uOttawa

L'Université canadienne
Canada's university

FACULTÉ DES ÉTUDES SUPÉRIEURES ET POSTOCTORALES

uOttawa

L'Université canadienne
Canada's university

FACULTY OF GRADUATE AND POSDOCTORAL STUDIES

Didier Savard

AUTEUR DE LA THÈSE / AUTHOR OF THESIS

M.Sc. (Chemistry)

GRADE / DEGREE

Department of Chemistry

FACULTÉ, ÉCOLE, DÉPARTEMENT / FACULTY, SCHOOL, DEPARTMENT

The Versatile Chemistry of Aryl Substituted 1,2,4-Triazole Ligands in Molecular Magnetism

TITRE DE LA THÈSE / TITLE OF THESIS

M. Murugescu

DIRECTEUR (DIRECTRICE) DE LA THÈSE / THESIS SUPERVISOR

CO-DIRECTEUR (CO-DIRECTRICE) DE LA THÈSE / THESIS CO-SUPERVISOR

S. Barry

S. Gambarotta

D. Richeson

Gary W. Slater

Le Doyen de la Faculte des études superieures et postdoctorales / Dean of the Faculty of Graduate and Postdoctoral Studies

The Versatile Chemistry of Aryl Substituted 1,2,4-triazole Ligands in Molecular Magnetism

By
Didier Savard

University of Ottawa

Your file Votre référence
ISBN: 978-0-494-73756-9
Our file Notre référence
ISBN: 978-0-494-73756-9

I. Table of contents

II. Acknowledgements

I would like to express my sincere appreciation to Dr. Muralee Murugesu for his support, advice and guidance during the length of my thesis research.

I would like to thank Dr. Rodolphe Clérac from the Centre de Recherche Paul-Pascal in Bordeaux for his support and guidance. I also express my gratitude to Mr. Gary D. Enright from the National Research Council of Canada, Ms. Tara J. Burchell from the University of Ottawa Crystallographic Center, Dr. Ilia Korobkov from the University of Ottawa Crystallographic Center, Dr. Sadok Letaief from the Center for Catalysis Research and Innovation, Ms. Roxanne Clément from the Center for Catalysis Research and Innovation and Dr. Wolfgang Wernsdorfer from the Néel Institute, the National Center for Scientific Research for their technical support and advices, and finally Ph.D. student Po-Heng Lin for his appreciated guidance and help.

I would also like to thank the University of Ottawa, the Canada Foundation for Innovation (CFI), the Fonds France-Canada pour la Recherche, the National Research Council of Canada (Discovery and RTI grants), the University of Bordeaux, the Centre National de la Recherche Scientifique, and the Région Aquitaine for their financial support.

III. List of abbreviations

Single-Molecule Magnet	SMM
Single-Chain Magnet	SCM
Spin Crossover	SCO
Metal-Organic Framework	MOF
High Spin	HS
Low Spin	LS
Quantum Tunnelling of the Magnetization	QTM
4-(4'-carboxyphenyl)-1,2,4-triazole	Hcpt
4-(4'-nitrophenyl)-1,2,4-triazole	npt
4-(4'-methylphenyl)-1,2,4-triazole	mept
4-(4'-carboxyphenyl)-1,2,4-triazole	mpt
4-(3'-hydroxyphenyl)-1,2,4-triazole	Hhpt
4-(2'-pyridyl)-1,2,4-triazole	ptz

IV. List of Figures

V. List of Schemes

VI. List of Tables

VII. Publications from Thesis Work

Didier Savard, Po-Heng Lin, Tara J. Burchell, Wolfgang Wernsdorfer, Rodolphe Clérac and Muralee Murugesu*, "Two-Dimensional Networks of Lanthanide Cubane-Shaped Dumbbells", *Inorg. Chem.*, **2009**, *48*, 11748–11754

VIII. Abstract

The work presented in this thesis focuses on exploring the versatile chemistry of 4-aryl substituted 1,2,4-triazole derivatives. The ligands 4-(4'-nitrophenyl)-1,2,4-triazole (npt) and 4-(4'-carboxyphenyl)-1,2,4-triazole (Hcpt) were prepared following a modified known synthetic strategy. Reaction of either of these ligands with transition metal or lanthanide precursor salts resulted in two novel complexes, namely $[Fe^{II}_3(npt)_6(EtOH)_4(H_2O)_2](ptol)_6 \cdot 4(EtOH)$ (**1**) and $[Dy^{III}_4(\mu_3\text{-}OH)_2(\mu_3\text{-}O)_2(cpt)_6(MeOH)_6(H_2O)]_2 \cdot 15(MeOH)$ (**5**), and of five analogous compounds.

In the case of **1**, the structural analyses and the magnetic properties indicated that the complex consisted of a linear trinuclear Spin Crossover Fe^{II} compound with a $T_{1/2}$ of 148 K. For this complex, the SC-XRD analyses were performed at 100 and 181 K in order to characterize the structural changes occurring during the spin transition. For **5**, the magnetic and structural data indicated that the complex was a dumbbell-shaped cubane dimer $\{Dy^{III}_4\}_2$ for which each cubane unit is a Single-Molecule Magnet with a small effective energy barrier.

Chapter 1. Introduction

The development of novel materials for their usage in optical and electronic devices is an important area of chemistry that gave rise to a strong interest in the scientific community since the early 1980s.[1-10] One of the current limitations in this field of chemistry is the fact that the top-down approach, commonly known as the race towards miniaturization, will one day reach its limitation which corresponds to the size of one molecule. Hence, researchers have explored the possibility of using molecules themselves as relevant devices for applications that can not be achieved by using conventional solid-state materials.[11-12]

Since the 1980s, the scientific interest in the development of molecules with unique properties for relevant applications slowly shifted towards a new category of chemistry named molecular magnetism.[13] This new science consists of developing and designing novel materials that exhibit unique magnetic properties. To date, the researchers in this area have been focused mainly on the development of Spin Crossover (SCO) complexes, Single-Molecule Magnets (SMMs) and Single-Chain Magnets (SCMs), as these three kinds of compounds are very promising for their potential applications in electronic and optical devices.[14-22] They also are categorized as molecular switches, which are compounds that exhibit bistability between two distinct states.[12] In general, for a complex to be considered as such, the change between the two distinct states must be triggered by the alteration of a physical parameter such as the applied magnetic field, the temperature or the pressure. Commonly, the two states are regarded as either "ON" or "OFF", the

former case usually being the one exhibiting a measurable physical response. In addition, the change between the two states is usually reversible over multiple cycles and measurable with conventional methods including magnetometry. Often, the intensity of the chemical, electrical or optical output varies in intensity during the switching process.

1.1 Spin Crossover (SCO) Materials

SCO materials are relevant molecular switches because they exhibit bistability between two electronic configurations, namely the Low Spin (LS) state and the High Spin (HS) state. For such materials, triggering between either of these two states is performed by either 1) a variation in temperature, 2) a variation in pressure, 3) light irradiation or 4) pulsed magnetic fields.[23-25] The fact that SCO compounds exhibit a considerable stability over successive HS→LS transition cycles, a short addressing time in the scale of nanoseconds due to the electronic nature of the spin transition and, in some exceptional cases, a hysteresis effect are some of the main advantages of developing such materials for applications in electronic devices.[12]

To date, the most studied SCO phenomenon has been for the Fe^{II} $3d^6$ transition metal.[26-32] In this case, the spin transition occurs between the $t_{2g}^6 e_g^0$ and the $t_{2g}^4 e_g^2$ electronic configurations. The properties of the latter event, such as the crossover temperature or the behaviour, are strictly dependent on both the ligand-field strength and the cooperative behaviour of the ligands for a given complex. As shown in Figure 1.1, the crossover temperature is related to the ligand-field strength; the stronger it is, the higher the crossover temperature is going to be.[33] However, in some exceptional cases where

electron-donating or withdrawing effects are observed, the crossover temperature may not be in direct relation with the parameter in question. There are five different behaviours of spin transition: 1) gradual, 2) abrupt, 3) with hysteresis, 4) multi-stepped and 5) incomplete.[27] In general, the three first behaviours are associated to the level of cooperative interactions, such as hydrogen bonds or electrostatic interactions, between the ligands in a crystal lattice. For example, a gradual SCO is associated with complexes where cooperative interactions between the ligands are poor or non-existent. For compounds where hysteresis is observed, the complexes are usually interacting through hydrogen bonds in the crystal lattice. When multiple SCO steps are observed throughout the magnetic data, the behaviour is exclusively associated to the fact that two or more distinct lattice sites exist in either the crystal lattice or the molecule itself. Finally, an incomplete spin transition is associated to the presence of residual spin fractions in either the LS state (residual HS fraction) or the HS state (residual LS fraction). It is noteworthy to mention that a gradual spin transition is usually accompanied with an incomplete SCO behaviour.

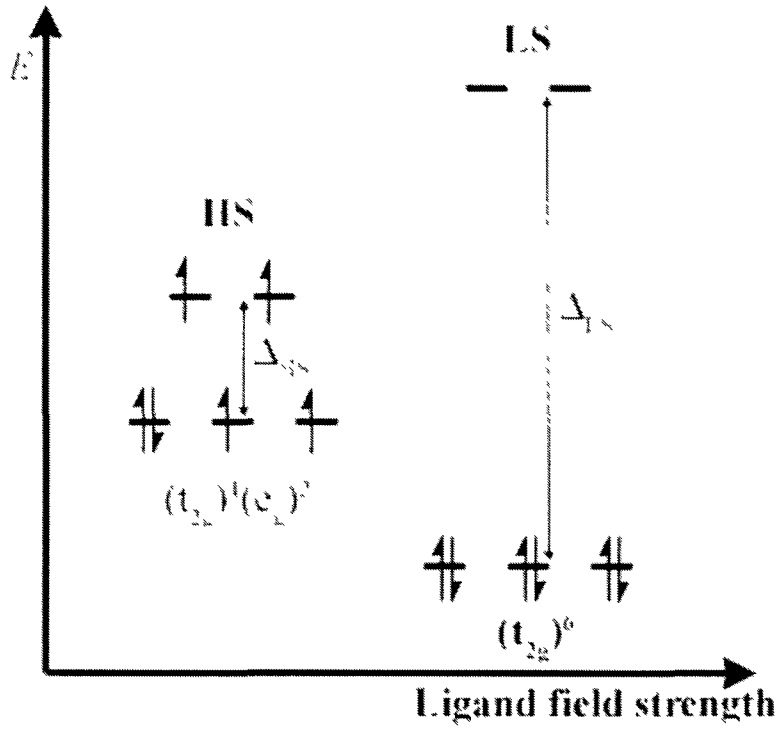

Figure 1.1 Representation of the LS and the HS states for Fe^{II} and of the relation between the cubic ligand field parameter (Δ) and the ligand field strength.

For their potential usage in electronic devices, the design of compounds with a crossover temperature ($T_{1/2}$) near or above room temperature is of strong interest.[14-22] Although many compounds with a $T_{1/2}$ above 300 K have already been reported, the design of SCO compounds with unique magnetic properties is still a considerable challenge. The main difficulty towards achieving the synthesis of novel SCO complexes is the design of novel ligands that will achieve the required ligand-field strength for the phenomenon to occur and that will provide a synthetic control over the SCO behaviour of the compound. As explained by Gütlich and co-workers,[26] SCO compounds can be synthesized by reacting ligands with a strong ligand-field, such as pyridines, triazoles and Schiff-base derivatives, with Fe^{II} precursor salts. Some examples of such ligands are shown in Scheme 1.1.

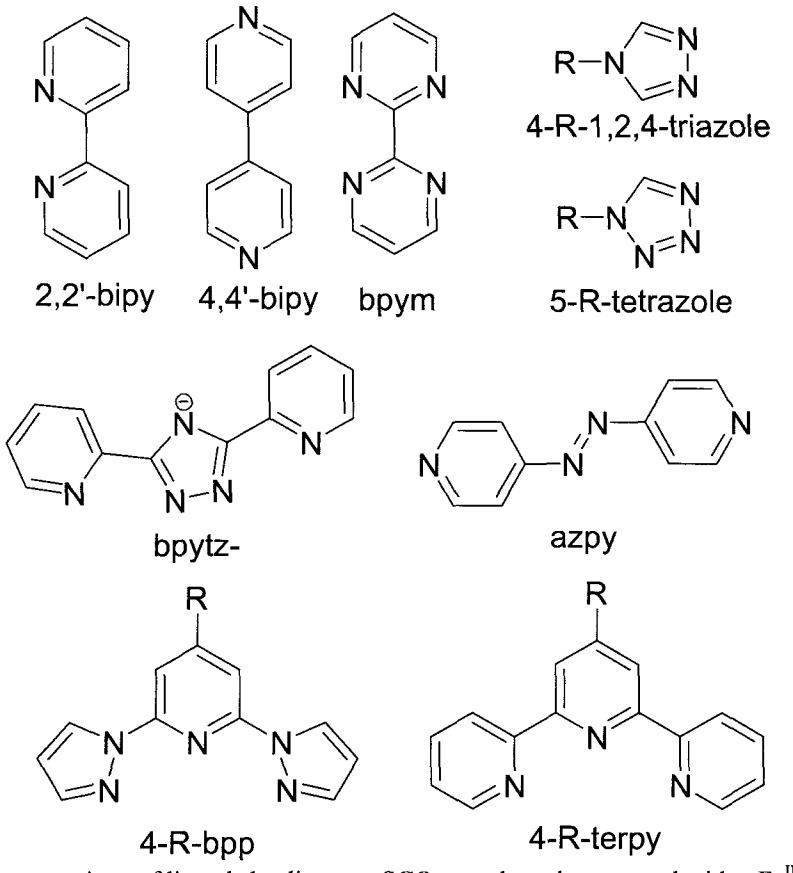

Scheme 1.1 Representations of ligands leading to a SCO complex when reacted with a Fe^{II} precursor salt.

It is noteworthy to mention that the SCO behaviour is usually accompanied with structural changes in the crystal lattice of a compound.[34-37] These changes in the distances and angles occur on two distinct levels; for a HS→LS transition, both the coordination distances of the metal ions and the distances between the molecules in a crystal lattice are shortened. The former case arises from a different orbital occupancy and, for Fe^{II}, is of approximately 0.15-0.20 Å which corresponds to an approximate decrease of 18-23% in the coordination sphere's volume of the ion. The decrease of intermolecular distances is also in direct relation with the SCO phenomenon and will usually result in a decreased unit cell volume. Currently, the major problem associated with these changes is the fact that crystals, upon spin transition, crack easily due to an increase in the crystal stress.

Hence, detailed structural data obtained through SC-XRD on SCO compounds in both their HS and LS states remains very elusive. The synthesis of complexes exhibiting a spin transition and that retain their crystallinity is still a difficult challenge to overcome.

For the purpose of this research, one of our goals consisted of exploring the possibility of synthesizing novel SCO compounds using 4-aryl substituted 1,2,4-triazole ligands and of analyzing their magnetic behaviour. The latter type of ligands is described in details in the following chapter of this work.

1.2 Single-Molecule Magnets (SMMs)

SMMs are categorized as molecular switches because they exhibit bistability between two distinct magnetization states when subjected to an applied magnetic field: the in-phase and the out-of-phase states.[38-44] For this type of complexes, the switching between the two states can be triggered by changing the direction of the magnetic field and the bistability phenomenon is caused by the presence of slow relaxation of the magnetization. The latter behaviour is observed due to the presence of an anisotropic energy barrier, U, which is the result of the combination of the spin ground state (S) and the uniaxial anisotropy (D). A representation of this energy barrier and of its behaviour giving rise to the slow relaxation of the magnetization is shown in Scheme 1.2. For most SMMs, the size of this energy barrier is approximated using the formula $U = S^2|D|$ for integer spin value or $U = (S-1/4)^2|D|$ for half-integer spin values.

The spin ground state of a given complex is determined by considering the magnetic coupling of its ions. There are two categories of magnetic coupling; ferromagnetic interactions, where the spins of two ions are coupled positively, and antiferromagnetic interactions, where the spins of the ions are coupled negatively. For example, for a complex where two Dy^{III} ions are coupled ferromagnetically, the spin ground state is S = 5 due to the addition of the spins of the Dy^{III} ion, each having five unpaired electrons (S = 5/2). For SMMs, since the anisotropic energy barrier is directly related to the spin ground state of the molecules, researchers are currently aiming at synthesizing molecules with large spin ground states. Usually, high spin first row transition metal centres or lanthanide ions are favoured in the preparation of SMMs due to their large spin ground state. In addition, ligands that promote ferromagnetic interactions between the ions, such as Schiff-base derivatives, are favoured over ligands promoting antiferromagnetic interactions.

For a given complex, the uniaxial magnetic anisotropy arises from the deformation of the orbitals along the easy axis of the complex, which can be the result of spin-orbit coupling and/or of a Jahn-Teller effect. For synthesizing SMMs, first row transition metals, such as Mn^{III}, Mn^{IV}, Fe^{II} and Co^{II}, or late lanthanide ions, including Tb^{III}, Dy^{III} and Ho^{III}, are favoured. For first row transition metals, spin-orbit coupling is most often observed for metal centres coordinated in an octahedral environment and takes place due to the presence of the d_{xy}, d_{yz} and d_{xz} orbitals degeneracy. In the case of lanthanide, the effect arises from the degeneracy of the *f* orbitals. When a Jahn-Teller distortion is observed

along the *z*-axis of an ion, the degeneracy of the $d_{x^2-y^2}$ and d_{z^2} orbitals is lost, which gives rise to the uniaxial magnetic anisotropy.

For SMMs, the size of this energy barrier not only determines the amount of energy required for such molecules to lose their magnetization, but also the blocking temperature, which is the temperature below which a complex exhibits the SMM behaviour. As mentioned above, the size of the energy barrier is directly related to the uniaxial anisotropy and the spin ground state of the complex. Hence, the size of this energy barrier is high dependent on the nature of the complex itself and is impossible to predict beforehand.

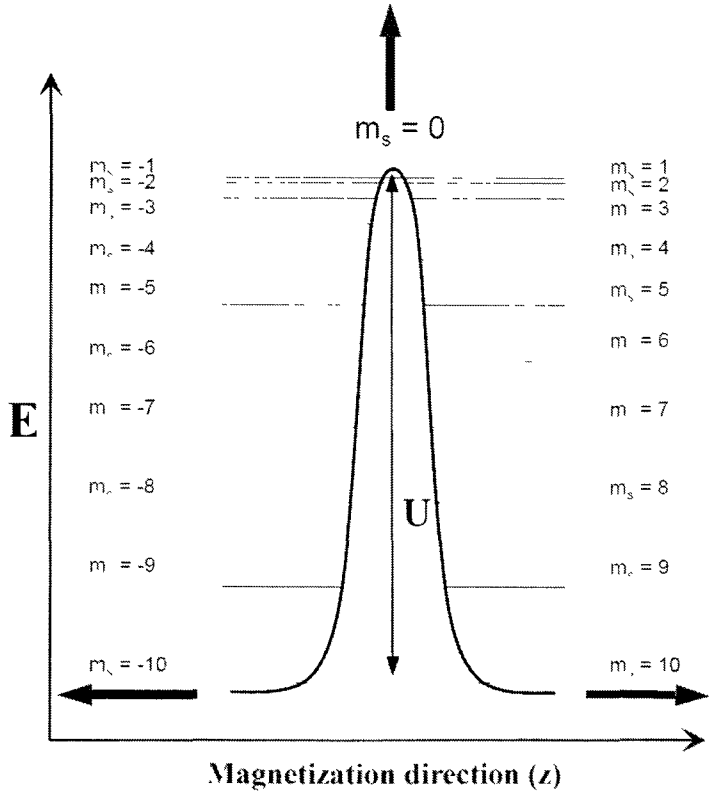

Scheme 1.2 Schematic representation of the anisotropic energy barrier of SMMs and of its relation with the direction of the applied magnetic field.

In the field of molecular magnetism, the assessment of the size of the energy barrier can be performed using two methods; the measurement of the alternate current (ac) susceptibility out-of-phase component or the measurement of the magnetization as a function of the direct current (dc) applied magnetic field. For the former case, when slow relaxation of the magnetization occurs, an out-of-phase component that is temperature and frequency dependent is observed. This signal arises from the few molecules that are not in-phase (i.e. aligned towards the same direction) with the applied magnetic field upon reversal of its direction at a specific frequency. For the latter case, the measurement is performed by slowly reversing the direction of the magnetic field upon multiple cycles. The magnetic moment of the sample, which is a projection of the magnetic moment of each individual molecule along the easy axis of the crystal, is then viewed as a function of the applied dc magnetic field. Upon reversal of the magnetization, the presence of a hysteresis loop that is sweep-rate dependent in the field dependence of the magnetization data confirms the presence of the SMM phenomenon. It is noteworthy to mention that the anisotropic energy barrier that is calculated from the experimental data is considered to be "effective" due to the presence of Quantum Tunneling of the Magnetization (QTM) between the two relevant magnetization states.

The first SMM[45] was synthesized by Lis in 1980 but its magnetic properties were not characterized before 1993 by Gatteschi and co-workers.[46] The compound, $[Mn^{III}_8Mn^{IV}_4(\mu_3\text{-}O)_{12}(CH_3COO)_{16}(H_2O)_4]\cdot 4(H_2O)\cdot 2(CH_3COOH)$ (Mn_{12}-Acetate), consisted of a Mn^{IV} cubane centered in a non planar ring of eight Mn^{III} ions. The molecular structure of this compound is shown in Figure 1.2. In this case, the ions were

linked by twelve μ_3-oxide moieties. The metallic core was encapsulated in sixteen acetate ligands and four coordinated water molecules, which acted as a protective shell surrounding the metallic core of the molecule. When an external magnetic field was applied, the complex exhibited slow relaxation of the magnetization caused by the presence of an effective anisotropic energy barrier of 62 K, which was the combination of an uniaxial anisotropy of -0.72 K and of a spin ground state of S = 10. In this case, the uniaxial anisotropy arose from the Jahn-Teller distortion of the Mn^{III} ions of the outer ring. The spin ground state of S = 10 resulted from the antiferromagnetic coupling of the ferromagnetically coupled $\{Mn^{IV}_4\}$ cubane core (S = 6) with the ferromagnetically coupled $\{Mn^{III}_8\}$ outer ring (S = 16). Since this discovery, researchers have been working towards the synthesis of novel SMMs with unique structural and magnetic properties and towards the synthesis of Mn_{12}-Acetate derivatives.

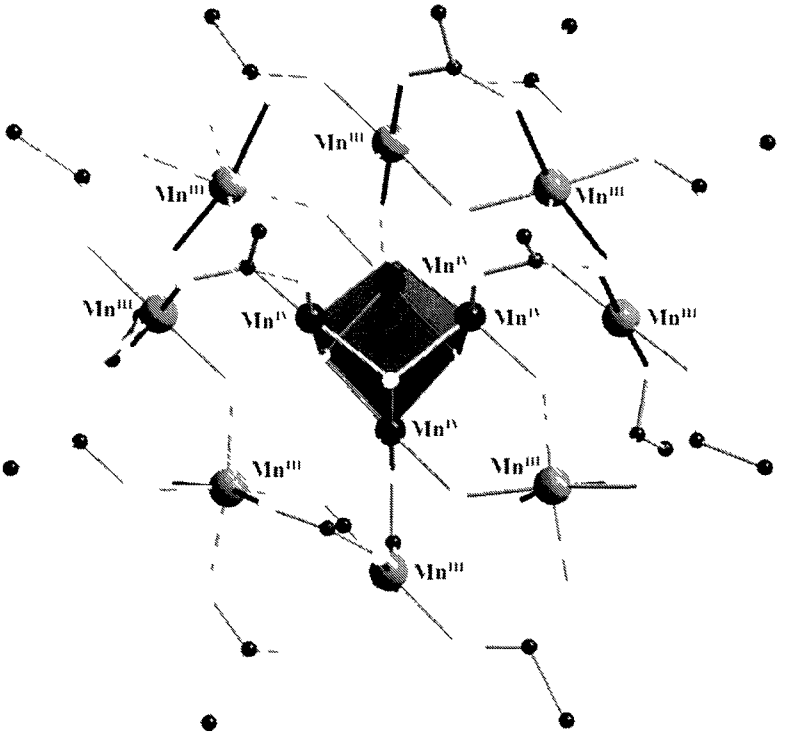

Figure 1.2 The molecular structure of Mn_{12}-Acetate. Colour code: Black (C), Dark Grey (Mn^{IV}), Grey (Mn^{III}), Light Grey (O).

Another example of SMM that was characterized in 2000 by Oshio and co-workers[48] consisted of the tetranuclear complex $[Fe^{II}_4(sae)_4(MeOH)_4]$ (H_2sae = 2-salicylideneamino-1-ethanol) which was composed of four Fe^{II} ions organized in a cubane connectivity. For this complex, the Fe^{II} ions were linked by four μ_3-oxide moieties from the ligands. Upon measurement of its magnetic properties, the complex exhibited a SMM behaviour with an energy barrier of 28.4 K. It is noteworthy to mention that in this case, the magnetic anisotropy arose from the spin-orbit coupling present for the Fe^{II} ions.

Currently, researchers are aiming towards increasing the size of the anisotropic energy barrier for the potential usage of SMMs at room temperature. To date, most of the synthesized SMMs of interest have exhibited energy barriers with sizes varying between 50 and 86 K. These complexes were synthesized by reacting either transition metal or lanthanide salts with Schiff-base,[49-56] carboxylate,[57-60] polyalcohol[61-64] and/or oximate[65-68] derivatives. Recently, our group published a novel complex for which the energy barrier was determined to be of 71 K.[69] To our knowledge, this consisted of the highest energy barrier reported to date. This compound, a dinuclear $\{Dy_2\}$ complex, was synthesized by reacting a novel Schiff-base ligand with a Dy^{III} precursor salt. We believed that the large anisotropic barrier was obtained due to the ferromagnetic combination of the intrinsic anisotropy and the large spin ground state of the Dy^{III} ions.

For the purpose of this research, we believed that the exploration of possible reactions between novel ligands, including 4-aryl substituted 1,2,4-triazoles, with lanthanide

precursor salts could result in complexes presenting SMM behaviour with large anisotropic energy barriers as shown in our previous work.

1.3 Summary of the thesis and scope of study

This research was focused on exploring the versatile chemistry of 4-aryl substituted 1,2,4-triazole ligands in the field of molecular magnetism. In Chapter 2, the previous literature regarding this category of ligand and the synthetic strategy that was used for the preparation of the ligands, Hcpt and npt, are described. The previously reported synthesis was altered in order to facilitate the purification process and to increase the yield of the reactions. For npt, the ligand was designed in order to synthesize a novel trinuclear linear complex with unique SCO properties. For Hcpt, we believed that the carboxylic acid functional group of the ligand could be reacted with lanthanide precursor salts in order to create lanthanide-only clusters, which are known to exhibit slow relaxation of magnetization. We also thought that the 1,2,4-triazolyl functional group of the ligand could promote unique topologies and supramolecular interactions between the molecular units in the crystal lattice. Chapter 3 describes the structural, optical, magnetic and thermogravimetric properties of the novel SCO trinuclear linear complex $[Fe^{II}_3(npt)_6(EtOH)_4(H_2O)_2](ptol)_6 \cdot 4(EtOH)$ (**1**, npt = 4-(4'-nitrophenyl)-1,2,4-triazole) and of three of its Co^{II} (**2** and **3**) and Ni^{II} (**4**) analogues. The measurement of the magnetic properties of **1** revealed that the compound exhibited a gradual SCO behaviour with a transition temperature ($T_{1/2}$) of 148 K. The characteristics of a novel Dy^{III} dumbbell-shaped cubane SMM, $[Dy^{III}_4(\mu_3\text{-}OH)_2(\mu_3\text{-}O)_2(cpt)_6(MeOH)_6(H_2O)]_2 \cdot 15(MeOH)$ (**5**, Hcpt = 4-(4'-carboxyphenyl)-1,2,4-triazole), and of its Ho^{III} (**6**) and Tb^{III} (**7**) analogues, are

described in Chapter 4. To our knowledge, this compound consisted of the first lanthanide-only cubane that exhibited slow relaxation of the magnetization. The structural analyses of **5** indicated that the dumbbell-shaped species were organized in a 2-D sheet due to the electrostatic interactions between the equatorial ligands of the complex. Finally, the general conclusions and recommendations for future work are described in Chapter 5 and all the experimental procedures are described in Chapter 6 of this work.

1.4 References

[1] O. Kahn and C. J. Martinez, *Science*, **1998**, *279*, 44

[2] O. Kahn, J. Kröber and C. Jay, *Adv. Mater.*, **1992**, *4*, 718

[3] P. Gütlich, Y. Garcia and H. A. Goodwin, *Chem. Soc. Rev.*, **2000**, *29*, 419

[4] R. N. Muller, L. V. Elst and S. Laurent, *J. Am. Chem. Soc.*, **2003**, *125*, 8405

[5] A. Galet, A. B. Gaspar, M. C. Muñoz, G. V. Bukin, G. Levchenko and J. A. Real, *Adv. Mater.*, **2005**, *17*, 2949

[6] B. Djukic and M. T. Lemaire, *Inorg. Chem.*, **2009**, *48*, 10489

[7] S. Qiu and G. Zhu, *Coor. Chem. Rev.*, **2009**, *253*, 2891

[8] J. Kim, Y. Piao and T. Hyeon, *Chem. Soc. Rev.*, **2009**, *38*, 372

[9] M. Liong, S. Angelos, E. Choi, K. Patel, J. F. Stoddart and J. I. Zink, *J. Mater. Chem.*, **2009**, *19*, 6251

[10] D. Gatteschi, L. Bogani, A. Cornia, M. Mannini, L. Sorace and R. Sessoli, *Solid State Sci.*, **2008**, 10, 1701

[11] J.-P. Sauvage, "Molecular machines and motors", *Springler-Verlag*, Berlin, **2001**, 306 pages

[12] J.-F. Létard, P. Guionneau and L. Goux-Capes, *Top. Curr. Chem.,* **2004**, *235*, 221

[13] D. Gatteschi, L. Bogani, A. Cornia, M. Mannini, L. Sorace and R. Sessoli, Solid State Sci., **2008**, *10*, 1701

[14] P. Gamez, J. S. Costa, M. Quesadaa and G. Aromi, *Dalton Trans.*, **2009**, 7845

[15] Y. Garcia, V. Ksenofontov and P. Gütlich, *Hyperfine Interact.*, **2002**, *139-140*, 543

[16] O. Kahn and C. J. Martinez, *Science*, **1998**, *279*, 44

[17] S. Brooker and J. A. Kitchen, *Dalton Trans.*, **2009**, 7331

[18] A. Bousseksou, G. Molnár, J. A. Real and K. Tanaka, *Coor. Chem. Rev.*, **2007**, *251*, 1822

[19] G. J. Halder, K. W. Chapman, S. M. Neville, B. Moubaraki, K. S. Murray, J.-F. Létard and C. J. Kepert, *J. Am. Chem. Soc.*, **2008**, *130*, 17552

[20] A. Naitabdy, J.-P. Bucher, P. Gerbier, P. Rabu and M. Drillon, *Adv. Mater.*, **2005**, *17*, 1612

[21] M. N. Leunenberger and D. Loss, *Nature*, **2001**, *410*, 789

[22] O. Roubeau and R. Clérac, *Eur. J. Inorg. Chem.*, **2008**, 4325

[23] J. A. Real, A. B. Gaspar, V. Niel and M. C. Muñoz, *Coord. Chem. Rev.*, **2003**, *236*, 121

[24] J. A. Real, A. B. Gaspar and M. C. Muñoz, *Dalton Trans.*, **2005**, 2062

[25] P. Gütlich, A. Hauser and H. Spiering, *Angew. Chem., Int. Ed. Engl.*, **1994**, *33*, 2024

[26] P. Gütlich and H. A. Goodwin, "Spin Crossover in Transition Metal Compounds", Springler, Berlin, **2004**

[27] P. Gütlich, Y. Garcia and H. A. Goodwin, *Chem. Soc. Rev.*, **2000**, *29*, 419

[28] P. Gütlich, Y. Garcia and T. Woike, *Coord. Chem. Rev.*, **2001**, *219*, 839

[29] A. B. Gaspar, M. Seredyuk and P. Gütlich, *J. Mol. Struct.*, **2009**, *924*, 9

[30] S. Brooker and J. A. Kitchen, *Dalton Trans.*, **2009**, 7331

[31] O. Kahn, "Molecular Magnetism", *VCH Publishers*, New York, **1993**, 396 pages

[32] N. T. Madhu, I. Salitros, F. Schramm, S. Klyatskaya, O. Fuhr and M. Ruben, *C. R. Chimie*, **2008**, 11, 1166

[33] A. Hauser, *Adv. Polym. Sci.*, **2004**, 23349

[34] Y. Garcia, P. Guionneau, G. Bravic, D. Chasseau, J. A. K. Howard, O. Kahn, V. Ksenofontov, S. Reiman and P. Gütlich, *Eur. J. Inorg. Chem.*, **2000**, 1531

[35] J. Li, R. L. Lord, B. C. Noll, M.-H. Baik, C. E. Schulz and W. R. Scheidt, *Angew. Chem. Int. Ed.*, **2008**, *47*, 10144

[36] T. Kosone, I. Tomori, C. Kanadani, T. Saito, T. Mochida and T. Kitazawa, *Dalton Trans.*, **2010**, *39*, 1719

[37] K. Yoshizawa, H. Miyajima and T. Yamabe, *J. Phys. Chem. B*, **1997**, *101*, 4383

[38] G. Christou, D. Gatteschi, D. N. Hendrickson and R. Sessoli, *MRS Bull.*, **2000**, *25*, 66

[39] L. Thomas, L. Lionti, R. Ballou, D. Gatteschi, R. Sessoli and B. Barbara, *Nature*, **1996**, *383*, 145

[40] E. Coronado and P. Day, *Chem. Rev.*, **2004**, *104*, 5419

[41] L. Bogani and W. Wernsdorfer, *Nature Mat.*, **2008**, *7*, 179

[42] J. J. Sokol, A. G. Hee and J. R. Long, *J. Am. Chem. Soc.*, **2002**, *124*, 7656

[43] S. Maheswaran, G. Chastanet, S. J. Teat, T. Mallah, R. Sessoli, W. Wernsdorfer and R. E. P. Winpenny, *Angew. Chem.*, **2005**, *44*, 5044

[44] J. Tang, I. Hewitt, N. T. Madhu, G. Chastanet, W. Wernsdorfer, C. E. Anson, C. Benelli, R. Sessoli and A. K. Powell, *Angew. Chem.*, **2006**, *45*, 1729

[45] T. Lis, *Acta crystallogr.*, **1980**, *B36*, 2042

[46] R. Sessoli, D. Gatteschi, A. Caneschi and M. A. Novak, *Nature*, **1993**, *365*, 141

[47] D. Gatteschi and R. Sessoli, *J. Magn. Magn. Mater.*, **2004**, *272-276*, 1030.

[48] H. Oshio, N. Hoshino and T. Ito, *J. Am. Chem. Soc.*, **2000**, *122*, 12602

[49] R. Singh, A. Banerjee, E. Colacio and K. K. Rajak, *Inorg. Chem.*, **2009**, *48*, 4753

[50] R. Ababei, Y.-G. Li, O. Roubeau, M. Kalisz, N. Bréfuel, C. Coulon, E. Harté, X. Liu, C. Mathonière and R. Clérac, *New J. Chem.*, **2009**, *33*, 1237.

[51] N. Hoshino, A. M. Ako, A. K. Powell and H. Oshio, *Inorg. Chem.*, **2009**, *48*, 3396

[52] G. Novitchi, W. Wernsdorfer, L. F. Chibotaru, J.-P. Costes, C. E. Anson and A. K. Powell, *Angew. Chem., Int. Ed.*, **2009**, *48*, 1614

[53] T. Kajiwara, M. Nakano, S. Takaishi and M. Yamashita, *Inorg. Chem.*, **2008**, *47*, 8604

[54] H. Miyasaka, A. Saitoh and S. Abe, *Coord. Chem. Rev.*, **2007**, *251*, 2622

[55] M. Ferbinteanu, H. Miyasaka, W. Wernsdorfer, K. Nakata, K. Sugiura, M. Yamashita, C. Coulon and R. Clérac, *J. Am. Chem. Soc.*, **2005**, *127*, 3090

[56] H. Miyasaka, R. Clérac, W. Wernsdorfer, L. Lecren, C. Bonhomme, K.-I. Sugiura and M. Yamashita, *Angew. Chem., Int. Ed.*, **2004**, *43*, 2801

[57] R. Sessoli, D. Gatteschi, A. Caneschi and M. A. Novak, *Nature*, **1993**, *365*, 141 and references cited therein

[58] R. Sessoli, H.-K. Tsai, A. R. Schake, S. Wang, J. B. Vincent, K. Folting, D. Gatteschi, G. Christou and D. N. Hendrickson, *J. Am. Chem. Soc.*, **1993**, *115*, 1804

[59] D. Gatteschi and R. Sessoli, *Angew. Chem., Int. Ed.*, **2003**, *42*, 268

[60] D. J. Price, S. R. Batten, B. Moubaraki and K. S. Murray, *Polyhedron*, **2007**, *26*, 305

[61] A. Ferguson, J. Lawrence, A. Parkin, J. Sanchez-Benitez, K. V. Kamenev, E. K. Brechin, W. Wernsdorfer, S. Hill and M. Murrie, *Dalton Trans.*, **2008**, 6409

[62] M. Murugesu, J. Raftery, W. Wernsdorfer, G. Christou and E. K. Brechin, *Inorg. Chem.*, **2004**, *43*, 4203

[63] T. C. Stamatatos, K. M. Poole, K. A. Abboud, W. Wernsdorfer, T. A. O'Brien and G. Christou, *Inorg. Chem.*, **2008**, *47*, 5006

[64] T. C. Stamatatos, V. Nastopoulos, A. J. Tasiopoulos, E. E. Moushi, W. Wernsdorfer, G. Christou and S. P. Perlepes, *Inorg. Chem.*, **2008**, *47*, 10081

[65] C. Papatriantafyllopoulou, M. Estrader, C. G. Efthymiou, D. Dermitzaki, K. Gkotsis, A. Terzis, C. Diaz and S. P. Perlepes, *Polyhedron*, **2009**, *28*, 1652

[66] C. J. Milios, R. Inglis, L. F. Jones, A. Prescimone, S. Parsons, W. Wernsdorfer and E. K. Brechin, *Dalton Trans.*, **2009**, 2812

[67] T. C. Stamatatos, D. Foguet-Albiol, S.-C. Lee, C. C. Stoumpos, C. P. Raptopoulou, A. Terzis, W. Wernsdorfer, S. O. Hill, S. P. Perlepes and G. Christou, *J. Am. Chem. Soc.*, **2007**, *129*, 9484

[68] F. Mori, T. Nyui, T. Ishida, T. Nogami, K.-Y. Choi and H. Nojiri, *J. Am. Chem. Soc.*, **2006**, *128*, 1440

[69] P.-H. Lin, T. J. Burchell, R. Clérac and M. Murugesu, *Angew. Chem., Int. Ed.*, **2008**, *47*, 8848

Chapter 2. Ligands Design and Syntheses

2.1 4-aryl substituted 1,2,4-triazoles ligands in inorganic chemistry

Since the early 1900s, triazole-based organic compounds have been widely studied in the fields of biology and biochemistry due to their presence in fish oils. However, before the work of Bayer and co-workers published in 1974,[1] their behaviour in the field of synthetic inorganic chemistry remained unexplored due to the difficulty of preparing 1,2,4-triazole-based ligands. To our knowledge, the first triazole-based coordination complex was reported by Haasnoot and co-workers in 1977.[2] In this work, a polymeric 1-D chain was synthesized by reacting three equivalents of 4-*H*-1,2,4-triazole with one equivalent of $[Fe^{II}(H_2O)_6](BF_4)_2$. The polymer, for which the optical and magnetic properties were measured, exhibited a SCO behaviour with a $T_{1/2}$ of approximately 378 K and presented a wide spin transition hysteresis of 32 K. Since its discovery, the characterization of this polymeric compound and of many analogous complexes has been of great interest due to their potential applications in polymer science.[3] The general structure of these 1-D chains is shown in Scheme 2.1. To date, the properties of these 1-D chains have been well studied by many researchers.[4-16] It has been demonstrated that functionalizing the 1,2,4-triazole ligand with an alkyl functional group on the 4th position or with small functional groups such as methyl-, ethyl- or amino- on the 3rd and 5th positions lead to analogous polymeric compounds.

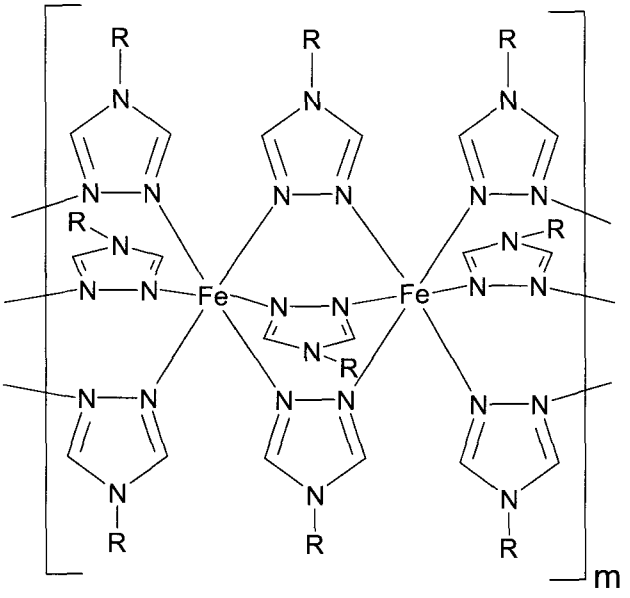

Scheme 2.1 Drawing of the general structure of 1-D triazoles-based chains.

Over the years, it has been demonstrated that the downside of these polymeric complexes was and still is the lack of structural information.[3] X-ray analyses of these compounds were difficult to achieve due to the polymeric nature of the compound itself and of the ligand, which favoured disorder in the crystal lattice. In most cases, structural analyses of these complexes were performed by either Powder X-ray Diffraction (PXRD) or by Extended X-ray Absorption Fine Structure (EXAFS). These analyses provided very little information on the properties of the chains in either the LS or the HS states and further investigations were often required. In addition to this lack of structural information, most of these Fe^{II} complexes were reported to be air-sensitive. However, it was established that the air sensitivity of these complexes is related to both the bulkiness of the counter anion, which acts as a protective shell for the polymeric chains, and the bulkiness of the substituting functional groups.

In 1984, Reedijk and co-workers[4] reported a trinuclear linear complex, $[Fe^{II}_3(Ettrz)_6(H_2O)_6](CF_3SO_3)_6$ (Ettrz = 4-ethyl-1,2,4-triazole), which was composed of two structurally unique Fe^{II} ions; the peripheral Fe^{II} ions, coordinated to three ligands and three solvent molecules, and the central ion, coordinated to six ligands. Structural analyses of this compound clearly demonstrated that the coordination environment of the central ion was similar to those previously reported for the Fe^{II} 1-D chains. In addition to this similarity, magnetic and mössbauer analyses revealed that the central ion also behaves in a similar SCO fashion, more specifically with a transition temperature of approximately 203 K. It is worth mentioning that this publication provided for the first time reliable structural information on such 1,2,4-triazoles-based complexes in both the LS and the HS states.

Later, in 1994, Kahn and co-workers[15] reported another trinuclear complex for which the substituting functional group on the 1,2,4-triazole ligand was 4-methoxyphenyl instead of ethyl. This complex, $[Fe^{II}_3(mpt)_6(H_2O)_6](ptol)_6 \cdot 2(MeOH) \cdot 8(H_2O)$ (mpt = 4-(4'-methoxyphenyl)-1,2,4-triazole), consisted of a trinuclear linear unit synthesized using a 4-aryl substituted 1,2,4-triazole ligand. In this work, the structural and magnetic observations in relation to the characteristics of the ligand and of the counter anions led to three major conclusions: 1) the bulkiness of the substituting functional group on the 4^{th} position of the triazole determines whereas a compound crystallizes as 1-D chain or as trinuclear linear complex, 2) the ligand's substituting functional group affects the magnetic behaviour of the trinuclear unit and 3) the nature of the counter anions also contributes to the magnetic behaviour of the complex. For example, as reported in this

work by Kahn *et al.*, using tetrafluoroborate instead of *p*-tolylsulfonate as a counter anion led not only to an absence of the crossover phenomenon, even if the coordination environment of the central ion was similar for both compounds, but also to a difference in the coordination behaviour of the peripheral Fe^{II} ions.

Since 1994, many studies and reviews[17] have been published regarding the magnetic properties and potential applications of 1,2,4-triazole-based 1-D chains and trinuclear complexes in relation to both the ligand's substituting functional groups and the counter anions. These studies not only allowed the development of a wide diversity of 1,2,4-triazole-based complexes but also confirmed the observations first stated by Kahn and co-workers mentioned above. It is now well established that using bulky substituting moieties on the triazole's fourth position favours the synthesis of trinuclear complexes while using less bulky derivatives leads to 1-D chains. Furthermore, in order to synthesize SCO triazole-based complexes, one should favour the usage of bulky counter anions such as triflate or *p*-tolylsulfonate in order to reach suitable ligand-field strengths and to prevent oxidation of the SCO metal centres.

Since 1984, many analogous Ni^{II}, Co^{II} and Cu^{II} trinuclear complexes[18-27] have been published for which the molecular structures were similar to the trinuclear unit first reported by Reedijk and co-workers. These reports proved that by changing the nature of both the ligand and the precursor salt, one can control the magnetic properties of these trinuclear units. For the purpose of this research, we believed that a large number of Fe^{II}, Co^{II} and Ni^{II} analogous 1-D chains or trinuclear complexes could be theoretically

synthesized in order to control the SCO properties of these 1-D chains, in the case of Fe^{II}, or to study the effect of the substituting functional group on the magnetic properties of the trinuclear units.

In 2005, Guo and co-workers reported[28] a mononuclear Co^{II} complex, $[Co^{II}(cpt)_2(H_2O)_4]\cdot 10H_2O$, for which the ligand's substituting functional group was 4-carboxyphenyl. The molecular structure of this compound is shown in Figure 2.1. Despite the statements mentioned above, reacting this aryl-based ligand with a cobalt precursor salt did not yield the expected trinuclear linear complex, but instead resulted in this mononuclear moiety. Structural analyses revealed that the complex consisted of a single Co^{II} ion with two deprotonated ligands in its axial positions and four coordinating water molecules in its equatorial positions. In addition, the study revealed that the packing arrangement of the molecules consisted of a 2-D sheet where the units are linked by hydrogen-bonds between the coordinating water molecules and the deprotonated carboxylate extremities of the ligands.

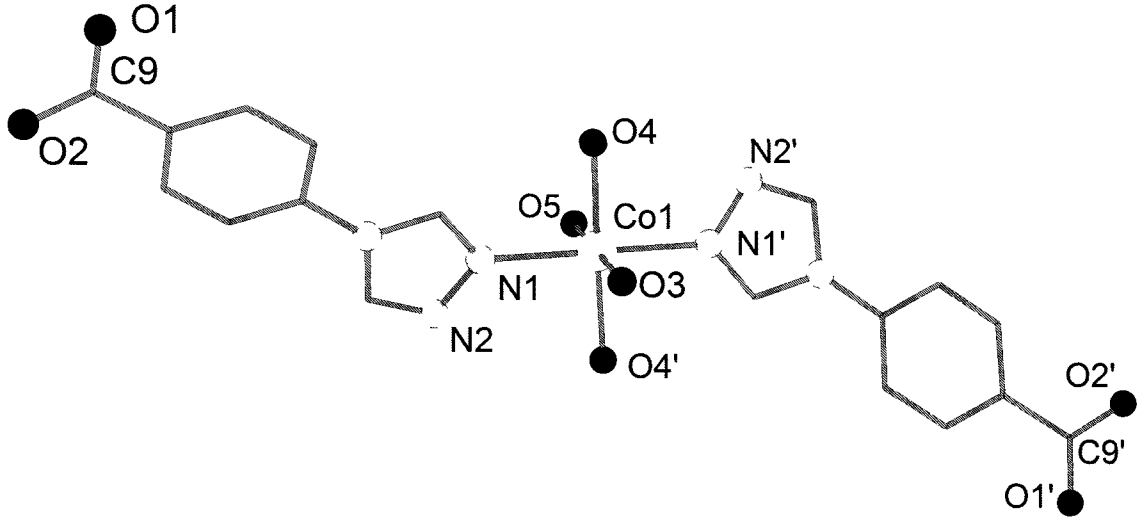

Figure 2.1 The molecular structure $[Co^{II}(cpt)_2(H_2O)_4]\cdot 10H_2O$. Colour code: Black (O), Grey (C), Light Grey (N), White (Co).

Later on, in 2007, Domasevitch and co-workers published[29] a similar compound, $[M^{II}(cpt)_2(H_2O)_2]$ (M = Co^{II}, Cu^{II} and Cd^{II}), for which the carboxylate functional group was coordinated to the metal centres along with two water molecules instead of the triazolyl functional group. The structural analyses of this compound revealed that the units were organized in a similar 2-D sheet reinforced by the presence of π-π stacking between the ligands and hydrogen-bonds between the triazolyl extremities and the coordinated water molecules.

The magnetic measurements for these two monomeric compound were not reported, but these publications opened the door to the possibility of using 4-aryl substituted 1,2,4-triazoles ligands for the synthesis of Metal-Organic Frameworks (MOFs), where both the triazoles and substituting functional group would be coordinated to metal ions, and to the possibility of synthesizing complexes where the carboxylic acid moiety of the reported ligand would act as the principal coordinating moiety. It is noteworthy to mention that these results also proved that 4-aryl functionalized 1,2,4-triazole ligands have the possibility of either electrostatically interacting or, as reported, π-π stack with similar species.

To our knowledge, only six complexes for which the ligands consisted of 4-aryl substituted 1,2,4-triazole derivatives have been reported to date. The ligands' structures and their coordination behaviour are shown in Scheme 2.2. In the case of Hcpt, the reported compounds[28, 29] consisted of mononuclear Co^{II}, Cu^{II} and Cd^{II} complexes for

which either the triazolyl or the carboxylate functional groups were coordinated to the metal centres, as mentioned above. For mept, two Fe^{II} complexes were reported as a pentanuclear assembly, $[Fe^{II}_2(mept)_5(NCS)_4]_2[Fe^{II}(mept)_2(NCS)_2(H_2O)_2]$, by Haasnoot and co-workers.[30] For these complexes, each of the Fe^{II} moieties are coordinated to mept ligands, water molecules and/or NCS^- units and the dinuclear complexes presented a SCO behaviour with a $T_{1/2}$ of approximately 111 K. For the three remaining ligands, mpt, hpt and ptz, the compounds consisted of linear Fe^{II}, Co^{II} and Ni^{II} trinuclear species, respectively, as previously mentioned.[15, 26, 27]

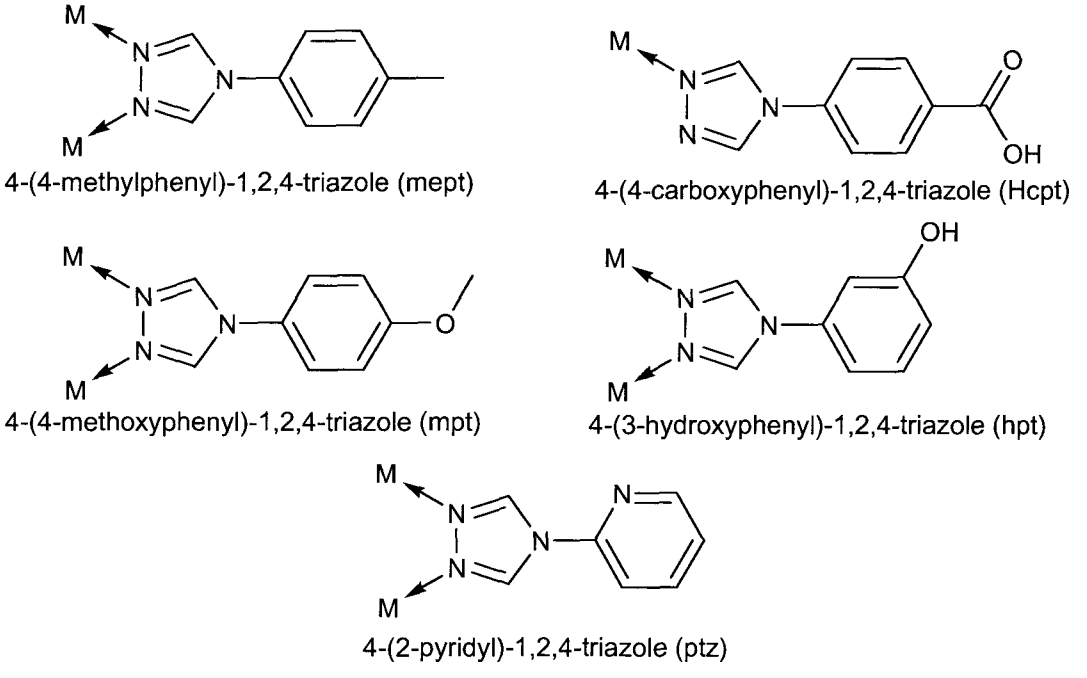

Scheme 2.2 Drawings of the reported 4-aryl substituted 1,2,4-triazole ligands and their coordination behaviour.

For most of these complexes, the coordination of the metal ions occurred strictly through the triazolyl functional group. It is noteworthy to mention that only mept and mpt were reacted with Fe^{II} precursor salts. For the purpose of this research, we believed that these compounds did not represent the versatile chemistry of this category of ligand for which

the chemistry is strictly dependent on the substituting phenyl aromatic ring. More specifically, for Hcpt, we believed that not only could this ligand be reacted with a Fe^{II} precursor salt in order to synthesize a SCO trinuclear unit but that it could also be reacted with other transition metal salts, such as Cr^{III}, Co^{II}, Co^{III}, Ni^{II} or Cu^{II}, or with lanthanides in order to either synthesize multidimensional MOFs or novel SMMs, respectively. We also believed that novel ligands, such as 4-(4'-nitrophenyl)-1,2,4-triazole (npt), could be synthesized and that reacting this type of ligand with an appropriate Fe^{II} precursor salt would result in novel SCO complexes. It is noteworthy to mention that the effect of the substituting functional group on the SCO behaviour of the trinuclear units has not been experimentally established; we believed that this avenue was also worth investigating.

2.2 The modified synthesis of 4-aryl substituted 1,2,4-triazole ligands

The synthesis of 4-aryl substituted 1,2,4-triazole was first reported by Bayer *et al.* in 1974.[1] In this work, the described preparation consisted of refluxing formylhydrazine and triethylorthoformate in methanol followed by the addition of a primary amide to the reaction, which resulted in a mixture of the triazolyl functionalized moiety and of the primary amine. In this work, the products were concentrated by slow evaporation of the solvent, leading to low purity oily materials. In order to purify the product, in the most recent publications referring to this synthesis, chromatography or recrystallization was performed. For the synthesis of Hcpt and npt, the protocol was modified in order to improve its overall yield.

For the purpose of this research, the modifications to the methodology consisted of 1) using ethanol instead of methanol as a solvent, 2) adding an acidic catalyst to the reaction and 3) using a microwave apparatus or a high pressure vessel.

First, methanol was replaced by ethanol in order to decrease the solubility of the final products, Hcpt and npt, in the reaction solution. When using methanol as the solvent, the products were not precipitating even at room temperature, which was rendering their purification long and difficult to achieve. Using ethanol as the solvent permitted the precipitation of the materials as either a pure product or as a mixture of the starting material, some impurities and the product for npt and Hcpt, respectively.

Second, the initially reported synthesis consisted of refluxing the reaction mixture over a long period of time in order to bring the reaction to completion. To improve the reaction time, a microwave apparatus was used in an attempt to heat the reaction above the boiling point of the reaction solvent, namely ethanol. This resulted not only in a very short reaction time, 5 minutes, but also in the precipitation of Hcpt as a pure powder that did not require further purification. In order to perform the reaction on a larger scale, a Synthware Glass high pressure vessel was used instead of the microwave apparatus, which allowed heating of the reaction mixtures up to 180 °C. The only inconveniences of this change were slightly longer reaction times, 30 minutes, and a less pure product in the case of Hcpt, which required an additional recrystallization step as detailled below.

Finally, as reported in the work of Bayer and co-workers, the reaction yields water through an amination reaction and the elimination of the aldehyde functional group during the ring-closing step, as shown in Scheme 2.3. For npt, adding sulphuric acid as a catalyst increased the yield of the reaction from 21% to 42% while in the case of Hcpt, the acid permitted a more efficient precipitation of the final product. It is noteworthy that at 180 °C, even in an acidic environment, 4-aminobenzoic acid was not totally soluble in the reaction mixture, which could have led to a lower yield than expected. A resume of the modified synthesis of the ligands, Hcpt and npt, is shown in Scheme 2.4.

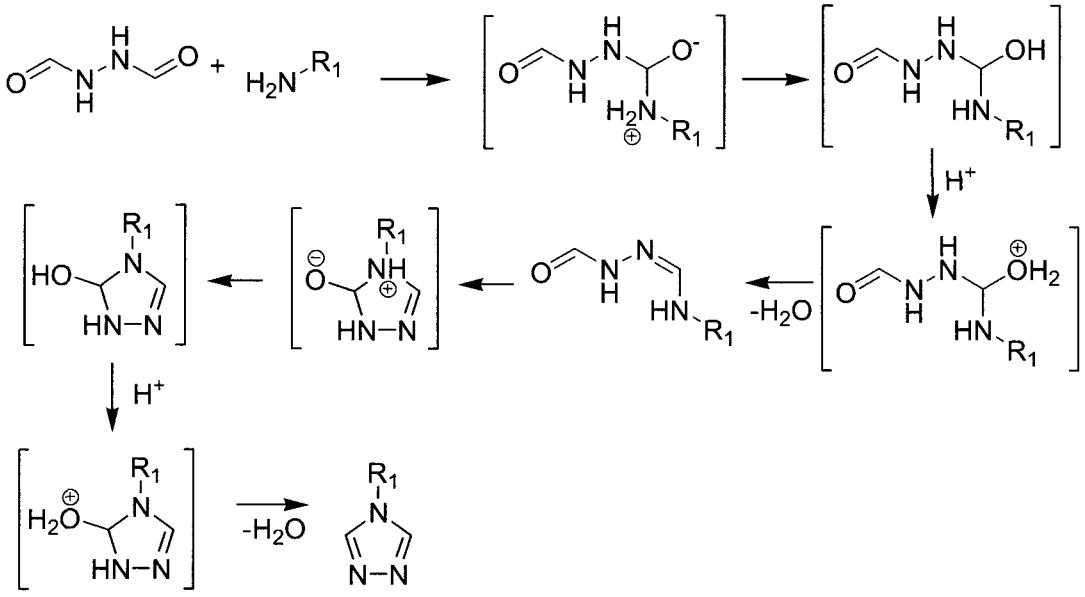

Scheme 2.3 The mechanism of the reaction between diformylhydrazine and a primary amine yielding the 1,2,4-triazole functional group.

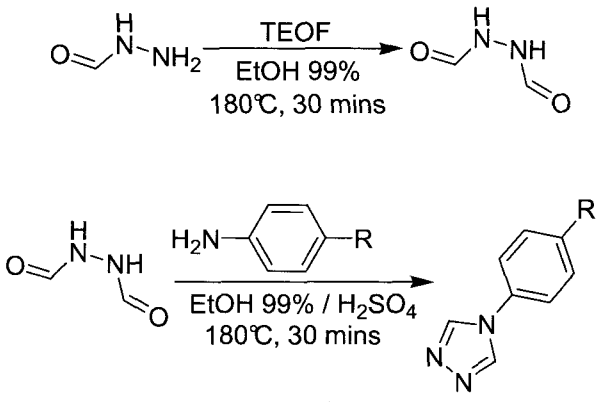

Scheme 2.4 The modified synthesis of 4-aryl substituted 1,2,4-triazole ligands. R = NO_2, COOH.

As mentioned above, the reaction between 4-aminobenzoic acid and diformylhydrazine using a Synthware Glass high pressure vessel led to an impure precipitate of Hcpt. Hence, an additional purification step was required. It was first determined that chromatography could not be used in order to purify the product since the latter is poorly soluble in any solvents when protonated. Solubility tests have demonstrated that Hcpt is fairly soluble in DMSO, DMA and DMF, poorly soluble in water, methanol and ethanol and insoluble in every other common organic solvents such as benzene, diethyl ether, toluene, nitromethane, acetonitrile, etc.. In order to purify Hcpt, recrystallization was performed by first dissolving the impure product in hot DMF. The mixture was then cooled at room temperature and diethyl ether was added in order to cause the precipitation of Hcpt. Once the majority of the product had precipitated, the filtrate was left undisturbed for 24 hours to yield colorless needles that were analyzed using SC-XRD.

2.3 Structural analyses of 4-(4'-carboxyphenyl)-1,2,4-triazole

The structural analyses of Hcpt, shown in Figure 2.2, demonstrated that the compound crystallized in the triclinic space group *P*-1 as a protonated organic compound and that,

as shown in Figure 2.3, the packing arrangement consisted of 2-D sheets of π-π stacked moieties. We believed that crystallization of the molecules from the unusual DMF/diethyl ether recrystallization mixture occurred due to the presence of a hydrogen bond [O-H...O = 2.57(1) Å] between the carboxylic acid functional groups and the DMF molecules of crystallization. The presence of such a hydrogen bond, along with π-π stacking between the aromatic rings of the ligands, allowed a better organization of the molecules on a supramolecular scale and thus crystallization of the compound. In this case, the crystals were analyzed not only to confirm the purity of the product but also to obtain information on the ligand's structural behaviour. It was observed that the triazolyl functional group was subjected to a dihedral angle of 33.5(1) ° towards the phenyl aromatic ring plane. This observation piqued our interest because such aromatic systems usually exhibit planarity between the aromatic rings. Hence, we believed that this dihedral angle could either be caused by a poor conjugation between the π systems of the two aromatic rings or by the presence of π-π stacking between the aromatic units in the crystal lattice. It is noteworthy that the crystal structure of this category of ligand was never reported before and may be worth further investigations.

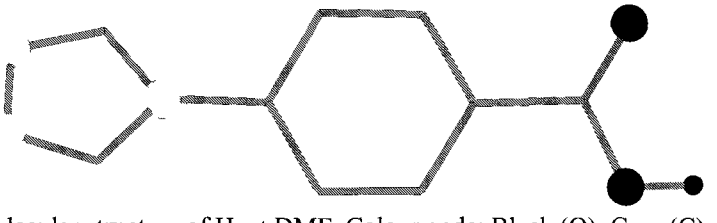

Figure 2.2 The molecular structure of Hcpt·DMF. Colour code: Black (O), Grey (C), Light Grey (N), Black (H, smaller).

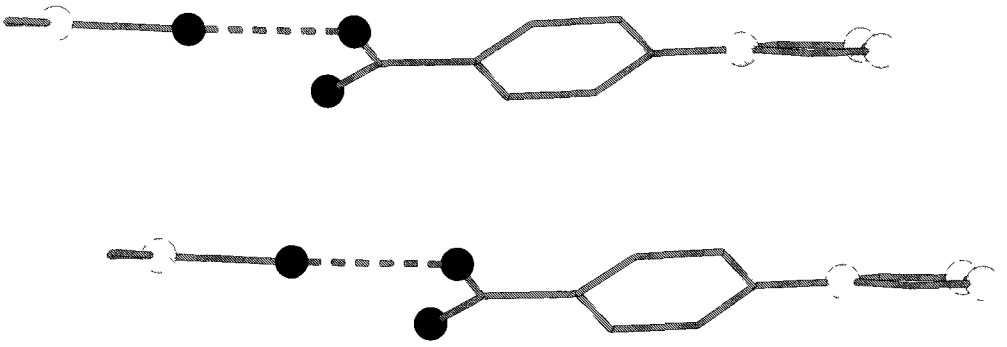

Figure 2.3 The packing arrangement of Hcpt·DMF viewed along the *b*-axis. Colour code: Black (O), Grey (C), Light Grey (N).

2.4 References

[1] H. O. Bayer, R. S. Cook and W. C. Von Meyer, *US Patent* 382137628, **1974**; *Chem. Abstr.* **1972**, *76*, 113224.

[2] J. G. Haasnoot, G. Vos and W. L. Groeneveld, *Z. Naturforsch.*, **1977**, *32b*, 1421

[3] K. S. Murray, Eur. J. Inorg. Chem., **2008**, 3101

[4] G. Vos, R. A. G. De Graaff, J. G. Haasnoot, A. M. Kraan, P. Vaal and J. Reedijk, *Inorg. Chem.*, **1984**, *23*, 2905

[5] G. Vos, R. A. Le Fêbre, R. A. G. De Graaff, J. G. Haasnoot and J. Reedijk, *J. Am. Chem. Soc.*, **1983**, *105*, 1682

[6] O. Roubeau, J. M. A. Gomez, E. Balskus, J. J. A. Kolnaar, J. G. Haasnoot and J. Reedijk, *New J. Chem.*, **2001**, *25*, 144

[7] J. J. A. Kolnaar, G. Van Dijk, H. Kooijman, A. L. Spek, V. G. Ksenofontov, P. Gütlich, J. G. Haasnoot and J. Reedijk, *Inorg. Chem.*, **1997**, *36*, 2433

[8] G. Vos, J. G. Haasnoot, G. C. Vershoor and J. Reedijk, *Inorg. Chim. Acta*, **1985**, *I05*, 31

[9] O. Roubeau, A. Colin, V. Schmitt and R. Clérac, *Angew. Chem. Int. Ed.*, **2004**, *43*, 3283

[10] M. M. Dîrtu, A. Rotaru, D. Gillard, J. Linares, E. Codjovi, B. Tinant and Y. Garcia, *Inorg. Chem.*, **2009**, *48*, 7838

[11] M. Seredyuk, A. B. Gaspar, M. C. Muñoz, M. Verdaguer, F. Villain and P. Gütlich, *Eur. J. Inorg. Chem.*, **2007**, 4481

[12] Y. Garcia, V. Niel, M. C. Muñoz and J. A. Real, *Top. Curr. Chem.*, **2004**, *233*, 229

[13] T. Fujigaya, D.-L. Jiang and T. Aida, *J. Am. Chem. Soc.*, **2003**, *125*, 14690

[14] M. M. Dîrtu, Y. Garcia, M. Nica, A. Rotaru, J. Linares and F. Varret, *Polyhedron*, **2007**, *26*, 2259

[15] M. Thomann, O. Kahn, J. Guilhem and F. Varret, *Inorg. Chem.*, **1994**, *33*, 6029

[16] M. Seredyuk, A. B. Gaspar, V. Ksenofontov, Y. Galyametdinov, M. Verdaguer, F. Villain and P. Gütlich, *Inorg. Chem.*, **2008**, *47*, 10232

[17] P. Gütlich and H. A. Goodwin, "Spin Crossover in Transition Metal Compounds", *Springler*, Berlin, **2004**

[18] F. J. Rietmeijer, J. G. Haasnoot, A. J. D. Hartog and J. Reedijk, *Inorg. Chim. Acta,* **1986**, *113*, 147

[19] L. R. Grovenveld, R. A. Le Fêbre, R. A. G. De Graaff, J. G. Haasnoot and J. Reedijk, *Inorg. Chim. Acta*, **1985**, *102*, 69

[20] W. Vreugdenhil, J. G. Haasnoot, M. F. J. Shoondergang and J. Reedijk, *Inorg. Chim. Acta*, **1987**, *130*, 235

[21] K. Drabent and Z. Ciunik, *Chem. Commun.*, **2001**, 1254

[22] P. J. Van Koningsbruggen, J. W. Van Hal, R. A. G. De Graaff, J. G. Haasnoot and J. Reejik, *J. Chem. Soc. Dalton Trans.*, **1993**, 2163

[23] Y. Garcia, P. J. Van Koningsbruggen, G. Bravic, D. Chasseau and O. Kahn, *Eur. J. Inorg. Chem.*, **2003**, 356

[24] Y. Garcia, P. J. Van Koningsbruggen, H. Kooijman, A. L. Spek, J. G. Haasnoot and O. Kahn, *Eur. J. Inorg. Chem.*, **2000**, 307

[25] B. Ding, L. Yi, W.-Z. Shen, P. Cheng, D.-Z. Liao, S.-P. Yan and Z.-H. Jiang, *J. Mol. Struct.*, **2006**, *784*, 138

[26] B. Liu, L. Xu, G.-C. Guo and J.-S. Huang, *J. Mol. Struct.*, **2006**, *825*, 79

[27] J. Liu, Y. Song, J. Zhuang, X. Huang and X. You, *Polyhedron*, **1999**, *18*, 1491

[28] R.-Q. Zoua, L.-Z. Caia and G.-C. Guo, *J. Mol. Struct.*, **2005**, *737*, 125

[29] L. V. Lukashuk, A. B. Lysenko, E. B. Rusanov, A. N. Chernegab and K. V. Domasevitch, *Acta Cryst.*, **2007**, *C63*, m140

[30] J. J. A. Kolnaar, M. I. de Heer, H. Kooijman, A. L. Spek, G. Schmitt, V. Ksenofontov, P. Gütlich, J. G. Haasnoot and J. Reedijk, *Eur. J. Inorg. Chem.*, **1999**, 881

Chapter 3. A Spin Crossover Trinuclear Linear Complex

3.1 Trinuclear Spin Crossover Complexes

As introduced in Chapter 2 of this work, the reaction of substituted 1,2,4-triazole ligands with late first row transition metal precursor salts generally yields 1-D chains or trinuclear linear complexes. For the purpose of this research, we chose to synthesize the ligand npt in order to explore its chemistry and to characterize the effect of the nitro- functional group on the SCO behaviour of a trinuclear complex. Previously, Kahn and co-workers[1] demonstrated that the reaction of a 4-aryl substituted 1,2,4-triazole ligand with $[Fe(H_2O)_6](ptol)_2$ leads to the formation of triazole-based trinuclear complexes due to the bulkiness of the ligand and of the counter anion. We opted for the nitro-functionalized ligand not only for the fact that the ligand would possess similar characteristics to the compound reported by Kahn *et al.* but also because the nitro- functional group is non coordinating. Furthermore, it is not known to favour the formation of hydrogen bonds between the molecular units or with the solvent molecules of crystallization. We believed that minimizing this type of intermolecular interactions by using the nitro- functional group would lead to a unique gradual SCO behaviour, as opposed to an abrupt spin transition observed for other similar trinuclear complexes.[2-3]

Furthermore, 4-aryl substituted 1,2,4-triazole ligands have been shown to exhibit either electrostatic interactions or π-π stacking with similar moieties, as shown in our work and by the work of Guo, Domasevitch and co-workers.[4-6] It is worth mentioning that, for npt, the nitro- functional group is coplanar with the phenyl aromatic ring. In our case, we

believed that the presence of this electron withdrawing group would promote electrostatic interactions between the aromatic ligands in the crystal lattice due to the delocalization of the electron density of the phenyl aromatic ring towards the nitro- functional group. It is well established that stronger intermolecular interactions favour the crystallization of coordination complexes and the formation of supramolecular arrays for the study of their structural and magnetic properties.

3.2 Synthesis of the complexes

The synthesis of the complex $[Fe^{II}_3(npt)_6(EtOH)_4(H_2O)_2](ptol)_6 \cdot 4(EtOH)$ (**1**) was carried out by reacting a Fe^{II} precursor salt, $[Fe(H_2O)_6](ptol)_2$, with the ligand npt in absolute ethanol, as shown in Equation 3.1. The solvent, in which the ligand exhibit low solubility, was chosen to promote crystallization of the complex. The counter anion, *p*-tolylsulfonate, was chosen because: 1) it prevents oxidation of the complex due to its bulkiness, 2) it favours crystallization of the complex through supramolecular interactions such as π-π stacking and 3) it is known to promote a SCO behaviour in Fe^{II} complexes. The crystallization was performed over 6 hours and yielded light-green plates suitable for SC-XRD. Three analogous compounds, complexes **2**, **3** and **4**, were synthesized using similar reaction conditions. For **3** and **4**, 20 mL of methanol was used instead of 30 mL of ethanol. The amount of solvent was lowered in order to yield a more saturated solution and thus promote crystallization of the complexes. At room temperature, the compounds exhibited rapid solvent loss, as observed by TGA (see Section 3.4). Prior to the analysis of their magnetic properties, **2**, **3** and **4** were dried under a constant flow of nitrogen until

constant mass. The magnetic properties of dried complexes **2**, **3** and **4** did not change significantly when compared to those of wet crystals.

$$6npt + 3Fe(ptol)_2 \cdot 6H_2O \xrightarrow[EtOH]{} [Fe^{II}_3(npt)_6(EtOH)_4(H_2O)_2](ptol)_6 \cdot 4(EtOH) \quad (3.1)$$

On the other hand, when exposed to air, **1** was subjected to a rapid oxidation as expected for Fe^{II} complexes. This oxidation was accompanied by a change of the crystal colour from light green to dark yellow and by an increase of the magnetic moment of the sample at room temperature upon measurement of its magnetic properties with a fixed molecular mass, confirming the $Fe^{II} \rightarrow Fe^{III}$ oxidation. The magnetic properties of **1** were thus measured in a N_2 or He inert environment. The samples were prepared in a glove box prior to the measurements and were directly transferred to the He environment of the SQUID magnetometer. In addition to the oxidation phenomenon, an absence of the SCO behaviour was denoted upon dryness. We believed that the absence of the spin transition could have been caused by the loss of solvent molecules of crystallization. Hence, the magnetic properties of **1** were measured on a wet sample suspended in the aforementioned inert environment.

3.3 Structural analyses

For **1**, structural analyses were performed using SC-XRD. These analyses revealed that the complex crystallized in the triclinic space group *P*-1. The molecular structure of **1** is shown in Figure 3.1. The +2 oxidation state of the Fe centres was confirmed by charge consideration and bond-valence sum calculations (see Table A1 in the annex) using the

parameters from the SC-XRD data collected at 181 K. The selected bond distances and angles of **1**, **2**, **3** and **4** are presented in Table 3.1, a labeled description of the core of **1** is presented in Figure 3.2 and the crystallographic data for all complexes is presented in Table A2 in the annex. Structural analyses indicated that **1** consisted of a linear trinuclear complex for which two structurally unique Fe^{II} metal centres were present: the central ion, hexacoordinated to six ligands, and the peripheral ions, hexacoordinated to three ligands, two solvent molecules (methanol or ethanol) and one water molecule. For **1**, at 181 K, the axial bonds of the central ion, M2-N10 and M2-N10', are elongated leading to symmetrical bond distances of 2.170(1) Å, which are longer than the symmetrical bond distances of 2.146(1) and 2.139(1) Å for M2-N1 and M2-N6, respectively. This elongation is expected for a HS Fe^{II} centre and may indicate the presence of spin-orbit coupling.[7] For the peripheral ions, no elongations were denoted along any of the axes. When compared to the data available in the literature, the coordination distances of the central ion corresponded closely to those expected for a HS Fe^{II} ion coordinated to six 1,2,4-triazoles ligands.[8] It is noteworthy to mention that the bond distances and angles were similar to those observed for the trinuclear units previously reported.[2-3] The main differences between these published compounds and **1** were the presence of coordinated solvent molecules to the peripheral ions, as opposed to water molecules only, and the different ligand substitutions. In order to compare the SCO properties of the complex with those of the literature, only the magnetic behaviour and the structural properties of the central ion were of interest.

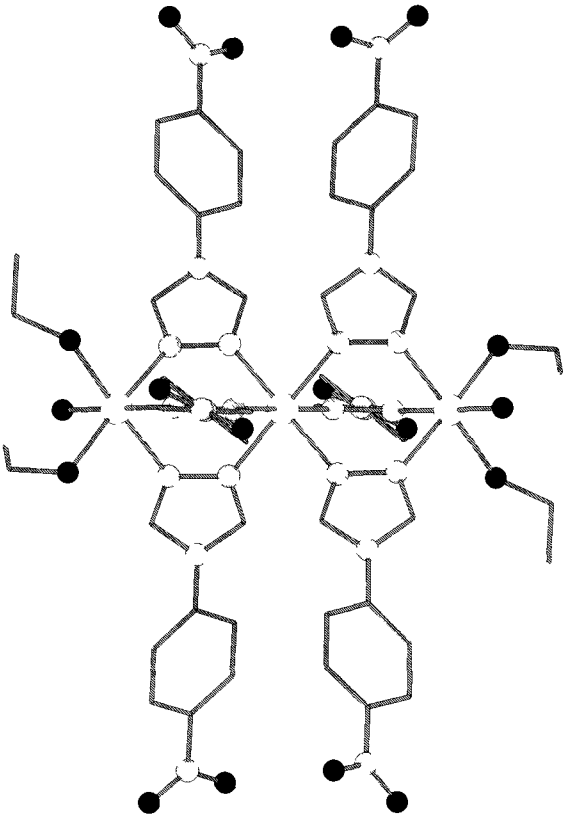

Figure 3.1 The molecular structure of **1** measured at 181 K. The hydrogen atoms and counter ions are omitted for clarity. Colour code: White (Fe), Black (O), Light Grey (N), Grey (C).

Table 3.1 Selected bond distances (Å) and angles (°) of **1**, **2**, **3** and **4**.

Complexes	**1**		**2**	**3**	**4**
T/K	181	100	202	202	202
M1-O7	2.133(1)	2.124(1)	2.077(4)	2.062(6)	2.071(5)
M1-O8	2.100(1)	2.085(1)	2.077(4)	2.083(5)	2.091(5)
M1-O9	2.098(1)	2.094(1)	2.140(4)	2.101(6)	2.075(4)
M1-N2	2.164(1)	2.145(1)	2.133(5)	2.118(6)	2.069(5)
M1-N5	2.159(1)	2.140(1)	2.115(4)	2.080(7)	2.044(5)
M1-N9	2.166(1)	2.149(1)	2.133(4)	2.116(6)	2.058(5)
M2-N1	2.146(1)	2.005(1)	2.129(4)	2.125(6)	2.102(5)
M2-N6	2.139(1)	2.004(1)	2.133(4)	2.147(6)	2.100(5)
M2-N10	2.170(1)	2.018(1)	2.162(4)	2.138(7)	2.105(5)
O7-M1-N9	176.24(5)	174.79(5)	178.5(2)	176.0(2)	177.6(2)
O8-M1-N5	176.73(5)	173.92(5)	178.5(2)	177.4(2)	179.8(2)
O9-M1-N2	178.75(5)	176.46(5)	176.4(2)	175.4(2)	179.2(2)
N1-M2-N6	88.88(5)	88.04(5)	88.5(2)	87.9(2)	89.8(2)
N1-M2-N10	90.25(5)	90.84(5)	90.3(2)	90.2(2)	90.2(2)
N10-M2-N6	90.87(5)	88.53(5)	90.6(2)	89.2(2)	89.4(2)

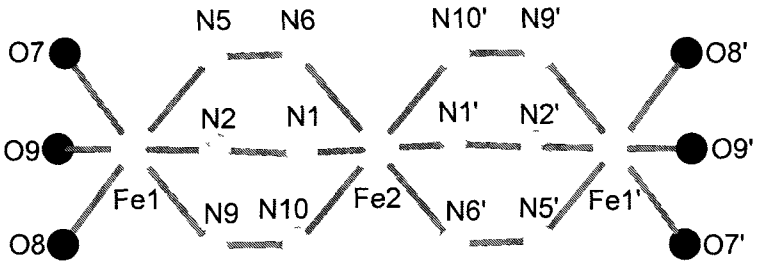

Figure 3.2 Labelled core of **1**. Colour code: White (Fe), Black (O), Light Grey (N).

As mentioned in section 3.2, the crystals of **1** were subjected to both a rapid oxidation upon exposure to air and a rapid solvent loss when taken out of the mother liquor. The packing arrangement of **1**, shown in Figure 3.3, demonstrated that the molecules were organized in a lattice-like arrangement. The first layer consisted of the cationic Fe^{II} metal centres and the anionic SO_3^- extremities of the *p*-tolylsulfonate counter anions. The second layer was made of the functionalized benzene aromatic rings of both the ligands and the *p*-tolylsulfonate counter anions and of the solvent molecules of crystallization. It is noteworthy to mention that the sulfonate extremities of the counter anions were located close to the metal centres due to supramolecular interactions between the ligands aromatic systems and the counter anions aromatic rings and to the ionic interactions between the negatively charged sulfonate groups and the Fe^{II} cations. This arrangement of the ligands and of the counter anions is shown in Figure 3.4.

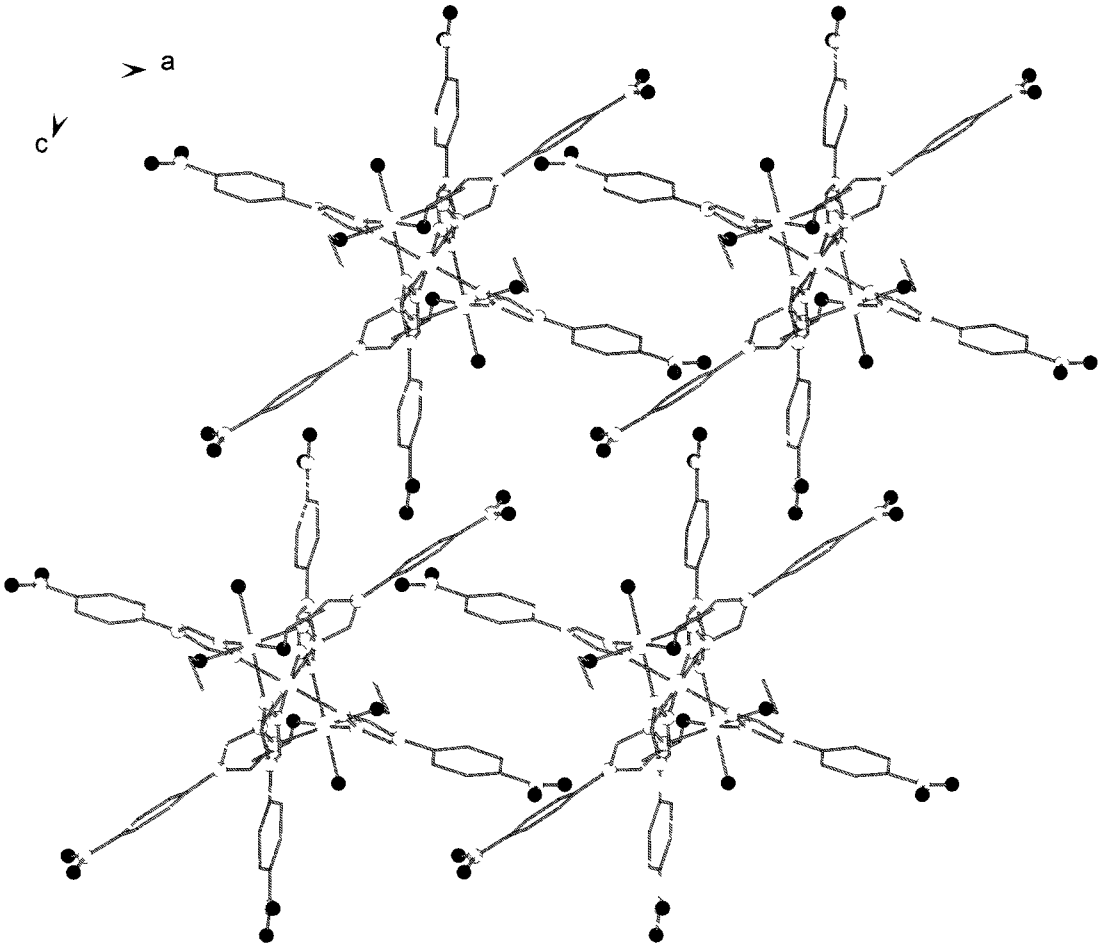

Figure 3.3 The packing arrangement of **1** viewed along the *b*-axis The *p*-tolylsulfonate counter anions, the solvents of crystallization and the hydrogen atoms are omitted for clarity Colour code: White (Fe), Black (O), Light Grey (N), Grey (C)

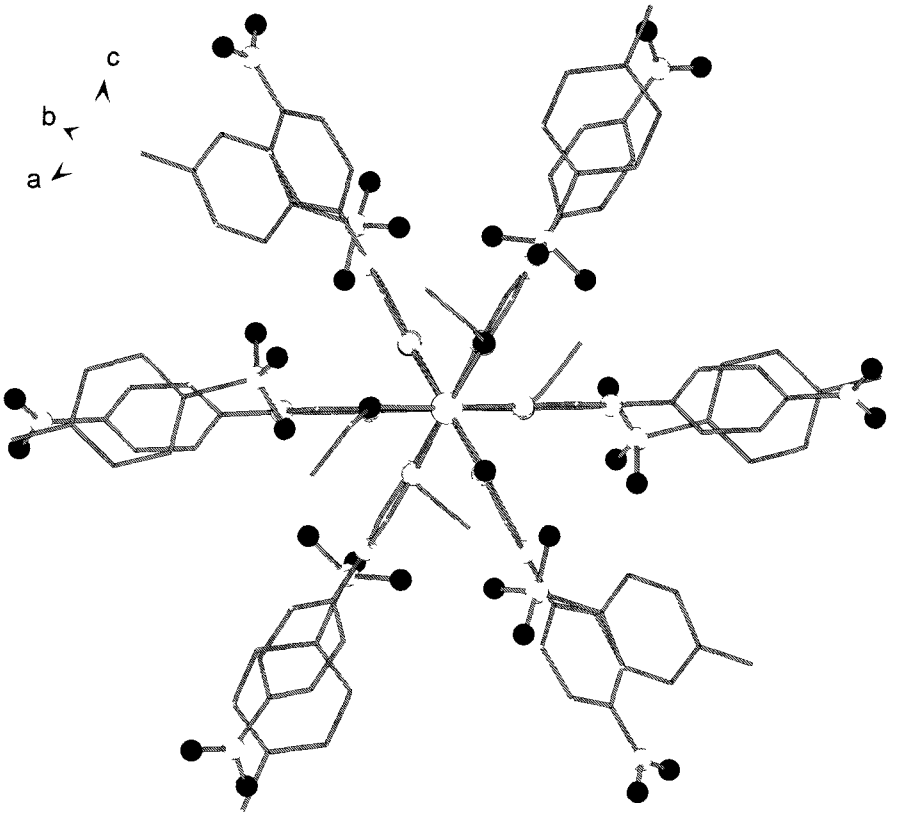

Figure 3.4 The packing arrangement of **1** viewed along the axial axis of the molecule. The solvents of crystallization and the hydrogen atoms are omitted for clarity. Colour code: White (Fe), Black (O), Light Grey (N).

As denoted by the magnetic measurements depicted in section 3.5, the central ion presented a spin transition with a $T_{1/2}$ of 148 K. It is important to mention that the coordination environment of the central ion of **1** was similar to those observed for triazole-based 1-D chains. Based on ligand-field strength considerations and on the different coordination environments of the ions, the ligand-field for the central ion was assumed to be stronger than the ligand-fields of the peripheral ions, which suggested the presence of two distinct SCO behaviours for **1**.

In order to confirm the occurrence of the spin transition in **1**, the same crystal was also measured at 100 K using SC-XRD. At this temperature, as shown in section 3.5, the

trinuclear unit would theoretically be in its HS-LS-HS state. For **1**, at 100 K, the bond distances between the six ligands and the central ion was of 2.005(1), 2.004(1) and 2.017(1) Å for Fe2-N1, Fe2-N6 and Fe2-N10, respectively. These were significantly shorter than those measured at 181 K with an average decrease of 0.14(1) Å. The latter corresponded closely to a Fe^{II} HS→LS spin transition for which the bond distances are shortened by approximately 0.15-0.20 Å. Furthermore, the coordination volume of the central ion was decreased by approximately 20%, which was also consistent with the data previously reported for a HS→LS SCO that would result in a decrease of 18-23%.[9-12] An ORTEP diagrams' comparison of the two central ions measured at 100 K and 181 K is shown in Figure 3.5 and a shadow superposition of the two structures is shown in Figure A1 in the annex.

The SCO phenomenon is usually accompanied by a decrease in the volume of the unit cell which causes crystal crumbling. For **1**, the unit cell volume decreased by approximately 60.5(4) $Å^3$, which was lower than the average decrease observed for similar compounds. For example, in the case of many trinuclear linear compounds, the average decrease consisted of approximately 150 $Å^3$.[2-3, 9-12] The bulkiness of the nitrophenyl functional groups on the triazole moiety and the presence of the bulky *p*-tolylsulfonate counter anions, which induced rigidity in the crystal lattice due to supramolecular interactions, could have been the cause of this smaller decrease. At low temperature, the shortest intermolecular distances for **1** were of 11.53(1), 9.25(1) and 14.14(1) Å along the *a*, *b* and *c*-axes, respectively, while at 181 K, these were of 11.55(1), 9.33(1) and 14.21(1) Å. The decrease of these intermolecular distances was very small

when compared to the large distance separating the trinuclear units in the crystal lattice. These observations could have indicated that **1** was most likely to retain its SCO behaviour upon multiple cool-thaw cycle, assuming that the crystals were kept in an inert environment during the measurement to prevent oxidation.

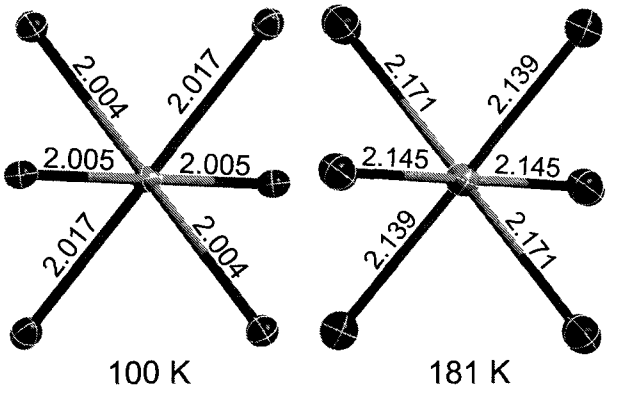

Figure 3.5 ORTEP diagrams comparison of the coordination environment of the central Fe^{II} ion of **1** at 100 and 181 K. Thermal ellipsoid plots are drawn at 50 %. Colour code: Light Grey (Fe), Dark Grey (N).

Structural analyses of **2**, **3** and **4** measured at 202 K revealed that all three complexes were analogous to **1**. In the case of **2**, the compound presented similar bond distances and angles and a comparable packing arrangement. For **3** and **4**, as aforementioned in section 3.2, the reaction solvent was changed to methanol. Hence, the coordinated solvent molecules on the peripheral ions were methanol molecules instead of ethanol molecules. Furthermore, for 4, the numbers of crystallization molecules was also different; two methanol molecules and one water. For each of the three complexes, the bond distances and angles of the metallic core were similar to those of **1**.

The molecular structure and the packing arrangement of **2** are shown in Figures 3.6 and 3.7, respectively. Regarding the packing arrangement, differences were noticed in the intermolecular distances which were of 11.59(1), 9.42(1) and 14.29(1) Å along the *a*, *b*

and *c*-axes, respectively. Similarly to **1**, an absence of intermolecular cooperative interactions was denoted which could suggest, along with the large intermolecular distances, an absence of long-range magnetic effect.

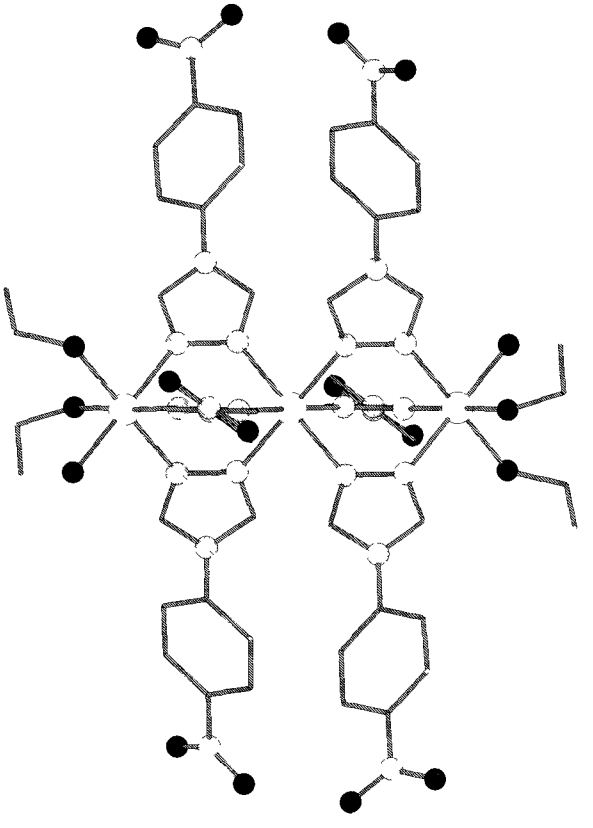

Figure 3.6 The molecular structure of **2**. The hydrogen atoms and counter ions are omitted for clarity. Colour code: White (Co), Black (O), Light Grey (N), Grey (C).

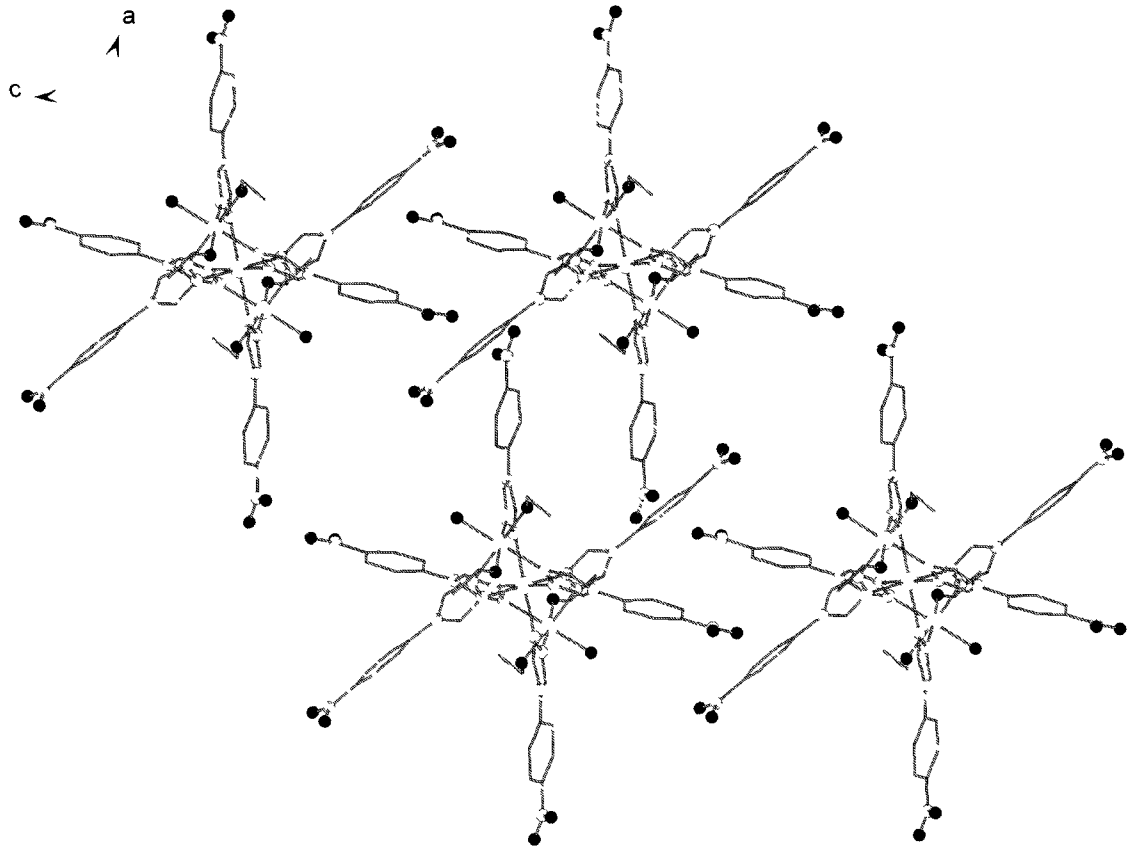

Figure 3.7 The packing arrangement of **2** viewed along the *b*-axis. The *p*-tolylsulfonate counter anions, the solvents of crystallization and the hydrogen atoms are omitted for clarity. Colour code: White (Co), Black (O), Light Grey (N), Grey (C).

The molecular structure of **3** is shown in Figure 3.8 while its packing arrangement is shown in Figure 3.9. Along with the different coordinated solvent molecules, structural differences were denoted in regard to the dihedral angles of the ligands. The dihedral angles of each symmetrical ligand for all four compounds are denoted in Table 3.2. For **3**, one of the three ligands of this complex presented a larger dihedral angle, namely a difference of 24.0(2) ° when compared to Ligand 2 of complex **1**. By considering the packing arrangement, it was denoted that intermolecular electrostatic interactions were present between these ligands of the trinuclear units. The distance between these interacting ligands, shown by fragmented lines in Figure 3.9, was of 3.24(1) Å. We

believed that these short distances were due to the nature of the interactions between the phenyl aromatic rings and the nitro- functional group. These interactions were occurring along the *c*-axis and led to a much different unit cell and a more pronounced lamellar organization of the molecules.

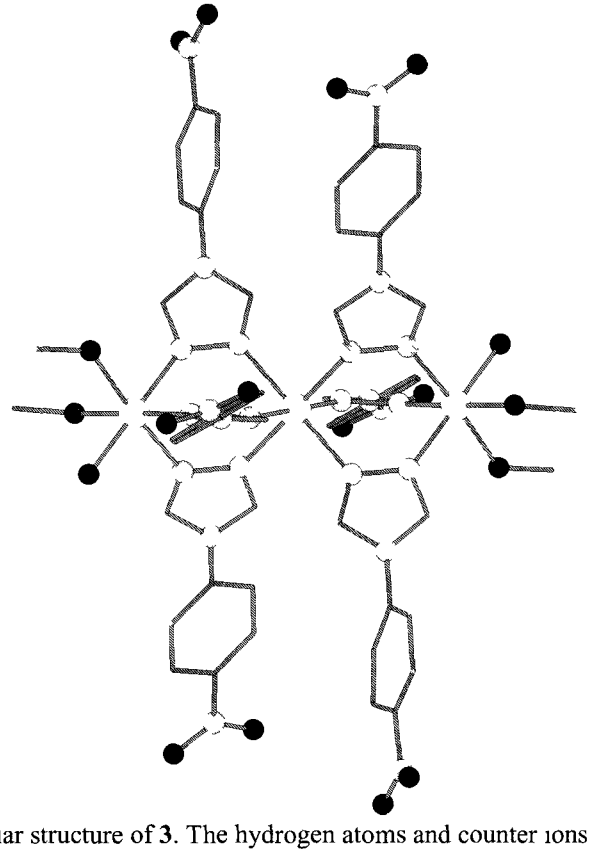

Figure 3.8 The molecular structure of **3**. The hydrogen atoms and counter ions are omitted for clarity. Colour code: White (Co), Black (O), Light Grey (N), Grey (C).

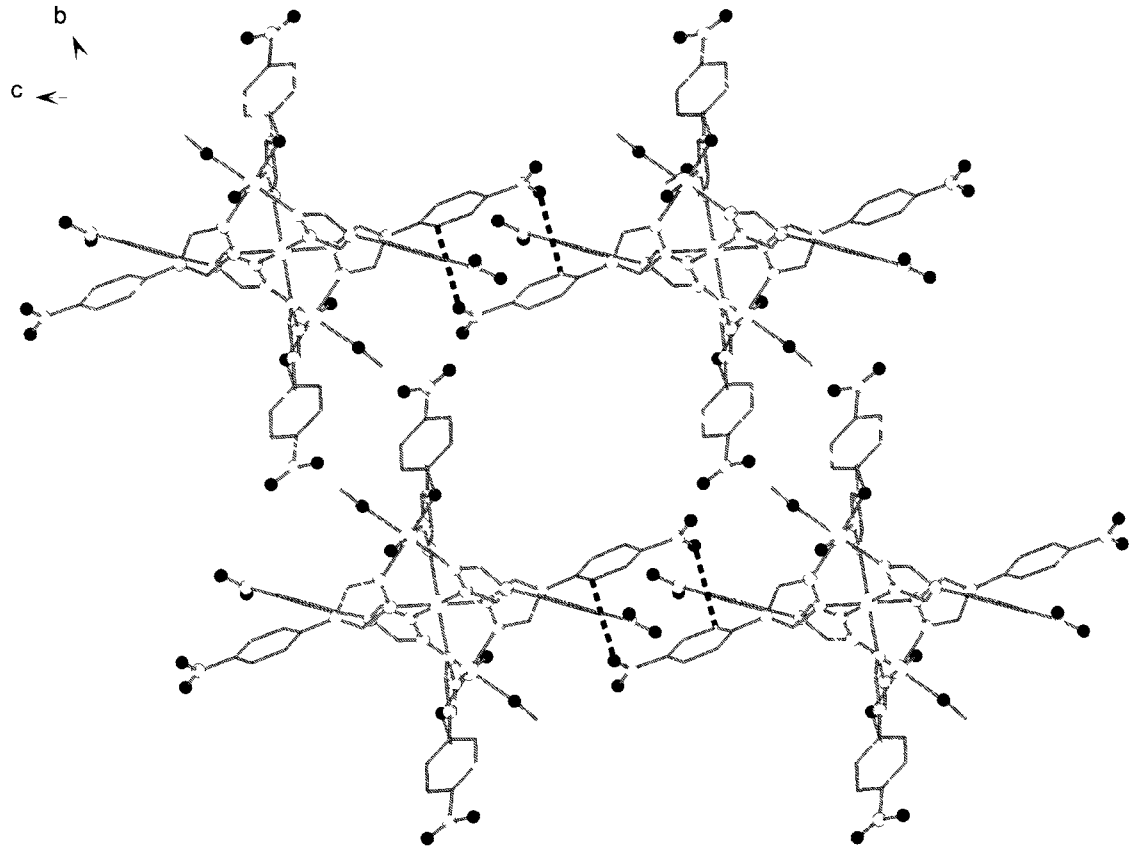

Figure 3.9 The packing arrangement of **3** viewed along the *a*-axis. Electrostatic interactions between the ligands are represented by the dark black fragmented lines. The *p*-tolylsulfonate counter anions, the solvents of crystallization and the hydrogen atoms are omitted for clarity. Colour code: White (Co), Black (O), Light Grey (N), Grey (C).

Table 3.2 Dihedral angles (°) of the ligands of **1**, **2**, **3** and **4**.

	Ligand 1	**Ligand 2**	**Ligand 3**
1	40.6(1)	39.1(1)	36.8(1)
2	41.8(1)	38.2(1)	34.9(1)
3	35.5(1)	63.1(1)	29.9(1)
4	52.5(1)	37.2(1)	37.3(1)

In the case of **4**, the molecular structure is shown in Figure 3.10 and the packing arrangement is shown in Figure 3.11. In this case, two occurrences of electrostatic interactions between the ligands of the trinuclear units were denoted. The distances between the interacting ligands were of 3.48(1) and 3.21(1) Å for Ligand 1 and Ligand 3. For Ligand 1, a difference of 11.9(2) ° in the dihedral angle of the ligand was denoted, which confirmed the presence of these electrostatic interactions. Again, these interactions

led to a much different packing arrangement, hence a different unit cell, and a better lamellar organization of the molecules. It is noteworthy to mention that for **3** and **4**, when exposed to air, the crystals were loosing solvent at a much faster rate than the crystals of **1** and **2**. This could have been either due to the different lamellar organization of the trinuclear units or to the different nature of the solvents of crystallization.

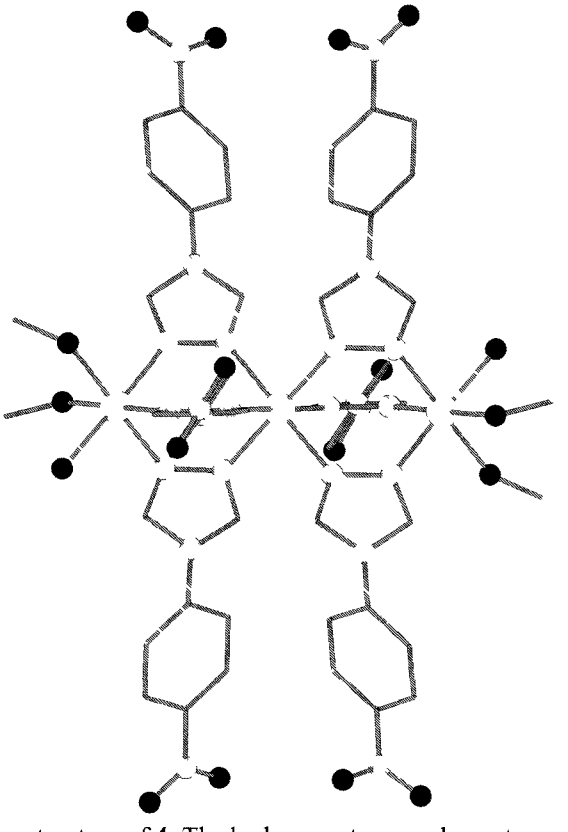

Figure 3.10 The molecular structure of **4**. The hydrogen atoms and counter ions are omitted for clarity. Colour code: White (Ni), Black (O), Light Grey (N), Grey (C).

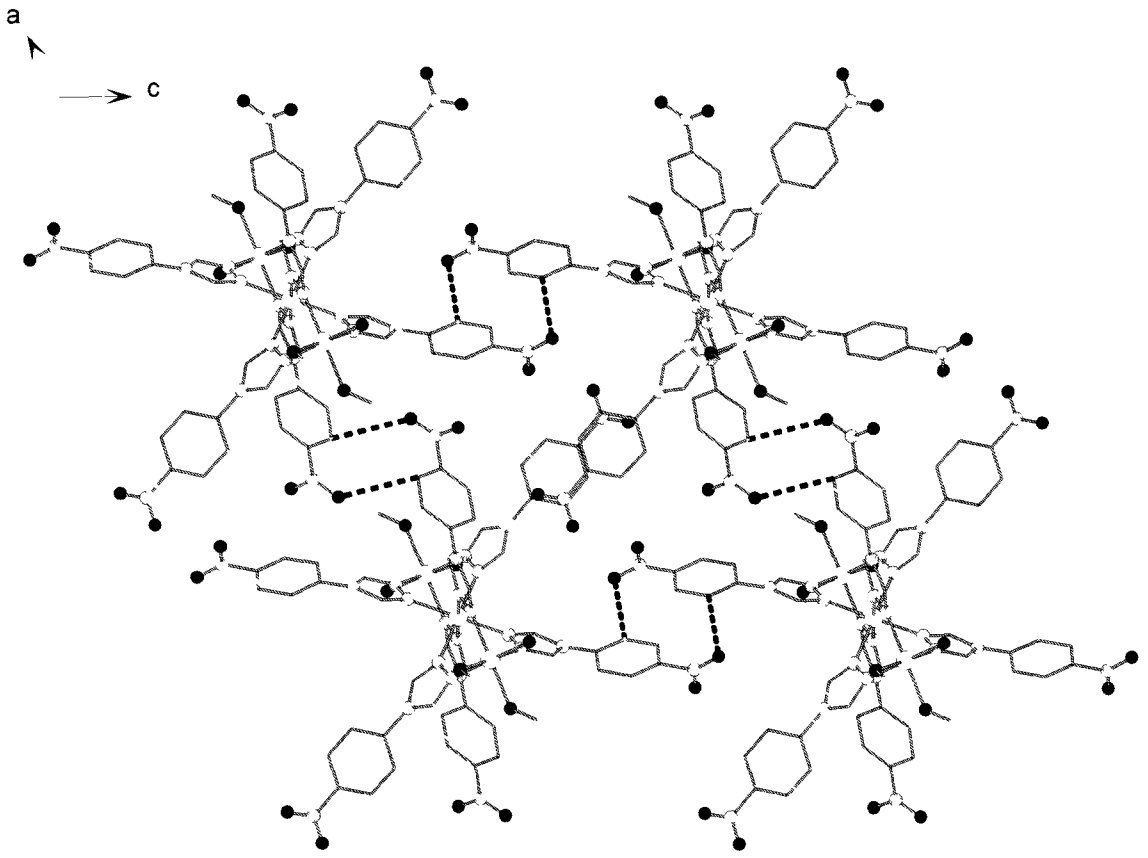

Figure 3.11 The packing arrangement of **4** viewed along the *b*-axis. Electrostatic interactions between the ligands are represented by the dark black fragmented lines. The *p*-tolylsulfonate counter anions, the solvents of crystallization and the hydrogen atoms are omitted for clarity. Colour code: White (Ni), Black (O), Light Grey (N), Grey (C).

3.4 Thermogravimetric analyses

Thermogravimetric analyses of each complex were performed between 25 and 300 °C at the rate of 10 °C/min under a constant nitrogen flow. For **1**, the data, shown in Figure 3.12, indicated a four steps desolvation process. At room temperature, a positive derivative was denoted. The decrease of less than 1% in the total mass of the sample could have been caused by the loss of a small amount of solvent of crystallization and could have indicated that the first desolvation step occurs at or below 25 °C. The exact percentage of this loss could not be calculated due to the lack of data below 25 °C and to the presence of a shoulder at 41 °C. The two next desolvation steps were observed at 71

and 93 °C. When combined, these two steps accounted for 5.9% of the total mass of the sample, which would correspond to four ethanol molecules (Calc. 6.4%). Since the total percentage was lower than the theoretical one, the data was in agreement with the fact that a first desolvation step could occur below 25 °C. Furthermore, these two desolvation steps were in agreement with the structural data presented in section 3.3, which indicated the presence of four solvent molecules of crystallization located between the lamellas of trinuclear units. This lamellar organization of the molecules and the presence of *p*-tolylsulfonate counter anions could have been the cause of this rapid solvent loss at room temperature. For **1**, at 150 °C, a fourth desolvation step was observed which corresponded to a decrease of 3.1% in the sample's total mass. This accounted to the loss of two ethanol molecules (Calc. 3.2%). As denoted in section 3.3, the peripheral ions of **1** were coordinated to two ethanol molecules and one water molecule each. Hence, we believed that this decrease corresponded to the loss of one ethanol molecule per ion, leading to Fe^{II} peripheral ions with different coordination environments at higher temperature. Experimental assessments revealed that the losses of the solvent molecules of crystallization were reversible while the losses of the coordinated solvent molecules on the peripheral ions at 150 °C were not.

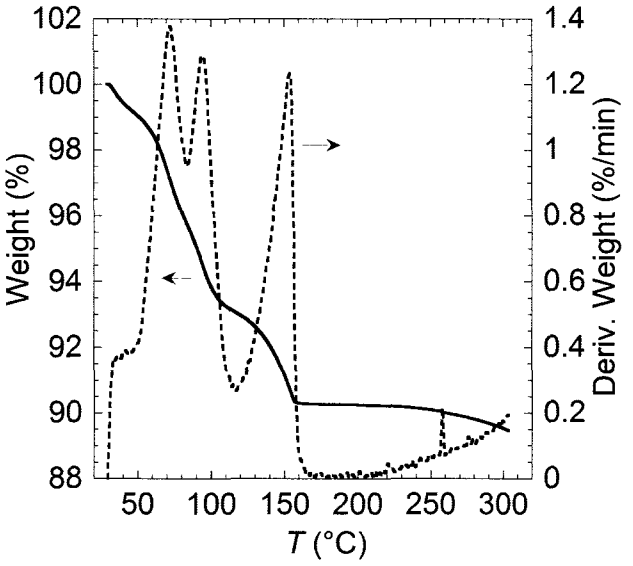

Figure 3.12 Thermogravimetric analyses of **1** measured between 25 and 300 °C at a rate of 10 °C/min under a constant nitrogen flow.

For **2** and **3**, for which the data are shown in Figure 3.13 and 3.14, similar behaviours were denoted over the same temperature range. In both cases, all four molecules of crystallization were lost below 100 °C and two additional coordinated solvent molecules were lost between 150 and 200 °C. For **2**, the temperatures at which these decreases occurred were 49 and 169 °C while for **3**, the temperatures were 55 and 170 °C.

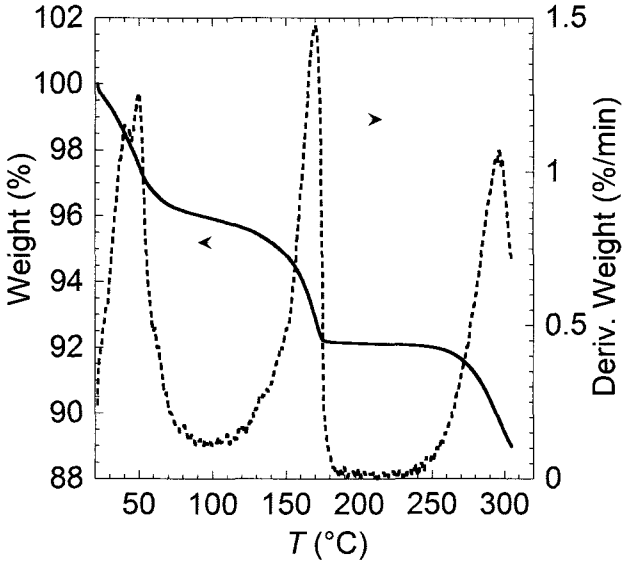

Figure 3.13 Thermogravimetric analyses of **2** measured between 25 and 300 °C at a rate of 10 °C/min under a constant nitrogen flow.

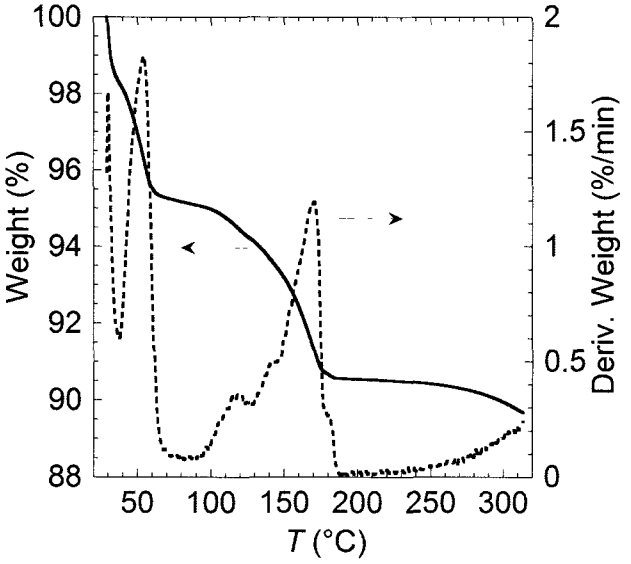

Figure 3.14 Thermogravimetric analyses of **3** measured between 25 and 300 °C at a rate of 10 °C/min under a constant nitrogen flow.

In the case of **4**, the data shown in Figure 3.15 indicated a more gradual loss of the solvent of crystallizations and of the coordinated solvent molecules. At room temperature, the positive derivative was even more pronounced than for the three other complexes. Since the decreases overlapped over each other in the data curve, it was difficult to assess the exact percentage loss for each step. However, at 225 °C, the total percentage loss was 8.2% which corresponded to the loss of one water and six methanol molecules (Calc. 8.1%). When compared to compounds **1**, **2** and **3**, two additional solvent molecules were lost in the heating process. As for the three other compounds, the losses of solvents of crystallization were reversible while the losses of coordinated solvent molecules were irreversible.

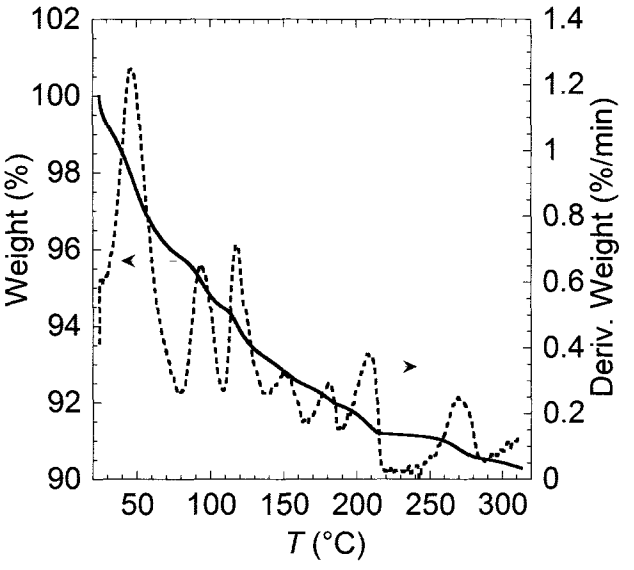

Figure 3.15 Thermogravimetric analyses of **4** measured between 25 and 300 °C at a rate of 10 °C/min under a constant nitrogen flow.

3.5 Magnetic properties

dc susceptibility measurements of **1** were performed between 1.8 and 300 K under an external dc field of 1000 Oe. The χT *vs* T plot of **1** is shown in Figure 3.16. At room temperature, the χT product was of 10.12 $cm^3 K mol^{-1}$ which was in the range of values expected for three Fe^{II} HS ions. Upon cooling, the compound presented a gradual spin transition with a $T_{1/2}$ of 148 K. The data then reached a plateau at approximately 100 K before decreasing again down to the value of 2.25 $cm^3 K mol^{-1}$. The rapid decrease at low temperature can be attributed to either the presence of magnetic anisotropy in the complex or to weak antiferromagnetic interactions between the peripheral metal centres. Due to a combination of both of these factors in these trinuclear units, their respective contribution could not be determined.

As mentioned in section 3.3, ligand-field strength considerations suggested that two different SCO behaviours are expected for the trinuclear molecules; one for the central

Fe^{II} ion coordinated to six ligands and one for the peripheral ion coordinated to three solvent molecules and three ligands. At 100 K, the χT product was of 7.71 $cm^3 K mol^{-1}$, which was higher than the range of values expected for two HS Fe^{II} ions linked through one LS Fe^{II} ion. This larger value was consistent with a spin transition where some of the central ions are trapped in the HS state, as expected for a gradual SCO. As described in the literature, the gradual SCO behaviour is associated with an absence of cooperative interactions between the molecular units in the crystal lattice. Such an observation was depicted in section 3.3. Furthermore, a large separation between the trinuclear units was also observed, which supported 1) the absence of intermolecular interactions between the units, 2) the gradual behaviour of the spin transition and 3) the absence of long-range magnetic ordering at low temperature.

These observations were consistent with the previously reported data for similar trinuclear units. In the cases where large distances between the species were observed in the crystal lattice, gradual SCOs were denoted. The opposite observation was presented when smaller distances where in hand. Usually, the large separations between the units were attributed to either the bulkiness of the ligands or to the bulkiness of the counter anions. The bulkier these were, the larger was the distance separating the units. In addition, a similar behaviour was denoted for triazole-based 1-D chains for which the size of the substituting functional group played an important role in the nature of the SCO behaviour.

The crossover temperature ($T_{1/2}$) for similar trinuclear complexes have been reported to vary between 180 K and 300 K depending on the size of the substituting functional group and on the nature of the counter anion. For **1**, the crossover temperature was of 148 K which was slightly lower than those observed for other trinuclear linear units. In the case where 4-methoxyphenyl was the substituting group, the crossover temperature was of 245 K. For this compound, the higher crossover temperature was attributed to an electron-donating effect from the *trans*-methoxy to the triazolyl group through aromatic conjugation between the two rings. Based on the ligand-field theory, we believed that the lower transition temperature was caused by an electron-withdrawing effect from the nitro- functionalized aromatic substitution instead of the more common alkyl substitution on the triazole's fourth position.[13]

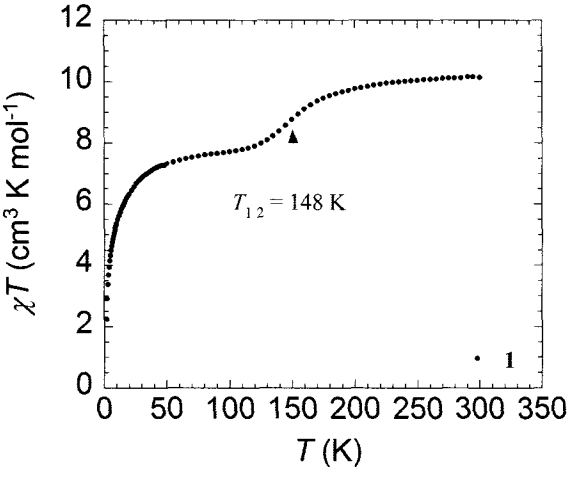

Figure 3.16 The dc susceptibility of **1** measured between 1.8 and 300 K under an applied dc field of 1000 Oe.

For **2** and **3**, the χT *vs* T plots are shown in Figure 3.17 and 3.18, respectively. At room temperature, the χT products were in the range of expected values for three HS Co^{II} ions. Upon cooling, the data decreased steadily down to the values of 2.16 and 1.98 cm^3 K mol^{-1}. At 5 K, the presence of a shoulder in the curve suggested a spin ground state of 3/2 for

either of the compounds, which was not confirmed due to the presence of magnetic anisotropy and/or intermolecular antiferromagnetic interactions at low temperature.

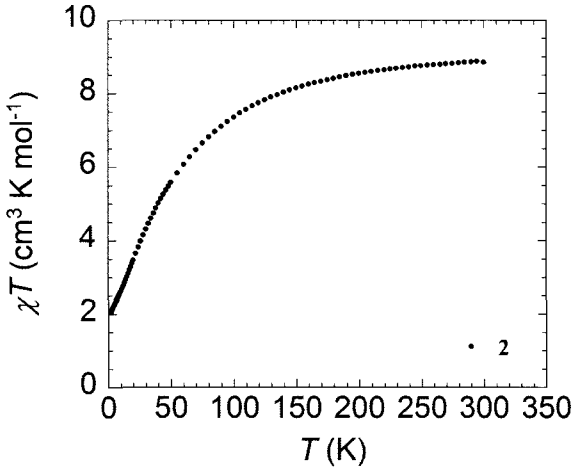

Figure 3.17 The dc susceptibility of **2** measured between 1.8 and 300 K under an applied dc field of 1000 Oe.

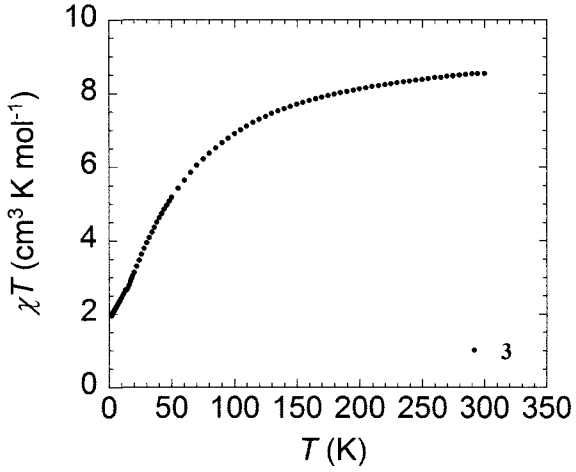

Figure 3.18 The dc susceptibility of **3** measured between 1.8 and 300 K under an applied dc field of 1000 Oe.

The dc susceptibility data for complex **4** is shown in Figure 3.19. At room temperature, the χT product was lower than the expected Curie constant of 3.36 cm^3 K mol^{-1} for three non-interacting Ni^{II} ions (Ni^{II} S = 1: g ~ 2.12, C = 1.12 cm^3 K mol^{-1}). Upon cooling, the data decreased down to the value of 1.15 cm^3 K mol^{-1} at 5 K, which indicated a spin ground state of S = 1. This decrease could be due to the presence of antiferromagnetic

interactions between the peripheral ions and the central ion. Below that temperature, the data further decreased down to the value of 0.56 $cm^3 K mol^{-1}$ at 1.8 K. Above 15 K, the data was well fitted to a Heisenberg model for a linear trinuclear HS Ni^{II} system (Equations 3.2 and Equation A1 in the annex), which resulted in the following fitting parameters: g = 2.116(2), J_1 = -8.5(1) cm^{-1}. In this case, the interaction between the peripheral units (J_2) was approximated to be 0 cm^{-1} in respect to the linear model.

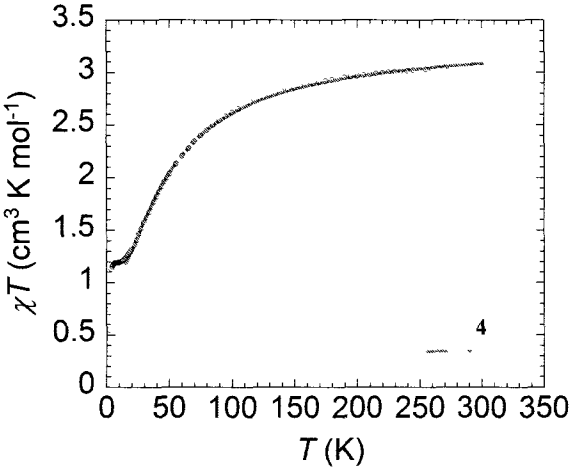

Figure 3.19 The dc susceptibility of **4** from 1.8 to 300 K under an applied dc field of 1000 Oe and fitting of the data, resulting in the following parameters: g = 2.116(2), J_1 = -8.5(1) cm^{-1} and J_2 ~ 0 cm^{-1}.

$$H = -2J_1\left[\hat{S}_1\hat{S}_2 + \hat{S}_2\hat{S}_3\right] - 2J_2\hat{S}_1\hat{S}_3 \qquad (3.2)$$

The field dependence of the magnetization of **1**, **2**, **3** and **4** was measured at 1.8, 3, 5 and 8 K between 0 and 7 T. For **1**, **2** and **3**, the data is presented in Figures A2, A3 and A4 in the annex while the data for **4** is shown in Figure 3.20. For the three former complexes, the magnetization data increased quickly below 1 T and then slowly to reach non saturated maximum values of 6.18, 2.85 and 2.63 μ_B at 1.8 K and 7 T for **1**, **2** and **3**, respectively. The absence of saturation in each three cases suggested the presence of significant magnetic anisotropy and/or the presence of low lying excited states. For **4**, the

data measured at 3 K increased slowly below 1 T to reach a saturation value of 2.00 μ_B at 7 T, which was consistent with a spin ground state of S = 1.

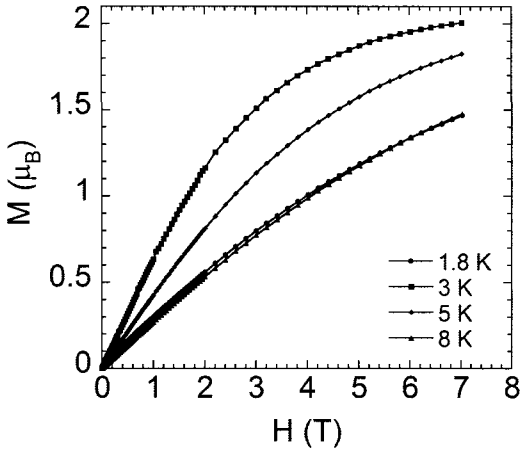

Figure 3.20 Field dependence of the magnetization of **4** at 1.8 (circles), 3 (squares), 5 (diamonds) and 8 K (triangles) measured between 0 and 7 T.

3.6 References

[1] M. Thomann, O. Kahn, J. Guilhem and F. Varret, *Inorg. Chem.*, **1994**, *33*, 6029

[2] G. Vos, R. A. G. De Graaff, J. G. Haasnoot, A. M. Kraan, P. Vaal and J. Reedijk, *Inorg. Chem.*, **1984**, *23*, 2905

[3] P. Gütlich and H. A. Goodwin, "Spin Crossover in Transition Metal Compounds", *Springler*, Berlin, **2004**

[4] R.-Q. Zoua, L.-Z. Caia and G.-C. Guo, *J. Mol. Struct.*, **2005**, *737*, 125

[5] L. V. Lukashuk, A. B. Lysenko, E. B. Rusanov, A. N. Chernegab and K. V. Domasevitch, *Acta Cryst.*, **2007**, *C63*, m140

[6] D. Savard, P.-H. Lin, T. J. Burchell, W. Wernsdorfer, R. Clérac and M. Murugesu, *Inorg. Chem.*, **2009**, *48*, 11748

[7] R. Janes and E. A. Moore, "Metal-ligand bonding", *Royal Society of Chemistry*, Cambridge, **2004**, 130 pages

[8] K. Yoshizawa, H. Miyajima and T. Yamabe, *J. Phys. Chem. B*, **1997**, *101*, 4383

[9] Y. Garcia, P. Guionneau, G. Bravic, D. Chasseau, J. A. K. Howard, O. Kahn, V. Ksenofontov, S. Reiman and P. Gütlich, *Eur. J. Inorg. Chem.*, **2000**, 1531

[10] J. Li, R. L. Lord, B. C. Noll, M.-H. Baik, C. E. Schulz and W. R. Scheidt, *Angew. Chem. Int. Ed.*, **2008**, *47*, 10144

[11] T. Kosone, I. Tomori, C. Kanadani, T. Saito, T. Mochida and T. Kitazawa, *Dalton Trans.*, **2010**, *39*, 1719

[12] K. Yoshizawa, H. Miyajima and T. Yamabe, *J. Phys. Chem. B*, **1997**, *101*, 4383

[13] A. Hauser, *Adv. Polym. Sci.*, **2004**, 23349

Chapter 4. Lanthanide-only Cubane-Shaped Dumbbells

4.1 Cubane Single-Molecule Magnets (SMMs)

The current major interest of the scientific community in the field of molecular magnetism is the formation of novel SMMs that will lead to higher energy barriers, and thus the potential usage of SMMs in high capacity data storage devices. To date, first-row transition metal complexes with cubane topologies have been extensively studied for their unique SMMs properties.[1-9] It has been previously demonstrated that reacting lanthanide precursor salts with carboxylic acid derivatives leads to cubane-shaped lanthanide-only complexes.[10-13] As mentioned in section 1.2, lanthanide ions possess an intrinsic anisotropy and a large spin ground state. Hence, we believed that reacting such salts with the Hcpt ligand could lead to the formation of a novel cubane complex with a high energy barrier. Furthermore, the ligand Hcpt have been known to exhibit electrostatic interactions or π-π stacking with similar moieties. We believed that using this ligand could lead to the formation of a supramolecular array of SMMs, which would allow scientists to characterize the exact nature of the SMM phenomenon.

The ligand, Hcpt, was chosen because it possesses two asymmetrical coordination sites, which favour the formation of complexes with unique topologies, and a rigid backbone, which supports the formation of Metal-Organic Frameworks (MOFs). Based on the hard-soft/acid-based concept,[14] it is well established that the hard lanthanide ions prefer to coordinate to acidic carboxylate functional groups instead of basic triazolyl groups. For the purpose of this research, we believed that the weakly coordinating triazolyl group of

the Hcpt ligand would promote electrostatic interactions between the ligands and thus improve the supramolecular arrangement of the molecules in the crystal lattice.

4.2 Synthesis of the complexes

In order to synthesize a novel lanthanide-only SMM, we decided to explore the reaction of the Hcpt ligand with various lanthanide precursor salts. The treatment of lanthanide trichloride or trinitrate hydrates with Hcpt in the presence of NaN_3 in a 2:1:2 molar ratio in 25 mL of a 5:1 mixture of methanol and DMF yielded compounds **5**, **6** and **7** for the lanthanides Dy^{III}, Ho^{III} and Tb^{III}, respectively. The chemical equation for the formation of the cubane clusters is summarized in Equation 4.1.

$$12\text{Hcpt} + 8\text{LnCl}_3\cdot 6\text{H}_2\text{O} \xrightarrow[\text{MeOH / DMF}]{} [\text{Ln}^{\text{III}}_4(\mu_3\text{-OH})_2(\mu_3\text{-O})_2(\text{cpt})_6(\text{MeOH})_6(\text{H}_2\text{O})_2]_2\cdot x(\text{MeOH}) \quad (4.1)$$

In these reactions, the sodium azide employed did not coordinate to the lanthanide ions. However, the azide salt acted as a mild base in order to deprotonate the Hcpt ligand. When stronger bases were used, the compounds usually precipitated very quickly, which was resulting in polycrystalline powders unsuitable for Single-Crystal X-ray Diffraction (SC-XRD). Using the exact 4:3 ligand-to-metal ratio was also resulting in such powders. A ligand-to-metal ratio of 2:1 and a cosolvent, namely dimethylformamide (DMF), were used in the reaction mixture in order to promote the crystallization of the complexes and to increase the solubility of the Hcpt ligand in the reaction mixture. In the absence of

DMF, the compounds were precipitating very quickly resulting in polycrystalline powders.

4.3 Structural analyses

Structural analyses of **5** revealed that the compound was composed of a tetranuclear cubane complex, $\{Dy_4\}$, that crystallized in its dimeric form, $\{Dy_4\}_2$. The dimeric molecular structure of **5** is shown in Figure 4.1. For complexes **6** and **7**, unit cell measurements and intensity data collections were carried out. From the collected data, the atoms connectivity was obtained, which confirmed that the complexes were isomorphous to **5**. However, due to the poor diffraction of the crystals, both structures could not be refined with acceptable R1 factors.

For **5**, the complex was composed of two cubane units, $\{Dy^{III}_4(\mu_3\text{-}O)_2(\mu_3\text{-}OH)_2\}^{6+}$, where each moiety was encapsulated by six carboxylate groups from the cpt$^-$ ligand. Two of the ligands linked the cubane moieties through coordination of the 1,2,4-triazolyl functional group to the Dy1 ion to form the dimeric cubane-shaped dumbbell complex. A fully labeled view of the core of **5** is shown in Figure 4.2 while the selected bond distances and angles are shown in Table 4.1. The core of the cubane units were composed of four Dy^{III} ions, two μ_3-O and two μ_3-OH. On average, the bond distances between O13 and O15 and their respective Dy^{III} ions, except between O15 and Dy1, were of 2.40(2) Å while the bond distances between O14 and O16 and their respective ions were of approximately 2.35(2) Å. These differences in the bond distances suggested that the cubane structure was most likely composed of two μ_3-hydroxides (O13 and O15) and two μ_3-oxides (O14

and O16). We believed that these differences in the bond distances were the cause of the asymmetrical distortion of the cubane core. It is noteworthy to mention that there was an absence of counter anions in the crystal lattice. Hence, the +3 oxidation states of the dysprosium ions were determined by charge considerations.

Table 4.1 Selected bond distances (Å) and angles (°) of **5**.

Bond distances (Å)		**Angles (°)**	
Dy1-O15	2.31(1)	Dy1-O13-Dy2	107.3(4)
Dy1-O14	2.35(1)	Dy1-O14-Dy2	108.9(5)
Dy1-O13	2.41(1)	Dy1-O15-Dy3	107.8(4)
Dy1-N12	2.77(2)	Dy1-O13-Dy3	105.1(4)
Dy2-O14	2.37(1)	Dy1-O15-Dy4	105.8(4)
Dy2-O13	2.36(1)	Dy1-O14-Dy4	104.8(4)
Dy2-O16	2.33(1)	Dy2-O13-Dy3	104.5(4)
Dy3-O16	2.36(1)	Dy2-O16-Dy3	106.4(5)
Dy3-O15	2.40(1)	Dy2-O14-Dy4	103.7(4)
Dy3-O13	2.39(1)	Dy2-O16-Dy4	106.6(5)
Dy4-O15	2.41(1)	Dy3-O15-Dy4	103.9(4)
Dy4-O16	2.34(1)	Dy3-O16-Dy4	107.4(5)
Dy4-O14	2.39(1)		

Each Dy^{III} ion was eight coordinated to three ligands, three μ_3 bridging units and two solvent molecules, or, in the case of Dy1, one solvent molecule and one coordinating triazolyl functional group from the symmetrical cubane moiety. This unique symmetrical coordination of the 1,2,4-triazolyl functional group of two of the ligands led to the formation of the dumbbell-shaped octanuclear complex, $\{Dy_4\}_2$. The coordination distance of the triazolyl nitrogen atom to the Dy1 atom was of 2.77(2) Å while the average Dy^{III}-N coordination distance is usually closer to 2.5 Å. Furthermore, the bond distances between non coordinated electrostatically interacting ligands and the cubane core were of approximately 4.63(1) Å. The combination of these two factors suggested a weak coordination strength for the ligands forming the $\{Dy_4\}_2$ dimer. We believed that the delocalization of the electron density of the triazolyl functional group towards the phenyl aromatic ring and the coordinated carboxylate functional group could have been

the cause of this weak coordination and of the presence of electrostatic interactions between the bridging ligands. The presence of this weak coordination was further supported by the fact that the bridging ligands had dihedral angles of 45.6(1) °, which was larger than the free ligand's dihedral angle of 33.5 ° (see section 2.3).

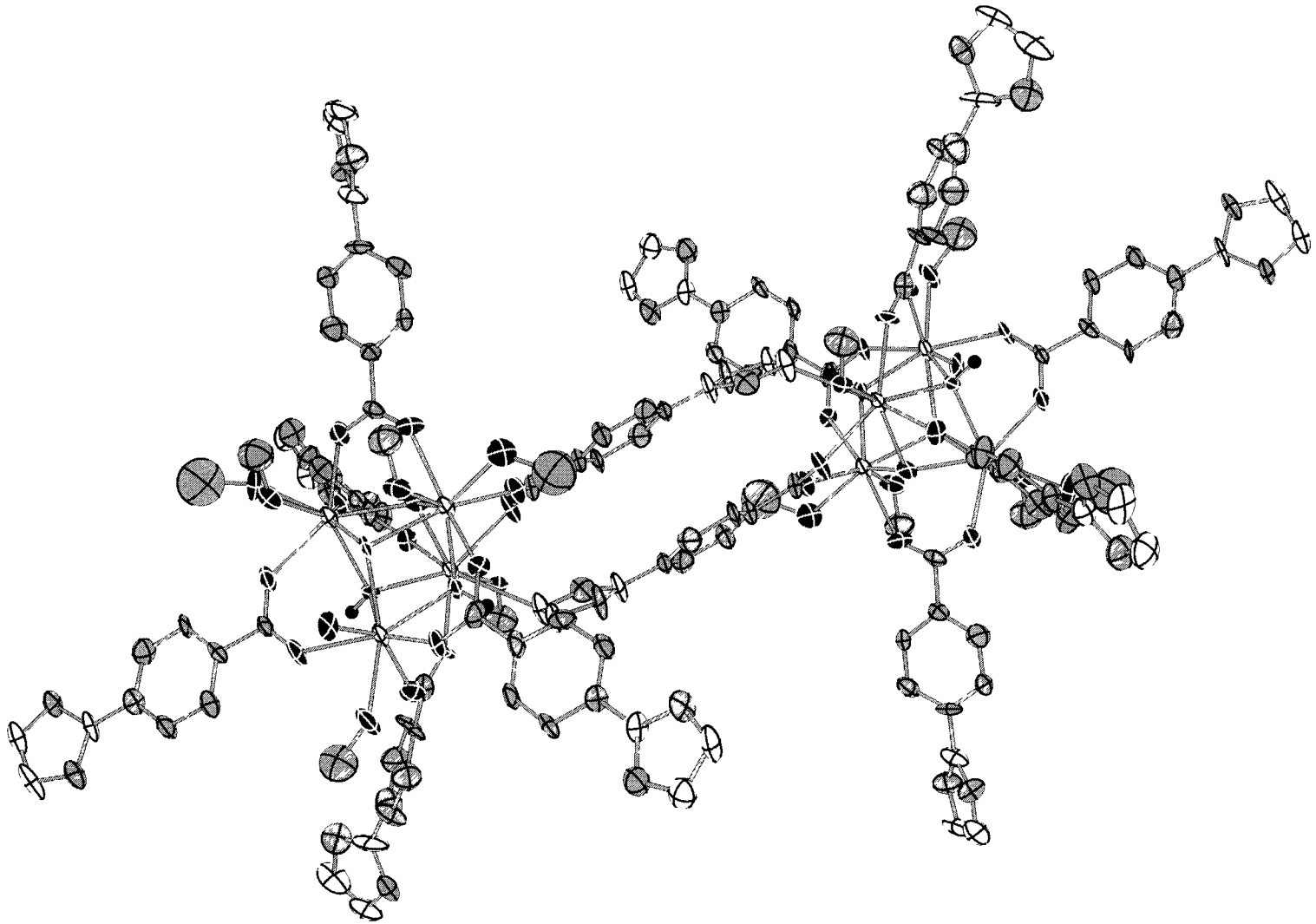

Figure 4.1 The molecular structure of **5**. Thermal ellipsoids are set at 50% probability. The hydrogen atoms and the solvent molecules are omitted for clarity Colour code: White (Dy), Black (O), Light Grey (N), Grey (C), and Black (H)

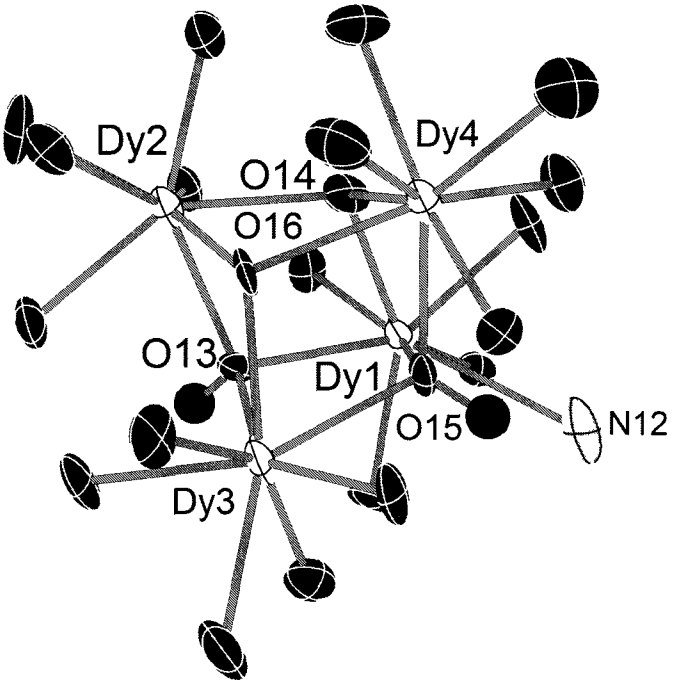

Figure 4.2 Ellipsoidal representation of the cubane core of **5** at 50% probability. Colour code: White (Dy^{III}), Black (O), Light Grey (N), Black (H).

The packing arrangement of **5** viewed along the *ab* plane is shown in Figure 4.3. The molecular $\{Dy_4\}_2$ moieties were organized in a 2-D sheet through electrostatic interactions of their equatorial ligands. We believed that the coordination of the carboxylate functional group to the Dy^{III} ions decreased the electron density located at the carboxylate end of the ligand and that the electron density located on the triazole aromatic ring was increased due to the delocalization of the π-nitrogen electrons in the aromatic system. Hence, we though that these two combined effects favoured the presence of electrostatics interactions between the ligands and the formation of the observed 2-D arrangement of the dumbbell-shaped species. For **5**, the equatorial spaces between the ligands, for which the distances and angles are described in Scheme 4.1, was occupied by four methanol molecules and two axial sheets' ligands.

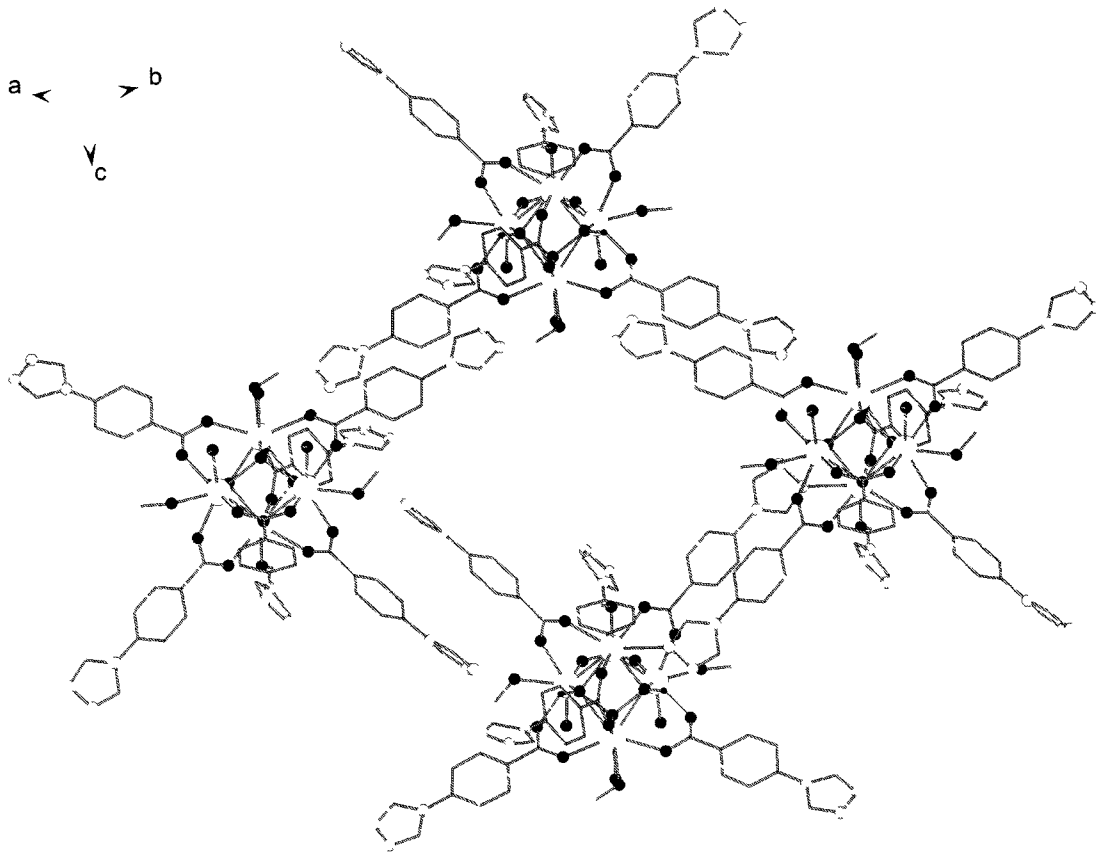

Figure 4.3 The packing diagram of **5** viewed along the *ab* plane. The hydrogen atoms, except for the core hydrogen atoms, and the solvent molecules are omitted for clarity. Color code: White (Dy), Black (O), Light Grey (N), Grey (C), Black (H).

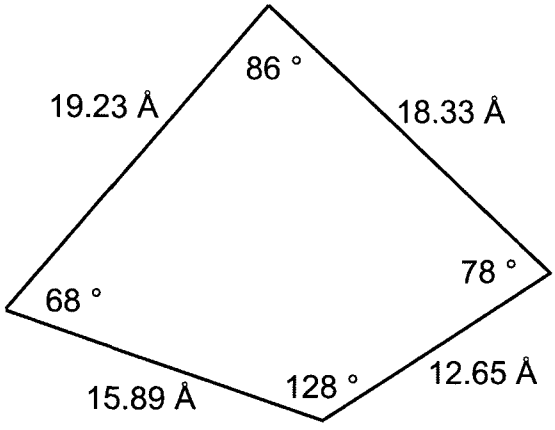

Scheme 4.1 Drawing of the quadrilateral space between the $\{Dy^{III}_4\}_2$ dumbbell units in the crystal lattice describing its edge distances (Å) and angles (°).

4.4 Magnetic properties

dc susceptibility measurements of **5**, which are shown in Figure 4.4, were performed on a polycrystalline sample between 1.8 and 300 K under an external field of 1000 Oe. At room temperature, the χT product was of 55.7 cm^3 K mol^{-1} which was close to the expected Curie constant[15] of 56.7 cm^3 K mol^{-1} for four non interacting Dy^{III} ions (Dy^{III}: S = 5/2, L = 5, g = 4/3, and C = 14.17 cm^3 K mol^{-1}). Upon cooling, the data slowly decreased to reach the minimal value of 33.1 cm^3 K mol^{-1} at 1.8 K. The declining χT product could be explained by three factors: 1) the presence of antiferromagnetic interactions between the lanthanide ions of the cubane core, 2) the depopulation of the ground-state Dy^{III} sublevels that result from spin-orbit coupling and a low symmetry crystal field or 3) magnetic anisotropy. Due to the combination of all these effects in these tetranuclear complexes, it was difficult to quantify the contribution of each factor.

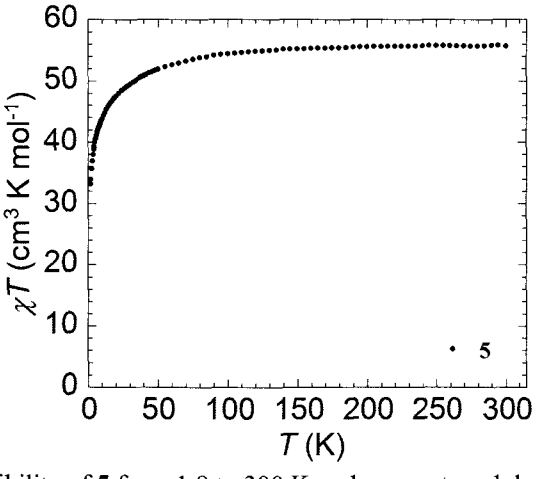

Figure 4.4 The dc susceptibility of **5** from 1.8 to 300 K under an external dc-applied field of 1000 Oe.

dc susceptibility measurements were also performed on samples of **6** and **7**, which exhibited a similar behaviour upon cooling. The data for these two compounds is shown in Figure 4.5 and 4.6. At room temperature, the χT products were of 54.2 and 46.5 cm^3 K

mol^{-1}, which were close to the expected Curie constants of 56.3 and 47.3 cm^3 K mol^{-1} at for four non interacting ions (Ho^{III}: $S = 2$, $L = 6$, $g = 5/4$, and $C = 14.08$ cm^3 K mol^{-1}, Tb^{III}: $S = 3$, $L = 3$, $g = 3/2$, and $C = 11.82$ cm^3 K mol^{-1}).

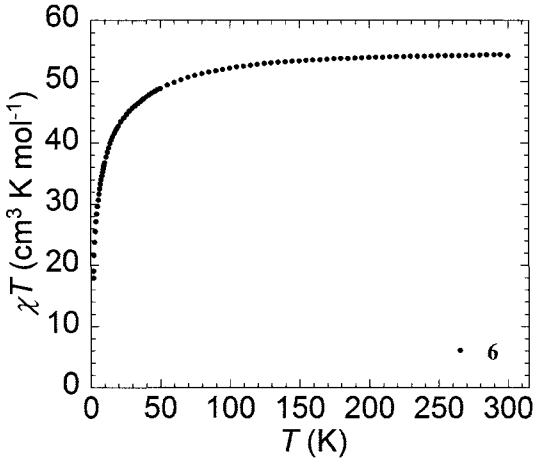

Figure 4.5 The dc susceptibility of **6** from 1.8 to 300 K under an external dc-applied field of 1000 Oe.

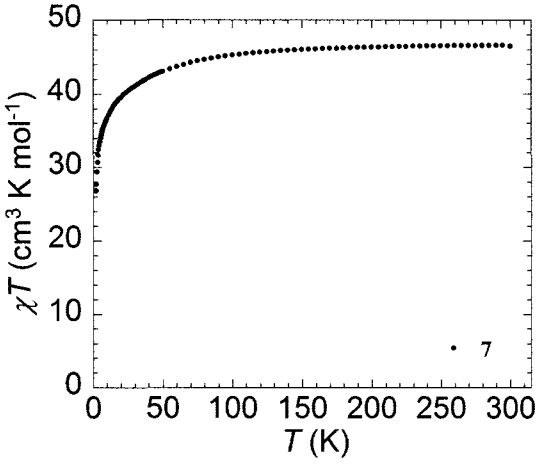

Figure 4.6 The dc susceptibility of **7** from 1.8 to 300 K under an external dc-applied field of 1 000 Oe.

For **5**, the field dependence of the magnetization between 1.8 and 8 K, shown in Figure 4.7, revealed an absence of saturation under large dc-applied fields. At 1.8 K and above 1 T, the magnetization increased slowly to reach a non-saturated value of 22.7 μ_B at 7 T. This lack of saturation is either indicative of the presence of magnetic anisotropy and/or

the presence of low lying excited state, which is in agreement with the dc susceptibility data described above. For **6** and **7**, the data, which is shown in Figure A5 and A6 in the annex, respectively, presented a similar behaviour; the magnetization value increased slowly to reach unsaturated values of 22.8 and 19.8 μ_β, respectively, at 1.8 K and under a field of 7 T.

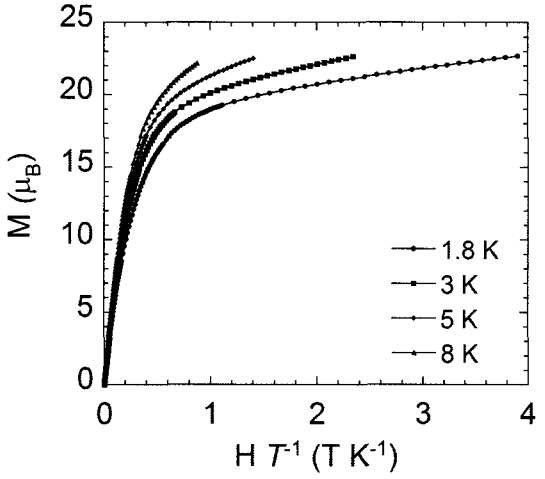

Figure 4.7 Field dependence of the magnetization of **5** measured at 1.8 (circles), 3 (squares), 5 (diamonds) and 8 K (triangles) between 0 and 7 T.

The temperature dependencies of the ac susceptibility were measured for all three complexes under an ac field of 3 Oe oscillating with frequencies ranging between 10 and 1500 Hz. For **6** and **7**, no out-of-phase susceptibility signals were observed at 1.8 K. For **5** (Figure 4.8), upon cooling, a frequency-dependent increment of the out-of-phase component was denoted. The data reached a maximum value of 1.5 $cm^3 mol^{-1}$ at 1.8 K and 1500 Hz. This suggested the presence of slow relaxation of the magnetization, which could have been the signature of a SMM behaviour.

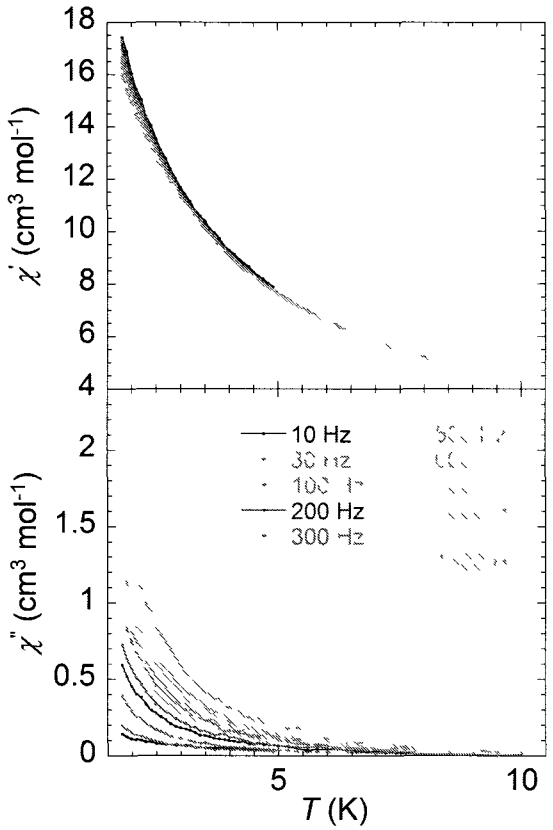

Figure 4.8 Temperature dependence of the in-phase (χ', top) and out-of-phase (χ", bottom) components of the ac susceptibility of **5** using frequencies between 10 and 1500 Hz.

In order to determine the exact nature of the possible SMM behaviour of **5**, field dependence of the magnetization measurements were performed on a single crystal of the complex between 0.04 K and 7 K and under dc applied fields ranging from -1.4 T to 1.4 T on a μ-SQUID apparatus. The measurements were performed by applying the magnetic field along the easy axis of the crystal. At 0.04 K, the complex exhibited a small M_S *vs* H hysteresis loop, which is shown in Figure 4.9. The sweep rate dependency of this hysteresis loop, shown in Figure 4.10, confirmed that **5** exhibited a slow relaxation of the magnetization that is characteristic for SMMs. We believed that the large separation between the tetranuclear units of **5** pointed to an absence of intermolecular magnetic interactions and thus confirmed this SMM behaviour. The occurrence of a step-like

behaviour indicated either the presence of quantum tunneling of the magnetization (QTM) or individual reversal of the magnetization of each Dy^{III} ion. The former is usually observed for polynuclear lanthanide systems. Furthermore, for such complexes, the shape and positioning of the steps usually originates from either the weak exchange interactions and from the orientation of the applied field in relation to the anisotropic plane of the molecule. The small coercivity of the hysteresis loop shown in Figure 4.9 suggested a small effective energy barrier for **5**, the size of which might be caused by the commonly occurring QTM in lanthanide systems.

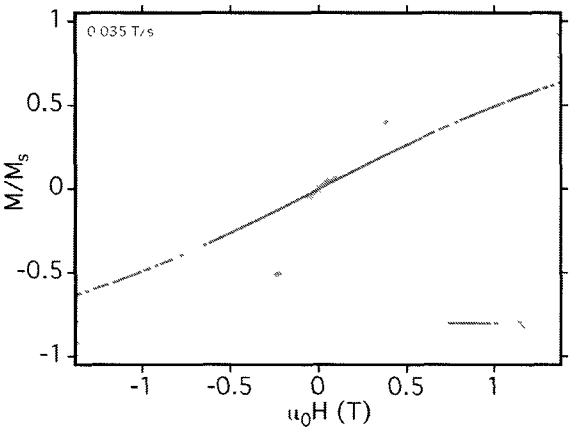

Figure 4.9 Field dependence of the normalized magnetization of **5** between 0.04 K and 7 K under dc-applied fields ranging from -1.5 to 1.5 T, where M_S is the magnetization at saturation.

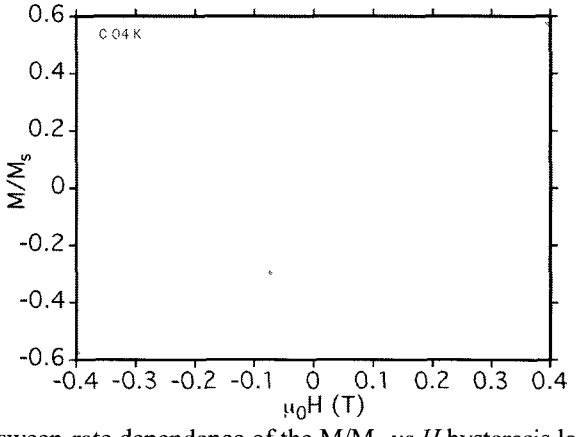

Figure 4.10 Field sweep-rate dependence of the M/M_S *vs H* hysteresis loop for **5** at 0.04 K.

4.5 References

[1] W. Wernsdorfer, N. Aliaga-Alcalde, D. N. Hendrickson and G. Christou, *Nature*, **2002**, *416*, 406

[2] S. M. J. Aubin, N. R. Dilley, L. Pardi, J. Krzystek, M. W. Wemple, L.-C. Brunel, B. M. Maple, G. Christou and D. N. Hendrickson, *J. Am. Chem. Soc.*, **1998**, *120*, 4991

[3] B. Moubaraki, K. S. Murray, T. A. Hudson and R. Robson, *Eur. J. Inorg. Chem.*, **2008**, 4525

[4] P. L. Feng, C. C. Beedle, C. Koo, W. Wernsdorfer, M. Nakano, S. Hill and D. N. Hendrickson, *Inorg. Chem.*, **2008**, *47*, 3188

[5] K. W. Galloway, A. M. Whyte, W. Wernsdorfer, J. Sanchez-Benitez, K. V. Kamenev, A. Parkin, R. D. Peacock and M. Murrie, *Inorg. Chem.*, **2008**, *47*, 7438

[6] P. L. Feng, C. C. Beedle, W. Wernsdorfer, C. Koo, M. Nakano, S. Hill and D. N. Hendrickson, *Inorg. Chem.*, **2007**, *46*, 8126

[7] H. Oshio, N. Hoshino and T. Ito, *J. Am. Chem. Soc.*, **2000**, *122*, 12602

[8] N. Aliaga-Alcalde, R. S. Edwards, S. O. Hill, W. Wernsdorfer, K. Folting and G. Christou, *J. Am. Chem. Soc.*, **2004**, *126*, 12503

[9] S. M. J. Aubin, M. W. Wemple, D. M. Adams, H.-L. Tsai, G. Christou and D. N. Hendrickson, *J. Am. Chem. Soc.*, **1996**, *118*, 7746

[10] B.-Q. Ma, D.-S. Zhang, S. Gao, T.-Z. Jin, C.-H. Yan and G.-X. Xu, *Angew. Chem., Int. Ed.*, **2000**, *39*, 3644

[11] T. Kajiwara, N. Iki and M. Yamashita, *Coord. Chem. Rev.*, **2007**, *251*, 1734

[12] X.-J. Zheng, L.-P. Jin and S. Gao, *Inorg. Chem.*, **2004**, *43*, 1600

[13] R. Wang, H. D. Selby, H. Liu, M. D. Carducci, T. Jin, Z. Zheng, J. W. Anthis and R. J. Staples, *Inorg. Chem.*, **2002**, *41*, 278

[14] X. Gu, D. Xue and H. Ratajczak, *J. Mol. Struct.*, **2008**, *887*, 56 and references cited therein

[15] C. Benelli and D. Gatteschi, *Chem. Rev.*, **2002**, *102*, 2369

Chapter 5. General conclusions and recommendations

The main goal of this work consisted on exploring the chemistry of 4-aryl substituted triazole ligands in the field of molecular magnetism. For the purpose of this research, two ligands, Hcpt and npt, have been synthesized using a modified synthetic strategy in order to ease the purification process and to increase the overall yield of the ligand preparation. Using these ligands, two new complexes presenting unique magnetic properties have been synthesized and characterized.

The first complex consisted of a trinuclear linear Fe^{II} compound, $[Fe^{II}_3(npt)_6(EtOH)_4(H_2O)_2](ptol)_6 \cdot 4(EtOH)$ (**1**). Using similar reaction conditions, three of its Co^{II} (**2** and **3**) and Ni^{II} (**4**) analogues were also synthesized. Structural analyses of these molecules indicated that the complexes were made of two structurally unique metal centres: the central ion and the peripheral ions. In the case of **1**, based on the ligand-field strength theory,[1] this suggested the presence of two distinct SCO behaviours, as expected for such trinuclear linear moieties. To our knowledge, only one other Fe^{II} trinuclear linear complex was previously published using a 4-aryl substituted ligand.[2]

The thermogravimetric analyses performed on compounds **1**, **2**, **3** and **4** revealed that they were subjected to rapid desolvation steps which were taking place between 25 °C and 200 °C. Above 150 °C, these measurements indicated that the complexes were losing two or four coordinated solvent molecules on either of the peripheral ions, and that this desolvation process was irreversible. In the case of **1**, **2** and **3**, we believed that the loss of

these coordinated solvent molecules was leading to five-coordinate peripheral ions and in the case of **4**, to four-coordinate peripheral ions.

The magnetic properties of each of these four complexes were measured. For **4**, the dc susceptibility data was well fitted to a Heisenberg model for a trinuclear linear moiety giving rise to the following fitting parameters: g = 2.116(2), J_1 = -8.5(1) cm^{-1}. J_1 represented the interactions between the central ion and the peripheral ions. The interaction between the two peripheral units (J_2) was approximated to be 0 cm^{-1} in respect to the linear model.

For **1**, the magnetic data revealed that the Fe^{II} complex exhibited a gradual SCO behaviour with a $T_{1/2}$ of 148 K. In this case, structural analyses were performed at 100 and 181 K. The latter measurements, along with the measurement of the magnetic properties, confirmed that the gradual nature of the spin transition was due to the absence of cooperative interactions between the molecules in the crystal lattice. In combination to the previously reported data on similar 1-D chains and trinuclear units,[3-4] these measurements proved that a control over the nature and the crossover temperature of the SCO behaviour can be achieved through ligand design. More specifically, the nitro-functionalization of the 4-aryl substituted 1,2,4-triazole ligand led to a lower crossover temperature and a gradual spin transition, while the methoxy- functionalization led to a higher crossover temperature and an abrupt spin transition. Not only did the measurements presented an insight on the magnetic properties of this complex, but they also provided relevant structural information on such systems which could help guide

researchers towards the design of a trinuclear unit for potential applications in electronic devices. Further work is currently underway in our laboratory to increase the amount of data available on this category of systems using 4-aryl substituted 1,2,4-triazole ligands.

The second complex of interest, $[Dy^{III}_4(\mu_3\text{-}OH)_2(\mu_3\text{-}O)_2(cpt)_6(MeOH)_6(H_2O)]_2 \cdot 15(MeOH)$ (**5**, cpt = 4-(4'-carboxyphenyl)-1,2,4-triazole), consisted of an octanuclear dumbbell-shaped $\{Dy_4\}_2$ compound where two cubane-shaped cores were linked by two bridging ligands. Two isomorphous analogues, namely the Ho^{III} (**6**) and Tb^{III} (**7**) complexes, were also synthesized using similar reaction conditions.

For **5**, the cubane-shaped cores were composed of two μ_3-oxides, two μ_3-hydroxides and four Dy^{III} ions. We believed that the asymmetrical nature of the bridging units of the cubane core caused a denotable structural distortion. In addition, the structural analyses of **5** indicated that the dumbbells were organized in a 2-D sheet due to electrostatic interactions between the equatorial ligands of the molecules. This arrangement of the molecules was similar to those observed for two dimensional MOFs.

The measurement of the magnetic properties of **5** indicated that the compound exhibited slow relaxation of magnetization below 1.8 K. In the literature,[5-8] similar cubane-shaped lanthanide-only complexes did not present SMM behaviour and the absence of the phenomenon was usually attributed to the presence of antiferromagnetic interactions between the ions. For **5**, we believed that the presence of slow relaxation of the magnetization was caused by the distortion of the cubane-shaped core.

It is worth mentioning that the design of the cubane-shaped complex **5** represented a first step towards a novel synthetic strategy based on supramolecular interactions between the ligands in order to organize and isolate SMMs in multidimensional environments. Further research is currently being done in our laboratory in order to increase the distortion of the cubane-shaped core, which would result in an improved SMM behaviour for the complex.

5.1 References

[1] A. Hauser, *Adv. Polym. Sci.*, **2004**, 23349

[2] M. Thomann, O. Kahn, J. Guilhem and F. Varret, *Inorg. Chem.*, **1994**, *33*, 6029

[3] G. Vos, R. A. G. De Graaff, J. G. Haasnoot, A. M. Kraan, P. Vaal and J. Reedijk, *Inorg. Chem.*, **1984**, *23*, 2905

[4] P. Gütlich and H. A. Goodwin, "Spin Crossover in Transition Metal Compounds", *Springler*, Berlin, **2004**

[5] B.-Q. Ma, D.-S. Zhang, S. Gao, T.-Z. Jin, C.-H. Yan and G.-X. Xu, *Angew. Chem., Int. Ed.*, **2000**, *39*, 3644

[6] T. Kajiwara, N. Iki and M. Yamashita, *Coord. Chem. Rev.*, **2007**, *251*, 1734

[7] X.-J. Zheng, L.-P. Jin and S. Gao, *Inorg. Chem.*, **2004**, *43*, 1600

[8] R. Wang, H. D. Selby, H. Liu, M. D. Carducci, T. Jin, Z. Zheng, J. W. Anthis and R. J. Staples, *Inorg. Chem.*, **2002**, *41*, 278

Chapter 6. Experimental methods

6.1 Ligand syntheses

6.1.1 4-(4'-carboxyphenyl)-1,2,4-triazole (Hcpt)

The ligand, 4-(4'-carboxyphenyl)-1,2,4-triazole (Hcpt), was synthesized according to a modified known procedure.[1] The intermediate, N,N'-diformylhydrazine, was prepared by heating an ethanolic solution (20 mL) of N-formylhydrazine (0.45 g, 7.5 mmol) and triethylorthoformate (TEOF) (1.87 mL, 11.3 mmol) at 180 °C for five minutes in a Biotage Initiator 60 microwave apparatus. To generate Hcpt, solid 4-aminobenzoic acid (PABA) (1.0 g, 7.5 mmol) was added to the solution and the mixture was heated again at 180 °C at 9 bar of pressure for five minutes with vigorous stirring. As the temperature decreased, the ligand precipitated as a pale-yellow powder, which was centrifuged for 15 minutes at 3000 RPM and dried *in vacuo* for 1 hour. Recrystallization of the ligand was carried out by dissolving the bulk pale-yellow powder in 45 mL of N,N'-dimethylformamide (DMF) at 120 °C for 30 minutes. The solution was then cooled to room temperature and 10 mL of diethyl ether was slowly added to the mixture. The precipitated pale-yellow powder was filtered and colorless needles were obtained from the filtrate after one week without disturbance. Yield = 0.78 g, 55%.

6.1.2 4-(4'-nitrophenyl)-1,2,4-triazole (npt)

The ligand was prepared according to a modified known synthetic strategy[1] by first mixing formylhydrazine (0.90 g, 15 mmol), triethylorthoformate (0.0037 L, 25 mmol) and ethanol (40 mL) in a Synthware Glass high pressure vessel. The solution was stirred

at 180°C for 30 minutes. The latter was cooled down to 60 °C in a warm water bath and 4-nitroaniline (2.1 g, 15 mmol) was slowly added to the solution. Four drops of sulfuric acid were added to the mixture as a catalyst. The mixture was heated again to 180°C for 30 minutes resulting in a dark red solution. Upon cooling, a dark yellow powder precipitated which was filtered, washed with ethanol (3 x 5 mL) and diethyl ether (3 x 5 mL) and dried *in vacuo* for 1 hour. Yield = 1.18 g, 42%.

6.2 Complexes syntheses

6.2.1 $[M^{II}_3(npt)_6(EtOH)_4(H_2O)_2](ptol)_6 \cdot 4(EtOH)$ (1, 2)

The complexes were synthesized by adding 5 mL of an ethanolic solution of $[M(H_2O)_6](ptol)_2$ (0.125 mmol, M = Fe (**1**), Co (**2**)) to a solution of npt (0.047 g, 0.25 mmol) in ethanol (25 mL). The solutions were stirred for 3 minutes at room temperature to obtain a clear solution. Crystallizations of the complexes were performed over a period of six hours to provide light green or light brown plate-like crystals of **1** and **2**, respectively, suitable for Single-Crystal X-ray Diffraction. Yield = 43% (**1**, 0.046 g) and 37% (**2**, 0.040 g), based on the metal salts.

6.2.2 $[M^{II}_3(npt)_6(MeOH)_4(H_2O)_2](ptol)_6 \cdot x(MeOH) \cdot y(H_2O)$ (3, 4)

Compounds **3** and **4** were synthesized by adding a solution of $[M(H_2O)_6](ptol)_2$ (0.125 mmol, M = Co (**3**), Ni (**4**)) in methanol (5 mL) to a solution of npt (0.047 g, 0.25 mmol) in methanol (15 mL). The solutions were stirred at room temperature for 10 minutes. The crystallizations of the complexes were done over two days to provide light brown or

purple plate-like crystals for **3** (x = 4, y =0) and **4** (x = 2, y = 1), respectively. Yield = 13% (**3**, 0.014 g) and 50% (**4**, 0.053 g), based on the metal salts.

6.2.4 $[Ln^{III}_4(\mu_3\text{-}OH)_2(\mu_3\text{-}O)_2(cpt)_6(MeOH)_6(H_2O)]_2 \cdot x(MeOH)$ (6, 7, 8)

The complexes, $[Ln^{III}_4(\mu_3\text{-}OH)_2(\mu_3\text{-}O)_2(cpt)_6(MeOH)_6(H_2O)]_2$ (Ln = Dy (**6**·15MeOH), Ho (**7**·14MeOH), Tb (**8**·18MeOH)), were prepared by slowly adding a solution of NaN_3 (0.016 g, 0.50 mmol) and Hcpt (0.024 g, 0.25 mmol) in DMF (2 mL) and MeOH (3 mL) to a solution of $LnCl_3 \cdot 6H_2O$ (0.25 mmol, Ln = Dy (**6**), Ho (**7**), Tb (**8**)) in MeOH (25 mL). The mixture was stirred for 15 minutes at room temperature and then filtered. The filtrate was left undisturbed for several days to provide plate-like crystals suitable for Single-Crystal X-ray Diffraction. Yields = 0.109 g (**6**, 76.0%), 0.019 g (**7**, 13.1%) and 0.034 g (**8**, 23.3%).

6.3 Infrared spectroscopy

Infrared analyses were obtained by using a Nicolet Nexus 550 FT-IR spectrometer in the 4000-650 cm^{-1} range. The spectra were recorded in the solid state by preparing KBr pellets and are shown below as Figures 6.1 through 6.7.

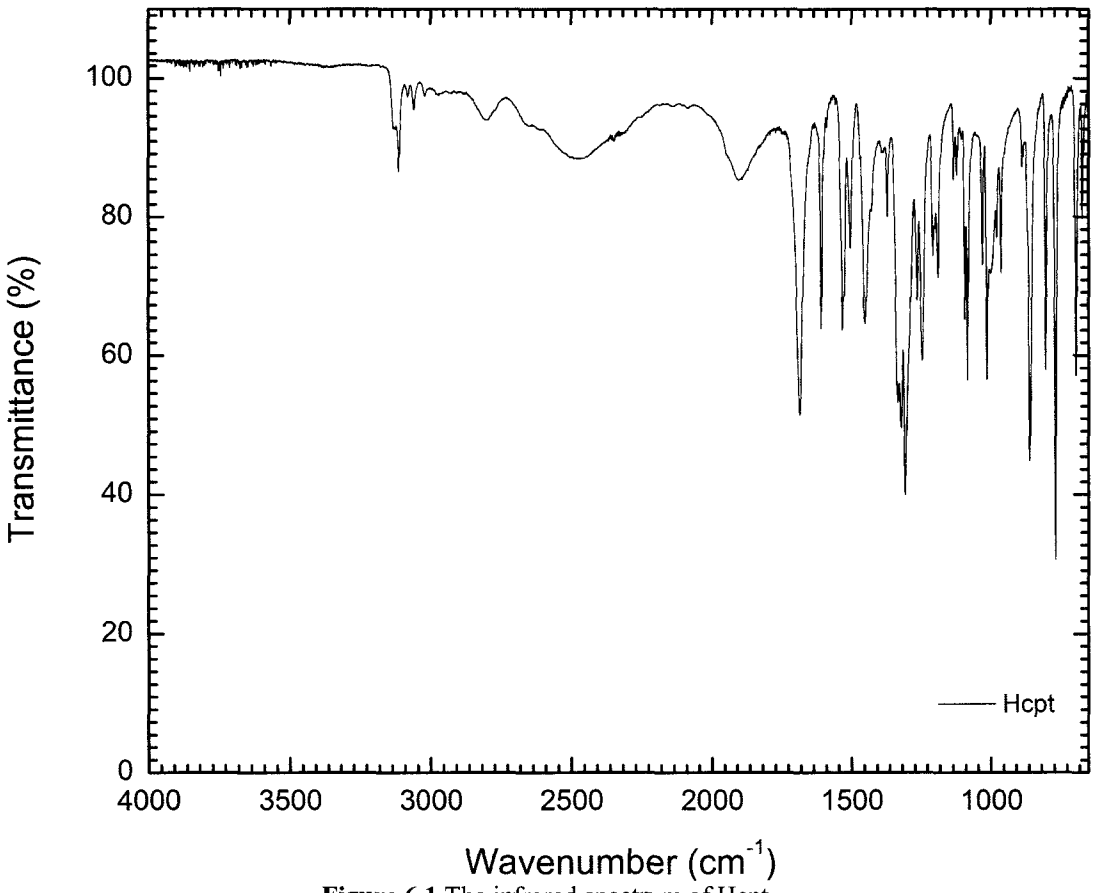

Figure 6.1 The infrared spectrum of Hcpt.

Hcpt (KBr, cm^{-1}): 3462 (br), 3026 (br), 2793 (s), 2501 (br), 1898 (m), 1696 (m), 1607 (m), 1529 (m), 1451 (m), 1373 (s), 1307 (br), 1249 (s), 1214 (s), 1183 (s), 1082 (s), 1016 (s), 868 (s), 771 (s), 694(s).

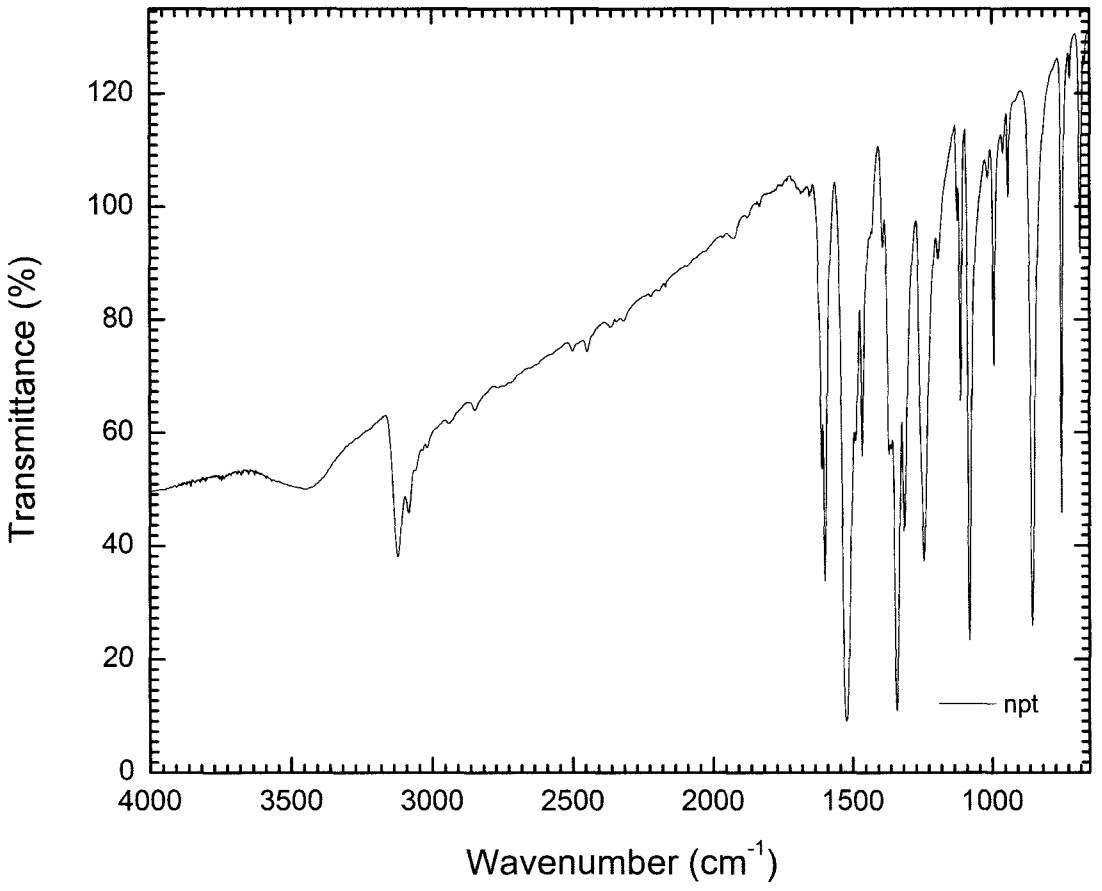

Figure 6.2 The infrared spectrum of npt.

npt (KBr, cm^{-1}): 3444 (br), 3120 (m), 1600 (m), 1528 (m), 1462 (s), 1342 (m), 1311 (s), 1244 (m), 1111 (s), 1080 (m), 991 (s), 848 (s), 751 (s), 680 (s). C,H,N analysis (%) found (calcd for npt): C 50.29 (50.53), H 2.04 (3.18), N 29.27 (29.46).

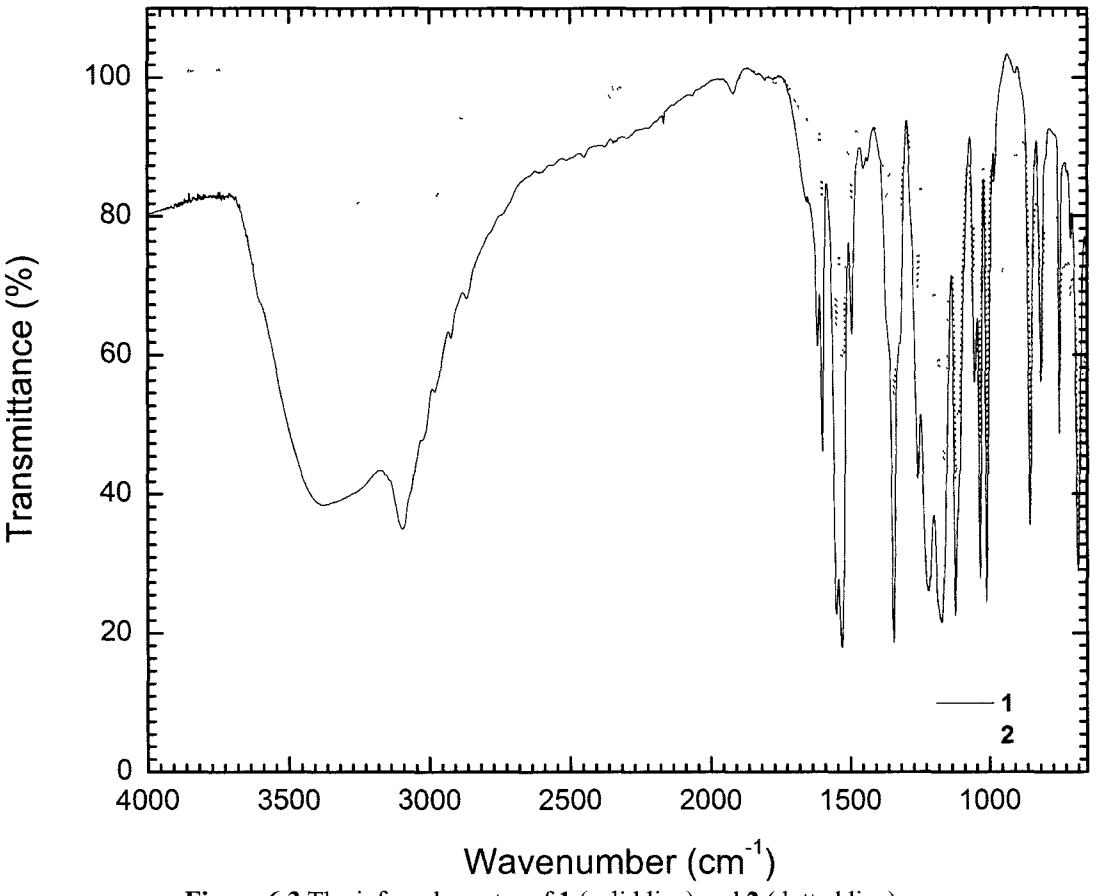

Figure 6.3 The infrared spectra of **1** (solid line) and **2** (dotted line).

1 (KBr, cm^{-1}): 3379 (br), 3097 (w), 1657 (s), 1618 (s), 1600 (s), 1526 (m), 1494 (s), 1441 (s), 1344 (s), 1258 (s), 1218 (s), 1173 (s), 1122 (s), 1051 (s), 1033 (s), 1010 (s), 854 (s), 815 (s), 750 (s), 682 (s).

2 (KBr, cm^{-1}): 3293 (br), 3097 (w), 2970 (s), 1617 (s), 1600 (s), 1531 (m), 1495 (s), 1442 (s), 1343 (s), 1256 (s), 1216 (s), 1164 (s), 1121 (s), 1061 (s), 1033 (s), 1008 (s), 952 (s), 850 (s), 815 (s), 749 (s), 678 (s).

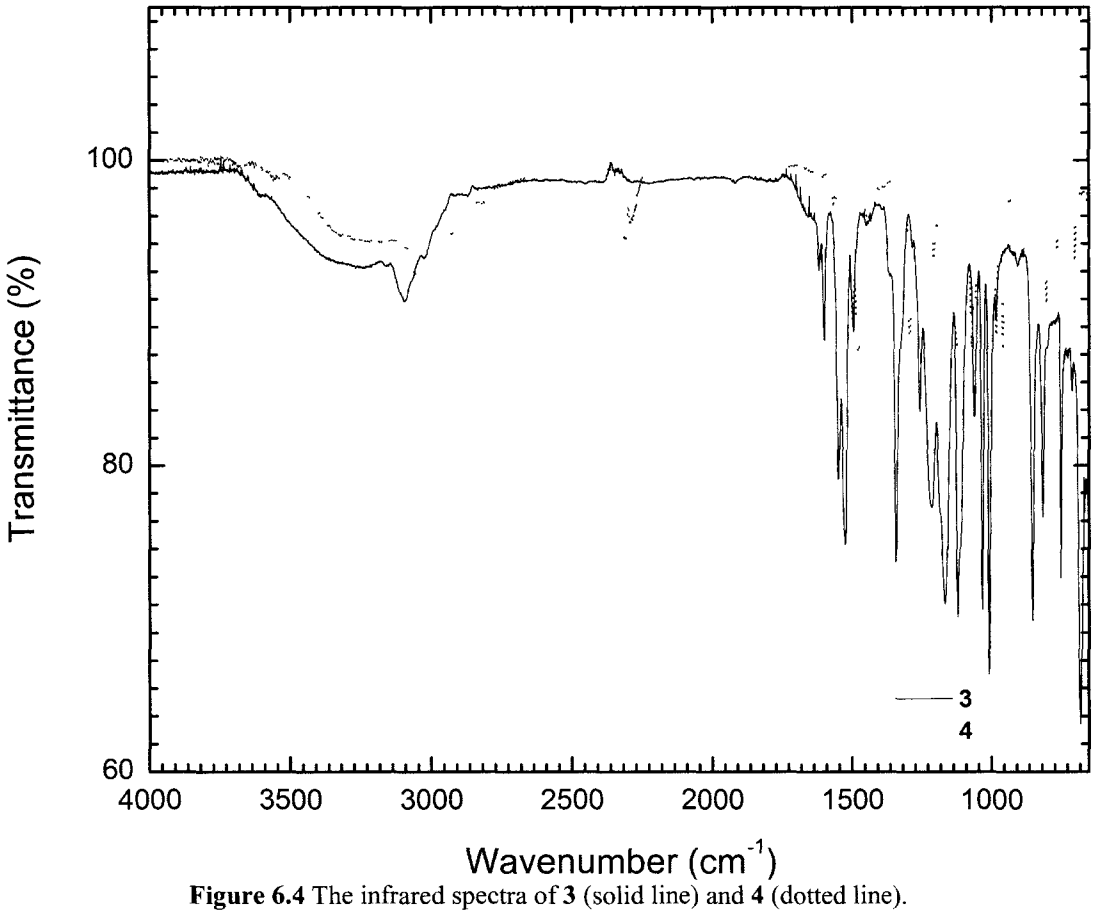

Figure 6.4 The infrared spectra of **3** (solid line) and **4** (dotted line).

3 (KBr, cm^{-1}): 3248 (br), 3097 (w), 1618 (s), 1601 (s), 1550 (s), 1526 (m), 1496 (s), 1343 (s), 1257 (s), 1216 (s), 1167 (S), 1121 (s), 1062 (s), 1033 (s), 1008 (s), 984 (s), 852 (s), 815 (s), 750 (s), 710 (s), 681 (s), 666 (s).

4 (KBr, cm^{-1}): 3249 (br), 3098 (w), 1617 (s), 1601 (s), 1551 (s), 1524 (m), 1496 (s), 1343 (s), 1258 (s), 1229 (s), 1168 (s), 1120 (s), 1069 (s), 1032 (s), 1009 (s), 985 (s), 852 (s), 815 (s), 750 (s), 710 (s), 679 (s), 653 (s).

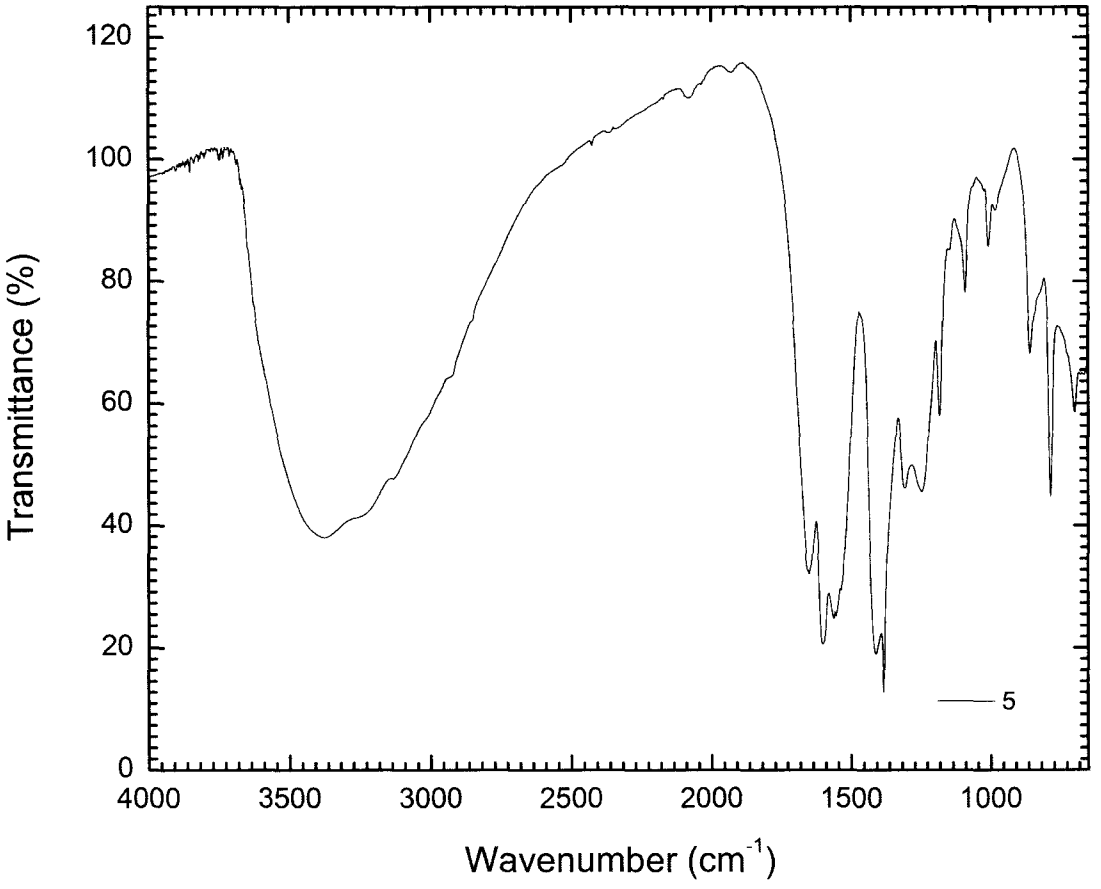

Figure 6.5 The infrared spectrum of **5**.

5 (KBr, cm^{-1}): 3451 (br), 1641 (m), 1600 (m), 1563 (m), 1522 (m), 1409 (m), 1375 (s), 1310 (s), 1243 (s), 1109 (s), 1093 (s), 865 (s), 777 (s), 689 (s).

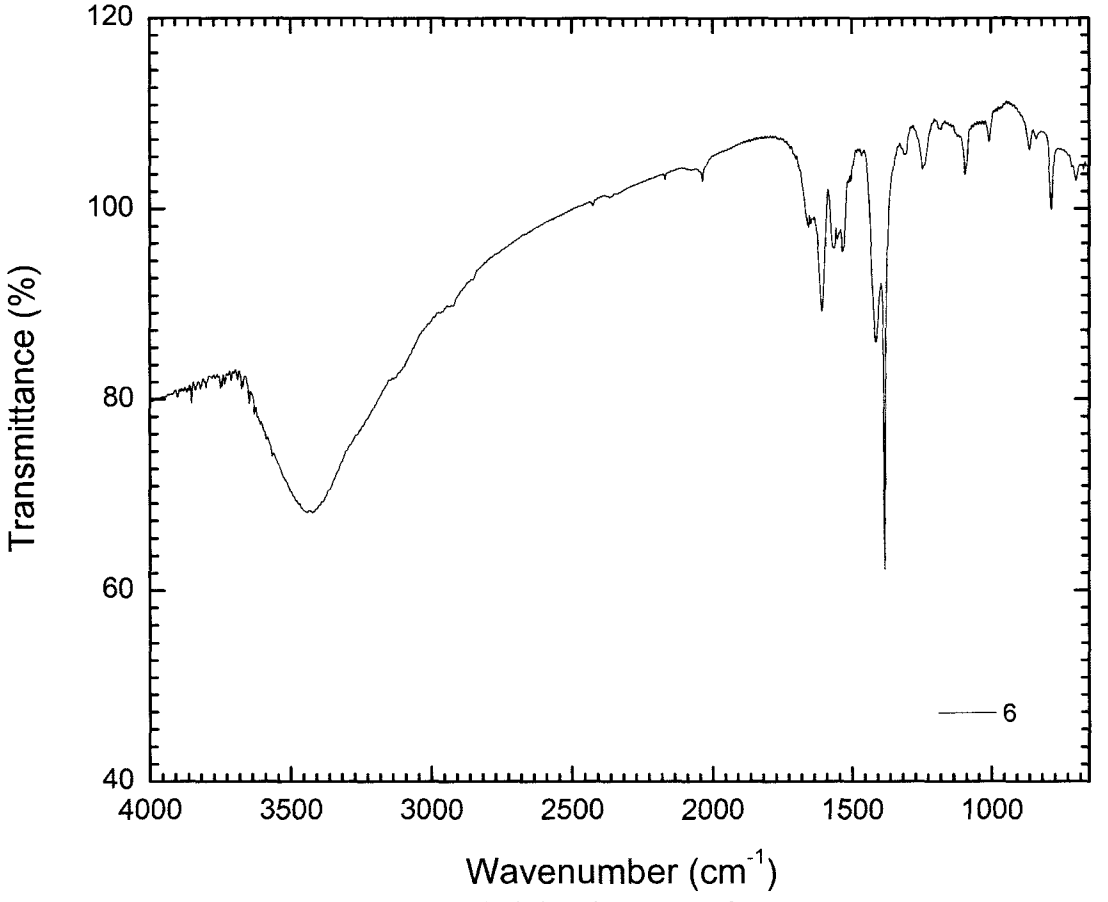

Figure 6.6 The infrared spectrum of **6**.

6 (KBr, cm^{-1}): 3441 (br), 1651 (m), 1605 (m), 1563 (m), 1528 (m), 1413 (m), 1384 (s), 1307 (s), 1244 (s), 1091 (s), 1006 (s), 865 (s), 789 (s), 699 (s).

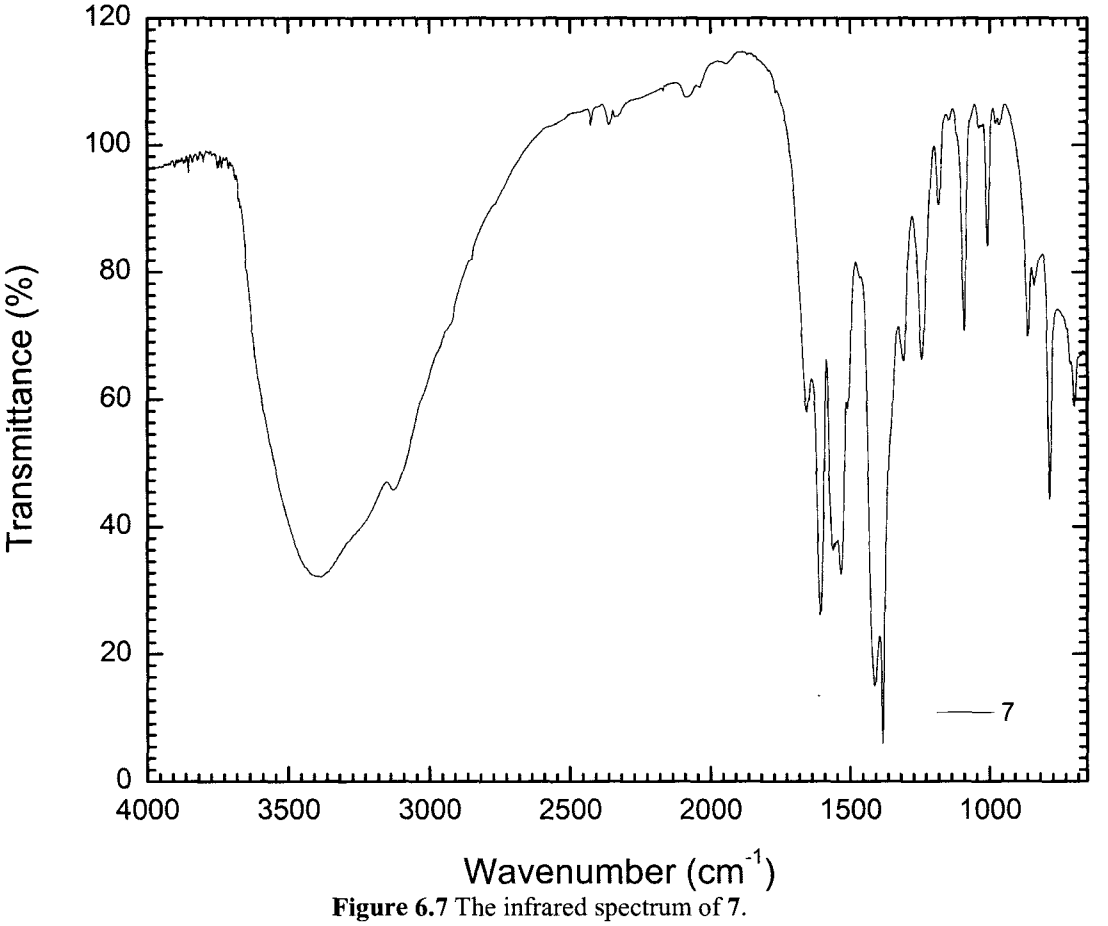

Figure 6.7 The infrared spectrum of **7**.

7 (KBr, cm^{-1}): 3436 (br), 1651 (m), 1605 (m), 1563 (m), 1532 (m), 1413 (m), 1310 (s), 1377 (s), 1243 (s), 1093 (s), 1005 (s), 865 (s), 787 (s), 705 (s).

6.4 NMR spectroscopy

NMR analyses were conducted on a Bruker Avance 400 spectrometer equipped with an automatic sample holder and a 5 mm auto-tuning broadband probe with Z gradient. The spectra of Hcpt and npt are shown below as Figures 6.8 and 6.9, respectively. ^{1}H NMR (Hcpt, DMSO-d^{6}, 400 MHz): 13.19 (s, 1H), 9.20 (s, 2H), 8.06 (d, 2H), 7.85 (d, 2H). ^{1}H NMR (npt, Acetone-d6, 400 MHz): 9.04 (s, 2H), 8.46 (d, 2H), 8.07 (d, 2H).

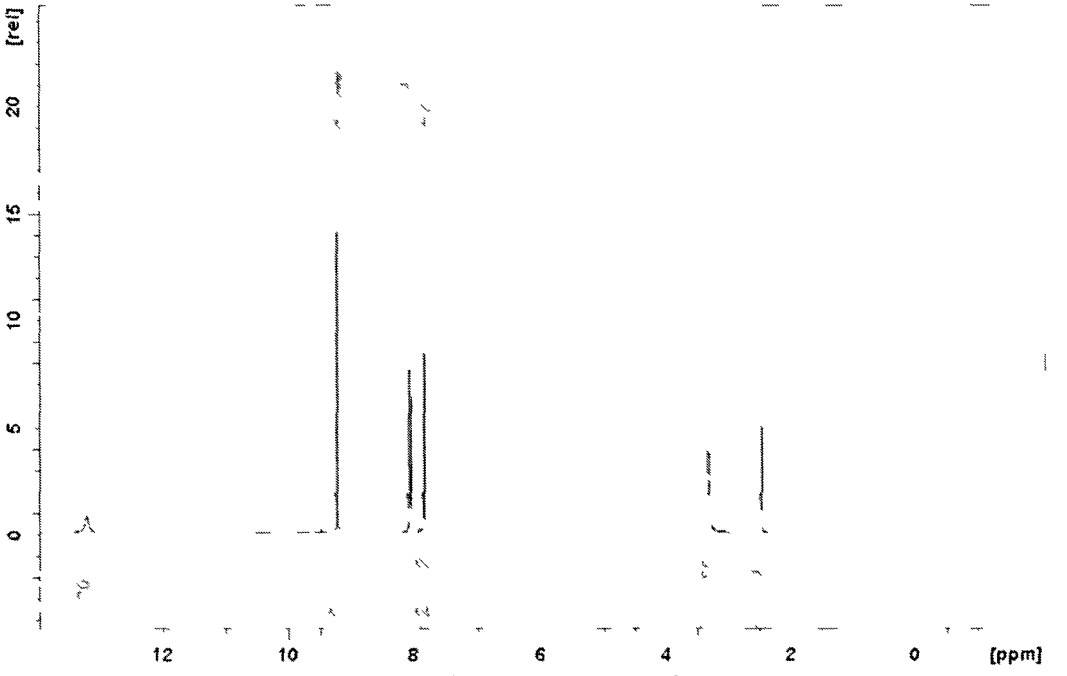

Figure 6.8 The NMR spectrum of Hcpt

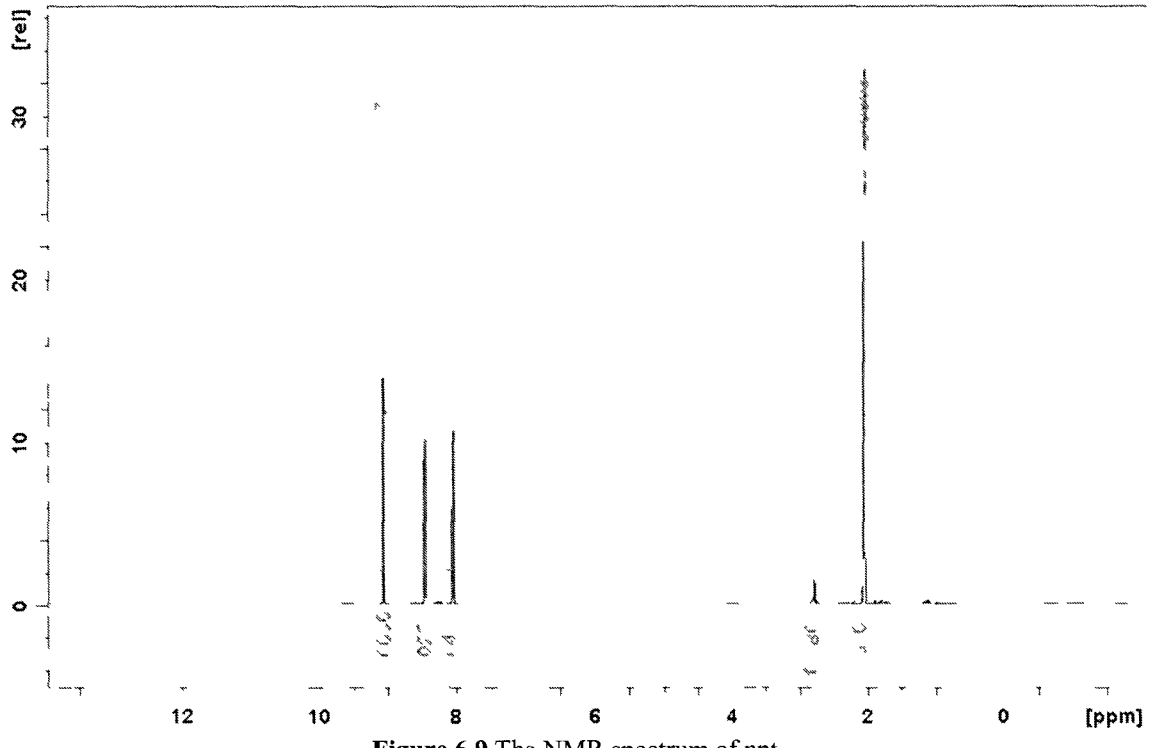

Figure 6.9 The NMR spectrum of npt

6.5 Single-Crystal X-ray Diffraction

Plate-like crystals of the compounds suitable for Single-Crystal X-ray Diffraction were mounted on glass fibers. Unit cell measurements and intensity data collections were performed on a Bruker-AXS SMART 1 k CCD diffractometer using graphite monochromated MoK_α radiation (λ = 0.71073 Å). The data reduction included a correction for Lorentz and polarization effects, with an applied multi-scan absorption correction (SADABS). In all cases, the reflection data were consistent with a triclinic system *P*-1. The crystal structures were solved and refined using the SHELXTL program suite. Direct methods yielded non-hydrogen atoms. All hydrogen atom positions were calculated geometrically and were riding on their respective atoms.

In the case of compound **1**, the data were measured on a Bruker Kryoflex diffractometer at 100 and 181 K. The positions of the coordinated ethanol molecules were calculated at both temperatures.

For **2**, the largest residual electron density peak (0.657 e/Å^3) was associated with a solvent molecule and full-matrix least-squares refinement on F^2 gave R_1 = 0.0671 and wR_2 = 0.1309 at convergence.

The data of complex **5** were truncated at 23.26°. The hydrogen atoms of the coordinated water molecules could not be located from the difference Fourier maps; they are therefore included in the chemical formula but absent from the res and cif files, creating a discrepancy in the cifcheck file. Some of the methanol solvent molecules of

crystallization were disordered and were either modeled at 50% occupancy or were modeled over two positions as a 50:50 isotropic mixture with light restraints. The largest residual electron density peak (2.550 $e^-/Å^3$) was associated with the Ln1 atom. Full-matrix least-squares refinement on F^2 gave $R_1 = 0.0813$ and $wR_2 = 0.2487$ at convergence.

For complexes **6** and **7**, unit cell measurements and intensity data collections were carried out. From the collected data, molecular structure and the connectivity were obtained which confirmed that the complexes were isomorphous. However, due to the poor diffraction of the crystals, both structures could not be refined with acceptable R_1 factors.

6.6 Magnetic Measurements

The magnetic susceptibility measurements were obtained using a Quantum Design SQUID magnetometer MPMS-XL operating between 1.8 and 300 K for dc applied fields ranging from -7 to 7 T. Polycrystalline samples of each complex were wrapped in a polyethylene membrane. dc susceptibility measurements were performed under a field ranging from 0 to 7 T between 1.8 and 300 K. ac susceptibility measurements were done under an oscillating ac field of 3 Oe and ac frequencies ranging from 1 to 1500 Hz. The magnetization data was collected at 100 K to check for ferromagnetic impurities that were absent in all samples. A diamagnetic correction was applied for the sample holder. The sample masses were of 13.8, 16.0, 16.8, 16.9, 6.6, 5.1, and 5.5 mg for **1**, **2**, **3**, **4**, **5**, **6** and **7**, respectively.

6.7 Thermogravimetric analysis

Differential thermal analyses (DTA) and thermal gravimetric analyses (TGA) were recorded using an SDT 2960 Simultaneous DSC-TGA instrument under N_2 flow (100 mL/min) at a heating rate of 10 °C/min between 25 and 300 °C.

6.8 Elemental analyses

Samples were weighed into aluminum capsules. The capsules were loaded into a Perkin-Elmer Series II 2400 CHNS/O Analyzer. Each sample is flash combusted at 924 °C and carried by helium through a column of reducing/oxidizing chemicals to get N_2, CO_2 and H_2O. The gases are separated as they pass through a gas chromatograph column so that the TCD (thermal conductivity detector) can detect each gas separately. The routine analytical precision (2sigma) is as follows: N, H and S = +/-0.1%, C = +/-0.3%. C,H,N analysis (%) found (calcd) Hcpt: C 56.32 (57.14), H 4.09 (3.73), N 23.35 (22.21). npt: C 50.29 (50.53), H 2.04 (3.18), N 29.27 (29.46).

6.9 References

[1] H. O. Bayer, R. S. Cook and W. C. Von Meyer, *US Patent* 382137628, **1974**; *Chem. Abstr.*, **1972**, *76*, 113224

[2] SHELXTL v 6.14, **2000**, *Bruker AXS, Inc.*, Madison, Wisconsin, USA.

Annex

Table A1 Bond valence sum calculations of **1**, **2**, **3** and **4**.

	$M1^{II}$	$M1^{III}$	$M2^{II}$	$M2^{III}$	Conclusion
1	2.12	2.35	2.13	2.41	$Fe1 = Fe^{II}$
					$Fe2 = Fe^{II}$
2	2.20	2.22	2.38	2 38	$Co1 = Co^{II}$
					$Co2 = Co^{II}$
3	2.51	2.53	2.69	2.69	$Co1 = Co^{II}$
					$Co2 = Co^{II}$
4	2.23	2 36	2 31	2 31	$Ni1 = Ni^{II}$
					$Ni2 = Ni^{II}$

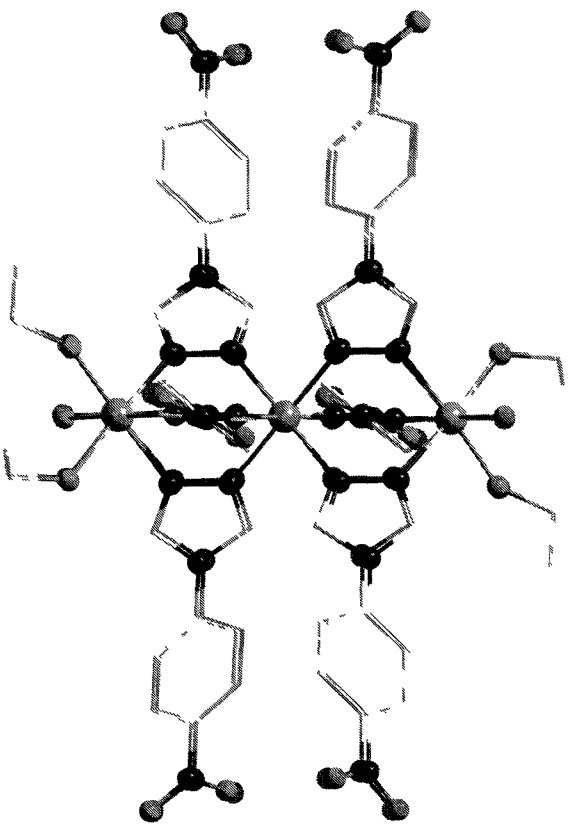

Figure A1 Shadow superposition of the molecular structures of **1** measured at 100 (shadow) and 181 K (clear).

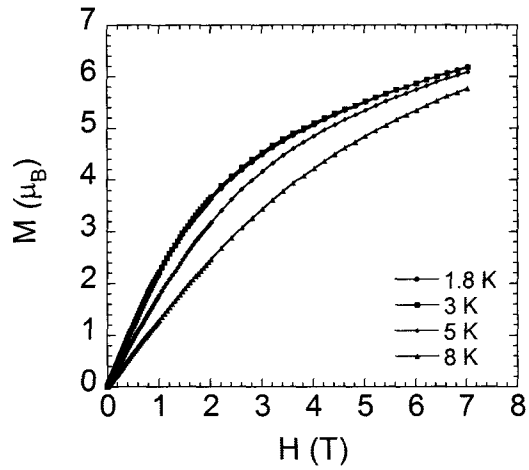

Figure A2 Field dependence of the magnetization of **1** at 1.8 (circles), 3 (squares), 5 (diamonds) and 8 K (triangles) from 0 to 7 T.

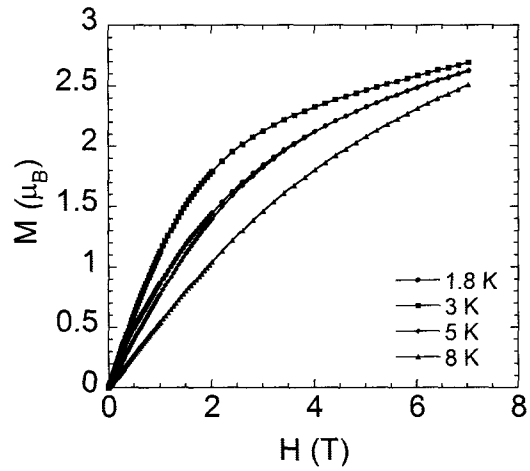

Figure A3 Field dependence of the magnetization of **2** at 1.8 (circles), 3 (squares), 5 (diamonds) and 8 K (triangles) from 0 to 7 T.

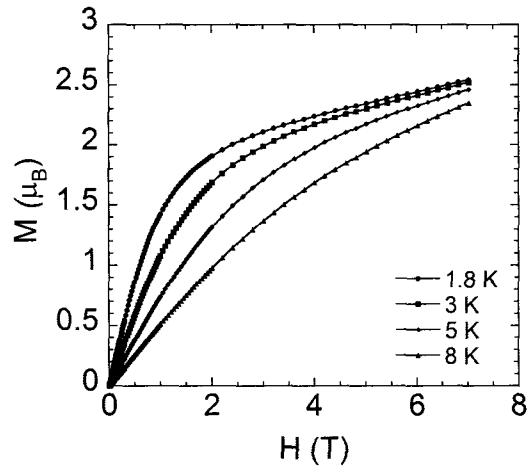

Figure A4 Field dependence of the magnetization of **3** at 1.8 (circles), 3 (squares), 5 (diamonds) and 8 K (triangles) from 0 to 7 T.

Equation A1

$$a = \frac{J_1}{kT}$$

$$b = \frac{J_2}{kT}$$

$$\chi T = \frac{Ng^2\mu_B{}^2}{3k}\left[\frac{84\exp(6a+6b)+30\exp(6b)+6\exp(-4a+6b)+30\exp(4a+2b)+6\exp(2b)+6\exp(2b)}{7\exp(6a+6b)+5\exp(6b)+3\exp(-4a+6b)+5\exp(4a+2b)+3\exp(2b)+1\exp(-2a+2b)+3\exp(2b)}\right]$$

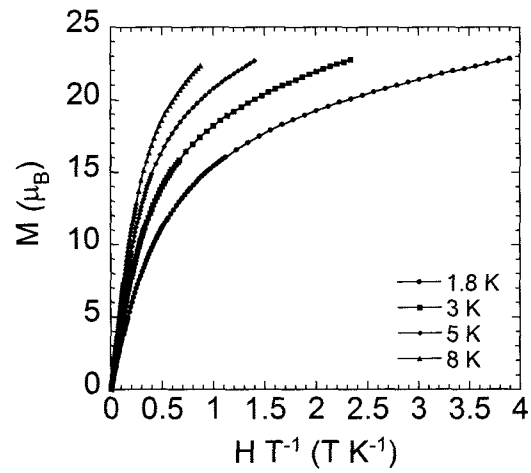

Figure A5 Field dependence of the magnetization of **6** measured at 1.8 (circles), 3 (squares), 5 (diamonds) and 8 K (triangles) between 0 and 7 T.

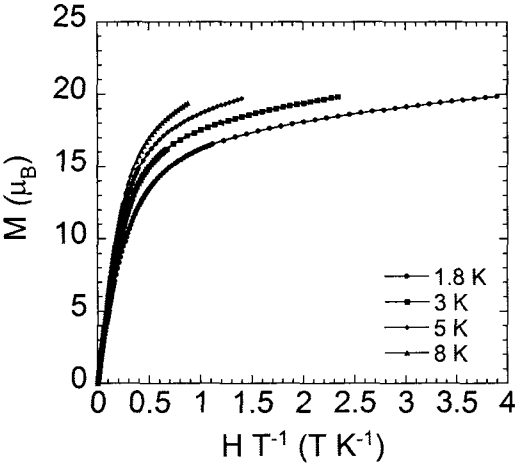

Figure A6 Field dependence of the magnetization of **7** measured at 1.8 (circles), 3 (squares), 5 (diamonds) and 8 K (triangles) between 0 and 7 T.

Table A2 Crystallographic data of **1**, **2**, **3**, **4**, **5** and Hcpt·DMF.

Complexes	**1**		**2**	**3**	**4**	**5**	Hcpt·DMF
T/K	181	100	202	202	202	202	202
Empirical formula	$C_{106}H_{130}Fe_3N_{24}O_{40}S_6$		$C_{106}H_{130}Co_3N_{24}O_{40}S_6$	$C_{98}H_{114}Co_3N_{24}O_{40}S_6$	$C_{96\ 32}H_{109\ 28}N_{24}Ni_3O_{39\ 32}S_6$	$C_{135}H_{188}Dy_8N_{36}O_{61}$	$C_{12}H_{16}N_4O_3$
Fw	2740.25		2749.49	2637.28	2600.81	4591.21	264.29
Cryst. syst.	Triclinic		Triclinic	Triclinic	Triclinic	Triclinic	Triclinic
Space group	*P*-1		*P*-1	*P*-1	*P*-1	*P*-1	*P*-1
a/Å	14.6130(7)	14.5077(7)	14.677(5)	13.5049(16)	15.056(2)	16.446(4)	3.917(1)
b/Å	15.1960(7)	15.0789(7)	15.268(5)	14.7832(18)	16.698(2)	16.476(4)	10.563(4)
c/Å	16.3954(8)	16.319(1)	16.480(5)	17.414(2)	16.718(2)	19.793(5)	15.144(6)
α/ °	107.505(2)	107.611(3)	107.590(4)	65.672(2)	103.588(2)	91.545(4)	81.941(5)
β/ °	99.989(3)	100.282(3)	99.874(4)	69.922(2)	109.528(2)	96.707(4)	89.277(9)
γ/ °	110.731(2)	110.437(2)	110.825(4)	83.052(2)	111.430(2)	101.977(4)	87.82(1)
V/Å^3	3083.3(3)	3022.8(3)	3124.9(17)	2974.6(6)	3368.0(8)	5203(2)	619.9(4)
Z	1		1	1	1	1	2
Radiation	Mo-Kα		Mo-Kα	Mo-Kα	Mo-Kα	Mo-Kα	Mo-Kα
D_c/g cm^{-3}	1.476	1.505	1.461	1.472	1.282	1.465	1.416
R_1 ($I > 2\sigma(I)$)[a]	0.0412	0.0389	0.0671	0.0670	0.0782	0.0813	0.0859
wR_2 ($I > 2\sigma(I)$)[b]	0.0995	0.1011	0.1541	0.1726	0.2361	0.2487	0.1477

[a] $R_1 = \Sigma(||F_o| - |F_c||)/\Sigma|F_o|$.

[b] $wR2 = [\Sigma[w(F_o^2 \_ F_c^2)^2]/\Sigma[w(F_o^2)^2]]^{1/2}$, $w = 1/[\sigma^2(F_o^2) + [(ap)^2 + bp]$, where $p = [\max(F_o^2, 0) + 2F_c^2]/3$.